A practical approach to accurate fault location on extra high voltage teed feeders

Coury, D. V.

Award date:
1992

Awarding institution:
University of Bath

A PRACTICAL APPROACH TO ACCURATE FAULT LOCATION ON EXTRA HIGH VOLTAGE TEED FEEDERS

Submitted by D.V. COURY

for the degree of Ph.D.

of the University of Bath

1992

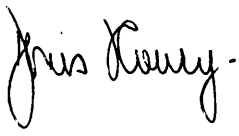

ProQuest LLC
789 East Eisenhower Parkway
P.O. Box 1346
Ann Arbor, MI 48106-1346

This thesis is dedicated to my parents,
Waldemar and Catarina.

SYNOPSIS

This thesis describes an alternative approach to accurately locating faults on teed feeders. In particular, the technique developed addresses some common problems in fault location and takes into account the practical limitations in the design, extending the range of applicability of the new scheme for a whole variety of practically encountered systems and fault conditions, without sacrificing the high accuracy requirements. The method is based on utilising voltage and current waveforms at all three ends of typical EHV teed feeders, which are then filtered using Discrete Fourier (DFT) techniques so as to produce a measure of the steady-state power frequency voltage and current phasors. The latter are obtained as data described by means of post-fault processing applied to data captured during the fault clearance process. The technique described makes use of superimposed, modal components of voltages and currents rather than total, phase values. Means is also developed for effectively synchronising the data from the three ends and an accurate identification of the faulted leg, both essential requisites for achieving high degrees of accuracy. A fault classification technique is also developed.

Finally, the fault location technique is evaluated using simulated results from practical 400 kV and 500 kV teed-feeder configurations, including those that pose some of the most difficult problems. A sensitivity analysis of the algorithm, whereby the effect of non-algorithmic errors introduced by incorrect setting parameters is also presented.

ACKNOWLEDGEMENTS

The author wishes to express his sincere thanks to DR. R.K. AGGARWAL for his supervision and encouragement throughout the course of the work and the preparation of this thesis. The author is grateful to PROF. J.F. EASTHAM and the Computer Centre for the provision of the facilities at Bath University. Thanks are extended to PROF. A.T. JOHNS for some very useful discussions on the subject and the colleagues of the Electrical Power Systems Research Laboratory.

The author's gratitude is also extended to MISS J.S. GODWIN for the constant help and emotional support throughout the course of the work.

Finally, the author acknowledges Coordenação de Aperfeiçoamento de Pessoal de Nível Superior (CAPES) for the financial support.

LIST OF CONTENTS

LIST OF PRINCIPAL SYMBOLS

V_F, I_F	Voltage and current at fault point for a two-ended line
V_A, I_A	Voltage and current at A terminal for a two-ended line
$V_A", I_A"$	Superimposed components of voltage and current at A terminal
$I_{AF}"$	Superimposed component of fault current from A terminal at point F
V_B, I_B	Voltage and current of B terminal for a two ended line
$I_{BF}"$	Superimposed component of fault current from B terminal at point F
$Z_L=R_f+jX_L$	Transmission line impedance per unit length for a two ended line
$Z_{LA}=R_{LA}+jX_{LA} = pZ_L$	Transmission line impedance between the fault and the end A
p	Fault distance as a percentage of the line length
L	Length of a two ended line
Z_{SA}, Z_{SB}	Sending and receiving end source impedances
a,b,c	Phase subscripts
$V_{P,Q,Ra,b,c}$	Multiphase pre-fault voltages for the ends P, Q and R respectively(three-ended system)
$I_{P,Q,Ra,b,c}$	Multiphase pre-fault currents for the ends P, Q and R respectively
$V_{TP,TQ,TRa,b,c}$	Multiphase pre-fault voltages for the T-point
$V'_{P,Q,Ra,b,c}$	Multiphase post-fault steady-state voltages

for the ends P, Q and R respectively

$I'_{P,Q,Ra,b,c}$ Multiphase post-fault steady-state currents for the ends P, Q and R respectively

$V''_{P,Q,Ra,b,c}$ Multiphase superimposed voltages for the ends P, Q and R respectively

$I''_{P,Q,Ra,b,c}$ Multiphase superimposed currents for the ends P, Q and R respectively

1,2,3 Modal subscripts

$V''_{P,Q,R1,2,3}$ Modal superimposed voltages for the ends P, Q and R respectively

$V''_{T1,2,3}, V''_{F1,2,3}$ Modal superimposed voltages at T and fault point

$I''_{P,Q,R1,2,3}$ Modal superimposed currents for ends P, Q and R respectively

$I''_{PT,QT,RT,1,2,3}$ Modal superimposed currents flowing to T-point

L_P, L_Q, L_R Line lengths for PT, QT and RT (three ended system)

Z_0, Z_{0k} Surge impedance and modal surge impedance

Y_0, Y_{0k} Surge admittance and modal surge admittance

Γ, Γ_k Propagation constant and modal propagation constant

$[\Gamma^2]$ Diagonal matrix

R_f Fault resistance

χ Distance to the fault point

$A(\chi), B(\chi), C(\chi), D(\chi)$ Terminal constants for two ended line

A_P, B_P Terminal constants for the leg PT

A_Q, B_Q Terminal constants for the leg QT

A_R, B_R	Terminal constants for the leg RT
[Z]	Line series impedance matrix per unit length
[Y]	Line shunt admittance matrix per unit length
$Z_{aa}, .., Z_{cc}$	Elements of [Z]
$Y_{aa}, .., Y_{cc}$	Elements of [Y]
[Q], [S]	Modal transformation matrices
[U]	Unit matrix
X/R	Reactance to resistance ratio
Z_{s0}, Z_{s1}	Zero and positive phase sequence source impedances
Z_s, Z_m	Self and mutual impedances
Y_s, Y_m	Self and mutual admittances

OPERATORS

j	$\sqrt{-1}$
-1	Inverse of a matrix
+	Conjugate transpose
*	Conjugate component
Re[.]	Real part of a complex variable
Im[.]	Imaginary part of a complex variable
arg[.]	Argument
exp[.]	Exponential

ABBREVIATIONS

CT	Current Transformer
CVT	Capacitor Voltage Transformer
EMTP	Electromagnetic Transient Program
EHV	Extra High Voltage
DFT	Discrete Fourier Transform
CAD	Computer Aided Design
CIM	Current Interface Module
DFR	Digital Fault Recorder

Types of fault:

a-earth	phase a to earth fault
a-b-earth	phase a to b to earth fault
a-b	phase a to b fault
abc	three phase fault

CHAPTER 1

INTRODUCTION

1.1 THE IMPORTANCE OF FAULT LOCATORS FOR TRANSMISSION LINES

Electric power systems are designed to ensure a reliable supply of energy with the highest possible continuity. Electrical faults can occur at any point in an electric power system and the most exposed parts are overhead transmission lines. A transmission line is also one of the most difficult parts of the power system to maintain and inspect, simply because of its dimension and the environment it is built in [1].

Determination of the point at which a fault occurs in an electric power transmission line is sometimes vital for economic operation of power systems. It allows the reduction of maintenance work and rapid service restoration following a permanent fault. A locator is also very useful for evaluating transient faults that could, otherwise, cause weak spots in transmission and distribution systems, resulting in future problems or faults.

The growing complexity of electric power systems demands a high performance of protection and control equipment. Fault locators have gained more importance

over the years since it has become more difficult to find the fault location as the visible damage of the line has decreased due to faster circuit breaker and faster protective systems.

The rapid progress in microprocessor technology, together with developments that have taken place in computer software, makes them ideally suitable for applications in electric power systems, in particular where high precision is necessary, such as in fault location. These new developments came as a replacement for analog techniques that were used in the past. The performance of such devices was not very precise and it demanded a fairly high requirement of maintenance and skilful operators.

A fault location technique can be implemented as part of a digital protection relay, a stand-alone device or an independent algorithm using data obtained by digital fault recorders for post fault analysis. Since fault locators process digitally recorded fault data in an off-line mode, they are, therefore, not subject to the same constraints, processing-wise, as protection relays that have to operate in an on-line mode. This thus allows an increase in sophistication and consequently, accuracy for the algorithms related to a digital fault location. Obviously, greater accuracy leads to an efficient post-fault service, the latter being particularly desirable on long lines or in rough terrain where even a few

kilometres of imprecision could jeopardise the forementioned continuity of supply.

The design of microprocessor-based fault locators includes the selection of a suitable algorithm and hardware to implement the selected technique. Several approaches to the problem of a transmission line fault location have been developed. Different principles have been applied to the problem and the techniques can be broadly classified in single-ended and multiple-ended data measurement.

Fault location techniques using fundamental frequency voltages and currents measured at one of the line terminals generally does not provide sufficient accuracy. A majority of such techniques are based on lumped parameter line models and the objective is to find a complex impedance of the system, from which fault distance can be deduced. The fault location estimates are particularly prone to inaccuracies if fault current is contributed by sources connected to both terminals of the line, especially in the presence of fault resistance. Some authors have offered improvements to this approach (as discussed in Chapter 2).

When data from multiple ends are used, it is possible to overcome some of the common problems associated with fault locating. In this respect, it should be mentioned that although a communication medium is required for

transmitting fault-recorded data to the processing end, however unlike fault detection (which operates in an on-line mode and therefore requires high-speed, continuous communication links), the communication requirements for fault locators are very modest (and non-continuous) since the latter operate in an off-line mode.

1.2 MULTI-TERMINAL LINES

Three-terminal lines, in which a tee connects new circuits into an existing transmission system, offer considerable economic advantages and environmental benefits over two-terminal lines for Extra High Voltage (EHV) power transmission. There is a natural conflict between the ever increasing demand for power or connections for new generation on one hand and the great difficulty in obtaining right of way for constructing new EHV lines. In this respect, a teed circuit offers a cheap and attractive alternative [2].

It is well known that such lines are difficult to protect by using conventional power system protection schemes. In this respect, the advent of fibre optical links for data communication between the three ends is making possible protection of such configurations which are, therefore, likely to find more widespread application in the future.

Like the demand for an adequate protection scheme for teed circuits, there is now also a growing demand for the development of an accurate fault location technique for such circuits and the work presented in this thesis is concerned with describing one such technique.

1.3 OBJECTIVES OF THE WORK

The main objectives of this thesis are:

- To present the basis of a new approach to accurately locate faults on three-terminal lines. The method is based on utilising voltage and current waveforms at the three ends of a circuit captured using digital fault recorders. The technique outlined also includes methods for synchronising data from the three ends, an accurate identification of the faulted branch and also a technique for classifying the type of fault. It is shown that these criteria are essential for achieving a high degree of accuracy. The signals for estimation of fault location are based on modal components rather than phase values. Some of the common problems associated with fault location are addressed in order to achieve the maximum accuracy.

- To establish the correct performance of the proposed fault locating technique. The approach adopted for this purpose was to model the fault locator on a computer and investigate the performance that might be expected when it is subjected to simulated fault transient data attained from in-house power system models. This approach provides an inexpensive and flexible method for assessing a variety of different system and fault conditions the fault locator would experience in practice.

  Simulation results using a number of different 400 kV transmission line configurations are presented. The simulation takes into account the effect of transducers (CTs and CVTs) and hardware errors such as the effect of interface modules, anti-aliasing filters and quantisation, so that the information processed through the fault locator algorithm is very close to a real-life situation.

  As part of the fault locating algorithm, a digital filter based on Discrete Fourier Transform (DFT) technique is also implemented to extract the fundamental frequency components of voltages and currents.

  The algorithm is extensively tested for a whole variety of practically encountered different systems and fault conditions. Furthermore, the effect on

accuracy of parameters like fault resistance, different fault inception angles, variation in the sampling rate, superimposed components, setting errors, etc is ascertained.

- To make suggestions for future work related to the proposed fault location technique.

1.4 SCOPE OF THE THESIS

Chapter 2

A literature review of fault locator techniques for transmission lines is presented in this chapter. The techniques reviewed are initially divided into two groups: (i) for two terminal lines and (ii) for three terminal lines. The first group is subdivided into algorithms using data from one end of the transmission line only and algorithms based on information from both ends. The second group is concerned with presenting the very limited techniques developed for fault location on three terminal configurations. The merits and demerits of each technique are also described.

Chapter 3

This chapter describes the basis of an alternative approach to accurately locating faults on three terminal lines. The different stages involved in the fault locating technique are presented. The fault calculation is implemented as the last step in the process. Steps like synchronisation of data from the three ends, fault inception time identification, extraction of fundamental phasors, superimposed components calculation, fault classification, modal transformation and identification of the faulted leg have to precede the actual fault distance calculation in order to maximise the accuracy for the latter. The theory related to each of the previous steps is also presented.

Chapter 4

A fault transient simulation package for three terminal lines, developed at The University of Bath, is utilised for testing the proposed algorithm. Although the fault location technique is based on Computer Aided Design (CAD) studies, practical considerations are included. The effect of transducers, interface modules/analog filters, quantisation, etc on primary system fault data are discussed in some detail in Chapter 4.

Chapter 5

Chapter 5 is devoted to the proposed algorithm testing. Some of the typical configurations encountered in practice are chosen for such purpose. The first one is a symmetrical tee with equal lengths to the T-point and equal source capacity terminations. A nonsymmetrical configuration with differing source capacities and line lengths up to the T-point is also analysed. The effect of feed-around paths on accuracy attained for both symmetrical and unsymmetrical systems as well as the performance of the proposed fault locator for double circuit tees is also outlined in Chapter 5. Results concerned with the outputs at different stages involved in the fault locating technique are then presented.

Chapter 6

Chapter 6 is divided into two main parts. The first part presents the performance evaluation of the fault locator algorithm under different fault conditions. The effect of data unsynchronism, source capacity, fault resistance, fault inception angle, fault cycle, sample rate and superimposed components on accuracy attained are examined. The second part is devoted to a sensitivity

analysis of the fault locator algorithm, whereby the effect of non-algorithmic errors, introduced by incorrect setting parameters, are investigated.

Chapter 7

Chapter 7 presents a summary of the work presented in this thesis and conclusions. It also includes suggestions for future work.

CHAPTER 2

LITERATURE REVIEW OF FAULT LOCATOR TECHNIQUES FOR TRANSMISSION LINES

2.1 INTRODUCTION

With the advent of microprocessor-based devices, better accuracy in locating faults in power systems has attracted great interest. Since then, considerable work has been done on developing digital techniques for locating faults in transmission lines. The fault locating techniques reviewed in this chapter are initially divided into two groups: (i) for two-terminal lines and (ii) for three-terminal lines. The first group is further divided into those algorithms using information from one end only and those based on information from both ends of the faulted line.

2.2 FAULT LOCATION TECHNIQUES FOR TWO-TERMINAL LINES

Figure 2.1 shows a single-line diagram of a power system in a faulted situation for a two-terminal line, which is useful to illustrate the principles, underlying some of the fault location techniques put forward in this group. Since the objective is only to present the fundamental ideas, the equations will not be extended for three-phase systems.

2.2.1 Algorithms Using Data from One-End Only

As mentioned in the previous chapter, algorithms using data from just one end of a transmission line are generally based on the calculation of the impedance (or more precisely reactance) up to the fault point, from which fault distance can be deduced. However, such techniques suffer from errors due to fault current contribution by sources connected to both terminals of the line and fault resistance.

Saint and Paithankar [3] have proposed a fault location technique based on the measurement of the ratio of reactance of the line from the fault locator up to the fault point to the total reactance of the line, i.e.; x_{LA}/x_n. Because x_n is a known value, the ratio x_{LA}/x_n determines the fault position. The following expression is derived for calculating this ratio:

$$\frac{x_{LA}}{x_n} = \frac{sin\Theta_3 \; cos\Theta_1}{sin\Theta_2} \qquad (2.1)$$

$$\Theta_1 = arg\left[\frac{I_A x_n}{V_A}\right]$$

$$\Theta_2 = -\frac{V_A}{I_A x_n - V_A} \qquad (2.2)$$

$$\Theta_3 = 180° - (\Theta_1 + \Theta_2)$$

Equation (2.1) shows that the fault position can be determined by the measurement of any two of the three phase angles θ_1, θ_2 and θ_3. The suggested technique is based on measurement of these angles by two digital counters. The fault locator is analysed only under single-end fed conditions. The fault location estimates are, therefore, not accurate if fault current is contributed by sources connected to both terminals of the line and if fault resistance is present.

Takagi et. al. [4] have presented a technique for reducing errors caused by various factors such as load flow, fault resistance, and the unsymmetrical arrangement of the transmission line. The method to calculate the distance to a fault point is based on the following equations, which express a fault point voltage V_F and current I_{AF}", using the one terminal data:

$$V_F = V_A cosh(\Gamma\chi) - Z_0 I_A sinh(\Gamma\chi) \qquad (2.3)$$

$$I_{AF}" = (V_A"/Z_0)\, sinh(\Gamma\chi) - I_A" cosh(\Gamma\chi) \qquad (2.4)$$

Adopting some approximations, the distance χ is obtained using the following equations:

$$\chi = \frac{Im[V_A I_A"^*]}{Im[Z_L I_A I_A"^*]} \qquad (2.5)$$

In equation (2.5), the effect of load flow is cancelled by using fault component current I_A", and the effect of fault resistance is reduced by a manipulation of the previous equations. The technique initially neglects the effect of shunt capacitance, but this effect is further compensated.

A digital fault locator has been implemented commercially by Toshiba Corporation (Muraoka et. al. [5]) using basically the same principles as above. The field tests show good accuracy for single phase-earth faults on a transmission line. The method offers some improvements, but it assumes that the impedance angles of the line up to, and beyond the fault, are the same. This simplified assumption can give rise to substantial errors in the calculated fault distance since the difference between the two arguments mentioned generally varies with the distance to fault.

A modification is offered also by Schweitzer [6], which provides an improvement to the performance of the Takagi algorithm.

In another method, Takagi et. al. [7] have used practically the same equations as before, i.e. (2.3) and (2.4), presenting another solution for the fault location problem, with the expression:

$$R_f\{1 + K(\chi)\} = -\left[\frac{A(\chi)V_A - B(\chi)I_A}{C(\chi)V_A" - D(\chi)I_A"}\right] \qquad (2.6)$$

Where:

$$K(\chi) \equiv \frac{I_{BF}''}{I_{AF}''} \quad \text{current distribution factor}$$

As the fault impedance is purely resistive, R_f is a real variable. The ratio $K(\chi)$ also becomes real on the condition that the transmission line is lossless and the source impedances at two ends are purely inductive. Therefore, the right hand side of the equation (2.6) must be a real value. Hence,

$$Im\left[\frac{A(\chi)V_A - B(\chi)I_A}{C(\chi)V_A'' - D(\chi)I_A''}\right] = 0 \qquad (2.7)$$

The solution χ of equation (2.7) is the distance from the local end to the faulted point. As this equation is a non-linear equation, the iterative solution technique based on Newton Raphson method is thus employed. The steps involved are: firstly, the primary data of transient waveforms is smoothed out by a digital filtering program; secondly, a transformation program extracts the voltage and current vectors (Fourier Techniques) and finally, the Newton-Raphson program is executed to solve the equations.

The digital fault locator is tested on an artificial transmission line (with no line resistance) and good results are attained. However, since the solution assumes lossless circuit elements, there are appreciable errors

in the computed distance when applied to a realistic lossy system.

Takagi et. al. [8] have also presented the same forementioned fault current distribution approach for locating faults, making use of Laplace Transform Technique. They have then applied the condition that the voltage across the fault resistance must have the same value, if calculated for two different values of the Laplace operators. However, the authors conclude that the Fourier method is superior to the Laplace one.

Wiszniewski [9] has presented a method based on the standard calculations of resistances and reactances using the fault current distribution factor, with an algorithm in which an attempt is made to compensate the error introduced by the fault resistance. The required calculations are noniterative.

The first expression, taking into account the current distribution factor, is:

$$Z_A = Z_{LA} + (R_f/K)\left[\frac{I_A - I_L}{I_A e^{j\lambda}}\right] \qquad (2.8)$$

The final expression for calculating a correct value of the reactance is obtained as:

$$X_{LA} = X_A - \frac{R_A tan(\Phi_L) - X_A}{(a/b)\, tan\Phi_L - 1} \qquad (2.9)$$

Where,

$$a = Re[\frac{I_A \_ I_L}{I_A e^{j\lambda}}]$$

$$b = Im[\frac{I_A - I_L}{I_A e^{j\lambda}}] \qquad (2.10)$$

and:

$K = ke^{j\lambda}$ fault current distribution factor

$Z_A = R_A + jX_A$ impedance measured at A

$\Theta_L = tan^{-1}(X_{LA}/R_{LA})$ phase angle of the phase impedance

I_L pre-fault current

The local signals V_A, I_A and I_L enable X_A, R_A, a and b to be calculated. Thus, the reactance X_{LA}, which is proportional to the true distance between the line end A and the fault may be determined by equation (2.9). The accuracy of the error compensation depends on the assumed values for Θ_L and λ. In fact, the fault current distribution factor depends on the configuration of the network, i.e. the line impedance between the fault and two ends and the source impedance at both ends of the line, but for simplification it is assumed that λ is equal to zero, which implies that the distribution factor

K is real. The angle θ_L is also considered as constant. However, in some cases, these assumptions may give rise to incorrect compensation.

Furthermore, the effect of shunt capacitance is ignored. Whilst, this assumption could be somewhat justified for relatively short lines, however, the line shunt capacitance can became quite significant as the line length goes up and this in turn could cause quite significant errors in the actual location of the fault.

Saha et. al. [1] and Erikson et. al. [10] have also developed an algorithm based on current distribution factor. The fault locator program utilises representative values of the source impedances to determine a correct description of the network.

Using an expression similar to equation (2.8) with a representation for the current distribution factor, the final expression is obtained as:

$$p^2 - pK_1 + K_2 - K_3R_f = 0 \qquad (2.11)$$

Where:

$$K_1 = \frac{V_A}{I_A Z_L} + 1 + \frac{Z_{SB}}{Z_L}$$

$$K_2 = \frac{V_A}{I_A Z_L} \left[\frac{Z_{SB}}{Z_L} + 1\right] \qquad (2.12)$$

$$K_3 = \frac{I_{FA}}{I_A Z_L} \left[\frac{Z_{SA}+Z_{SB}}{Z_L} + 1\right]$$

By separating the complex equation (2.11) into real and imaginary parts, two simultaneous equations are obtained. By eliminating the unknown fault resistance R_f, a single expression results with the single unknown variable p. This is solved using the magnitude and phase derived from Fourier analysis routine which yields the fundamental components of the signals. For a multiphase system, the fault type has to be defined before using the method.

The proposed equipment was tested under dynamic conditions and results are given only for a short line, with error of less than 1% of the total length. The effect of shunt capacitance is ignored. The authors use assumed values of source impedances to calculate the current distribution factor. However, equivalent source impedances are not readily available in all cases. Also, the system configuration changes from time to time, modifying distribution factors and introducing setting errors into the algorithm. The technique is in commercial use in the ASEA equipment.

Cook [11] has presented another approach dealing with the current distribution factor. The technique also requires an assumed value of remote end source impedance, which is then used to determine the argument of this factor, rather than its magnitude. Smaller errors are claimed by the author for such a technique. The effect of shunt capacitance is also neglected.

Another different fault location method using data from one end only, has been presented by Richards and Tan [12]. The line is represented as a lumped parameter circuit. The fault location problem is then treated as a parameter estimation problem of a dynamic system, in which the response of the physical system is compared to the lumped parameter model. The model's parameters are varied until an adequate match is obtained with the physical system response. Simplification of the equations is achieved by using instantaneous symmetrical components. The estimation does not require filtering of DC offset and high frequency components.

Several tests were conducted using the simulated transmission line and the final estimates are within 1% accuracy. However, the effect of some problems relating to real transmission lines, like untransposition or mutual coupling of parallel lines, are not investigated. The shunt capacitance is also neglected.

Morrison and Yang [13] have presented a method for fault locating, using solid state disturbance recorders. The algorithm is also based on the well known differential equation for the line. The fault equation is based on the instantaneous current and voltage at one end of the system. The technique neglects the effect of shunt capacitance.

Christoupoulos and Wright [14] have presented a different approach for locating faults on transmission lines. They use the theory of travelling waves for such a task. More details about this idea is given later in the fault location methods for three-terminal lines.

2.2.2 Algorithms Using Data from Two-Ends

Improvements in accuracy for transmission line fault location equipments are claimed by some authors using information measured at both ends of the line. The techniques are generally independent of fault impedance or changes in the power system source operating configuration. However, communication between the ends and a method to determine the phase angle of the voltages and currents at a common reference axis are necessary. The location of the fault can only be determined accurately if the measurements at both ends are synchronised.

Schweitzer [6],[15] has presented a technique which uses steady-state voltage and current data from both ends of the line. The first approach is for a short line model. In figure 1.1, the voltage at the fault point V_F, using A bus data is:

$$V_F = V_A - pZ_L I_A \tag{2.13}$$

and the voltage at the fault point using B bus data:

$$V_F = V_B - (1-p) Z_L' I_B \tag{2.14}$$

When these are equated so as to eliminate V_F, the result obtained is:

$$p = [(V_A - V_B) + Z_L I_B] / [Z_L (I_A + I_B)] \tag{2.15}$$

Using the steady-state values for currents and voltages, equation (2.15) gives the value of p, which represents the fractional distance to the fault point.

The short-line approximation assumes the currents at both ends of the line to be the same under normal, unfaulted conditions. This gives the pre-fault condition as:

$$I_B = -I_A \tag{2.16}$$

Thus, observation of the pre-fault current yields the phase relationship between the clocks at the two substations, making possible the synchronisation of the data for maximum accuracy.

Where the short line approximation is unjustified, the derivation may be repeated using distributed-parameters equations. Equations (2.13) and (2.14) are replaced by:

$$V_F = V_A cosh(\Gamma pL) - Z_0 I_A cosh(\Gamma pL) \qquad (2.17)$$

$$V_F = V_B cosh[\Gamma(1-p)L] - Z_0 I_B sinh[\Gamma(1-p)L] \qquad (2.18)$$

The solution obtained for the location, using the above equations and the first order approximations for the exponetials in the hyperbolic functions is:

$$p = \frac{[(V_A - V_B) - Z_0 \Gamma L I_B]}{[Z_0 \Gamma L (I_A + I_B) - (V_A - V_B)(\Gamma L) - (V_B + Z_0 I_B)(\Gamma L)^2]} \qquad (2.19)$$

where $Z_0 \Gamma L = Z_L$.

An A-bus estimate of pre-fault I_B is needed to synchronise the clocks. Using the same approximations, the estimate is:

$$I_{BA} = V_A[\Gamma L / Z_0] - I_A \qquad (2.20)$$

where the BA subscript denotes the estimate of the B-end quantity at the A-bus.

The two-ended method described above does not require or assume values of the system parameters external to the line being monitored. No results are presented in the reference using either of the forementioned techniques and zero error is claimed by the authors. In reality the accuracy is limited by the degree of accuracy of the line model used in a particular implementation, by the accuracy to which the parameters of the lines can be determined, and by the hardware and software used, including efficiency of the digital filtering method for obtaining the steady-state values.

Jeayasurya and Rahman [16] use equation (2.15) to estimate the location of a transmission line fault. They also used a method to determine the relative phase angle between the relay currents on a common reference axis.

As mentioned before, equation (2.15) neglects the shunt capacitance of the transmission lines. For long EHV lines, where charging currents are substantial, the authors claim that the method will give accurate estimation of the fault location provided that the high frequency transients due to shunt capacitance are filtered using suitable filters.

Accurate estimation of fault location is obtained with one cycle of post fault data, when the line capacitance is neglected. When the capacitance is considered, it is noted that almost two cycles of post fault data is required for an accurate estimation of the fault location.

Johns and Jamali [17] have also used equations (2.17) and (2.18) for an exact evaluation of the distance to the fault. The method involves monitoring and filtering the voltages and currents measured at each end of a line so as to produce a measure of the steady-state power frequency voltage and current phasors. The distance is then computed using the theory of natural modes and matrix function theory. In all cases, the algorithm error is less than approximately 1.5%.

Sachdev and Agarwall [18] have proposed an approach in which use is made of local apparent line impedance and positive sequence current measured by relays, as well as corresponding data from the remote end. From this information, different types of fault are analysed using symmetrical component theory in order to obtain the distance to fault for each case. Source impedances, distribution factors and pre-fault currents are not used in the estimation process.

The technique was tested using simulated data for single phase to ground and two phases to ground faults

only. The results indicate that the estimation errors are less than 5% of the line length, except for a section near the mid-point of the line where the fault current contributions from both line terminals are equal and where the error is much higher. The measurements taken at the two line terminals are not required to be synchronised. The effect of shunt capacitance is neglected.

Cook [11] has also presented two methods, which use the information available at local and remote ends. The first method requires only the measured impedance at each line end and generates a quadratic equation involving the unknown parameter distance. The second method requires two impedances and two relay currents, similar to the one proposed by Sachdev and Agarwall, but the developed algorithm is considerably easier to apply because it is a simplified form of the quadratic algorithm.

These methods are also accurate in general, but do not give satisfactory results in case of faults involving ground at certain locations. The effect of the line shunt capacitance has also been neglected and the algorithm can only be used accurately for transposed lines since sequence components are used.

2.3 FAULT LOCATION TECHNIQUES FOR THREE-TERMINAL LINES

Not much work has been done for fault location on three-terminal configurations, hitherto.

Ibe and Cory [19] have developed an algorithm for two- and three-terminal network based on the travelling wave phenomena. The high frequency components in the faulted waveforms present undesirable effects to most fault location algorithms and as a consequence filtering of post fault signals, to remove the high frequency transients, is essential for accurate fault location. The proposed algorithm, however, makes use of the travelling waves present for fault location purposes.

The transmission line is represented by the telegraph equations, based on the distributed parameter line model. These hyperbolic partial differential equations are solved by the travelling wave method. Criterion functions based on estimated voltage and current profiles on the line during the fault are used to determine the fault position. For the two-terminal networks, data sampled at the local terminals is sufficient for fault location, but for three-terminal networks, an additional recording from any of the two remote terminals may be necessary for confirmation of the faulted branch. A location accuracy of between 0.07 and 3.2% is achieved for a 33 kV system.

Despite the fact that a reasonable accuracy is attained using the proposed algorithm, problems can be present in a practical implementation. Difficulties are often experienced when using travelling wave methods, particularly with conventional CVTs. They are generally incapable of passing the necessary higher frequency phenomena, especially for faults close to a recording end, due to the very limited bandwidth of the transducer.

Girgis, Hart and Peterson [20] have also presented a method for the computation of fault location in two- and three-terminal lines. It considers the power frequency three-phase voltage and current phasors at each end of the line to be obtained and communicated to another processor to calculate the fault position. The local phasors are considered to have a common reference, but synchronisation at the different terminals is not required. The authors claim that the method is independent of fault type and insensitive to source impedance variation and fault resistance.

Considering a three-terminal line with Z_{abc1}, Z_{abc2}, and Z_{abc3} representing the series impedance matrix of the line sections L_1, L_2 and L_3 respectively, for a fault in line L_1, the relationship amongst the parameters of the line is given by:

$$\begin{bmatrix} Y_{1a} \\ Y_{1b} \\ Y_{1c} \end{bmatrix} = \begin{bmatrix} M_a \\ M_b \\ M_c \end{bmatrix} \chi \qquad \text{or} \qquad Y_1 = M\chi \tag{2.21}$$

$$\begin{bmatrix} Y_{2a} \\ Y_{2b} \\ Y_{2c} \end{bmatrix} = \begin{bmatrix} M_a \\ M_b \\ M_c \end{bmatrix} \chi \qquad \text{or} \qquad Y_2 = M\chi \tag{2.22}$$

where:

$$Y_{1j} = V_{j1} - V_{j2} + \sum_{k=a,b,c} (L_1 Z_{1jk} + L_2 Z_{2jk}) I_{k2} + L_1 \sum_{K=a,b,c} Z_{1jk} I_{k3}$$

$$Y_{2j} = V_{j1} - V_{j3} + \sum_{k=a,b,c} (L_1 Z_{1jk} + L_3 Z_{3jk}) + L_1 \sum_{K=a,b,c} Z_{1jk} I_{k2}$$

$$M_j = \sum_{k=a,b,c} (I_{k1} + I_{k2} + I_{k3})$$

$V_{j1,2,3}$ = three-phase voltage at terminals 1,2,3

$I_{j1,2,3}$ = three-phase current at terminals 1,2,3

j = a,b,c

χ = distance

Each of the equations (2.21) and (2.22) represents three complex equations in one unknown (real) or six real equations in one unknown. A solution for χ can then be obtained using least square estimates as:

$$\chi = (M^{+}M)^{-1} M^{+} Y_1 \tag{2.23}$$

or

$$\chi = (M^{+}M)^{-1}M^{+}Y_2 \qquad (2.24)$$

A technique for branch identification is proposed and the use of the same process as above using unsynchronised data is also implemented.

The method developed is tested using power frequency voltage and current phasors from very simple steady-state models of the high voltage system and the fault location algorithm totally ignores the line shunt capacitance. Furthermore, although the authors have also presented a limited study using more realistic voltage and current waveforms obtained from Electromagnetic Transient Program (EMTP), however, there is no mention of the effect of CVTs, CTs, transducer/recording equipment interfaces and in particular, the filtering technique used for extracting the fundamental components of voltage and current phasors from the fault generated noisy waveforms.

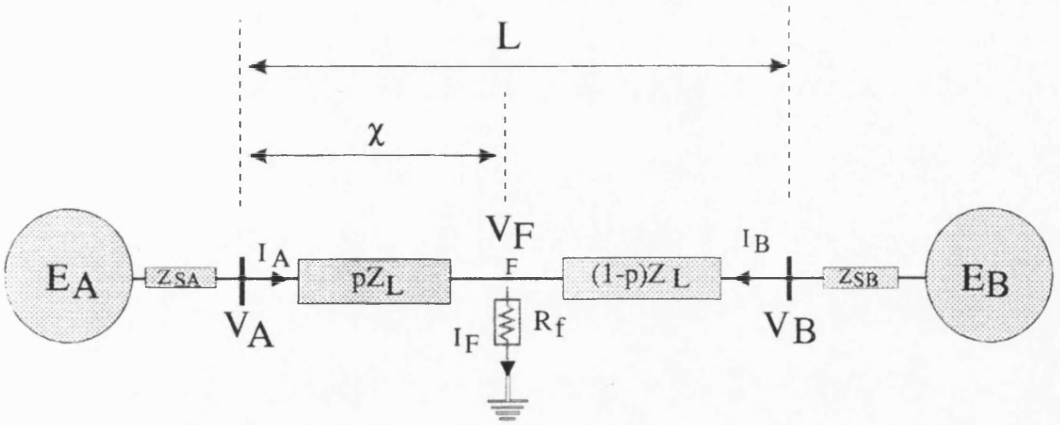

Figure 2.1 Single line diagram for faulted two-ended line

CHAPTER 3

ACCURATE FAULT LOCATOR FOR THREE-TERMINAL LINES

3.1 INTRODUCTION

Three-terminal lines, as mentioned before, although attractive both from environmental and economical points of view, however, pose additional problems caused by the intermediate infeed from the third terminal (and in some cases by an outfeed due to the presence of a tenuous feed-around path) and therefore require special attention.

This chapter describes the basis of an alternative approach to accurately locating faults on teed feeders which has been recently developed specifically for two-terminal lines [21]. The technique not only addresses some common problems in fault location, but also takes into account the practical limitations in the design, thus extending the range of applicability of the new scheme for a whole variety of practically encountered system and fault conditions, without sacrificing the high accuracy requirements. Some practical considerations relating to the fault location process are presented in the next chapter.

The method is based on utilising voltage and current waveforms at all three ends of typical EHV teed feeders,

which are then filtered using Discrete Fourier Transform (DFT) techniques so as to produce a measure of the steady state power frequency voltage and current phasor. The latter is obtained as data described by means of post-fault processing applied to data captured during the fault clearance process. The technique described makes use of superimposed, modal components of voltages and currents rather than total, phase values for the calculation of the fault distance. Means are also developed for effectively synchronising the data from the three ends and an accurate identification of the faulted leg, both essential requisites for achieving high degree of accuracy. A technique for classifying the type of fault is also presented.

3.2 THE FAULT LOCATION TECHNIQUE

Figure 3.1 shows a block diagram of the different stages involved in the fault locating technique. The starting point is the digitised voltages and currents at all three ends during a fault and include a number of cycles of pre-fault data. Figure 3.2 shows the typical digitised voltage and current waveforms for a faulted system, with pre-fault data, seen by one of the ends.

As can be seen in Figure 3.1, the fault calculation is implemented as the last step in the process, since steps like synchronisation of data from the three ends,

faulted leg identification, etc have to precede the actual fault distance calculation in order to maximise the accuracy for the latter.

3.2.1 Synchronisation of Data From Three Ends

Since data is recorded independently from three different ends, in some cases it might not be possible to avoid synchronisation errors due, for example, to unsynchronised clocks in the recording equipment at each end of the line. A direct consequence of this unsynchronisation is that the phasor quantities deviate from a common time reference. In this respect, it should be mentioned that in practice, if one end is designated as reference, then the mismatch in recorded data at any of the other two ends rarely exceeds two samples when compared to the reference-end data [22]. The technique is designed to tolerate these levels with in an acceptable degree of accuracy. It is nonetheless important to incorporate a means for synchronising data within the algorithm to maintain the high degree of accuracy, particularly in abnormal situations where there is an exceptionally large mismatch in data due, for example, to non-simultaneous triggering of fault recorders at the three ends, on fault inception.

The forementioned synchronisation could be achieved by means of a continuous data channel linking each end. However, an easier and cheaper solution is to make use of

the available pre-fault data for the voltage and current at the three ends obtained from the conventional fault recorders. One such approach is described in this section.

The technique employed here hinges upon evaluating the voltage at the tee point from a knowledge of the pre-fault power frequency voltage and current phasors which are obtained using the DFT technique (described in detail in section 3.2.3). With reference to the single line diagram shown in Figure 3.3(a), the voltage relationships attained at the tee point as functions of the multi-phase voltages and currents phasors at the three ends are given as:

$$[V_{TPa,b,c}] = A_P[V_{Pa,b,c}] - B_P[I_{Pa,b,c}] \qquad (3.1)$$

$$[V_{TQa,b,c}] = A_Q[V_{Qa,b,c}] - B_Q[I_{Qa,b,c}] \qquad (3.2)$$

$$[V_{TRa,b,c}] = A_R[V_{Ra,b,c}] - B_R[I_{Ra,b,c}] \qquad (3.3)$$

Where,

$$\begin{bmatrix} A_P & B_P \\ C_P & D_P \end{bmatrix} = \begin{bmatrix} \cosh(\Gamma L_P) & Z_0 \sinh(\Gamma L_P) \\ Y_0 \sinh(\Gamma L_P) & \cosh(\Gamma L_P) \end{bmatrix} \qquad (3.4)$$

and A_Q, B_Q, A_R and B_R are obtained in a similar way.

As it is a pre-fault model, the system is balanced and can be represented for one of the multi-phase quantities.

Having the phase a as reference, V_{Ta} can be calculated by the following equations:

$$V_{TPa} = cosh(\Gamma L_P) V_{Pa} - Z_0 sinh(\Gamma L_P) I_{Pa} \quad (3.5)$$

$$V_{TQa} = cosh(\Gamma L_Q) V_{Qa} - Z_0 sinh(\Gamma L_Q) I_{Qa} \quad (3.6)$$

$$V_{TRa} = cosh(\Gamma L_R) V_{Ra} - Z_0 sinh(\Gamma L_R) I_{Ra} \quad (3.7)$$

and the phasors obtained:

$$V_{TPa} = v_{tp} \angle \Theta_{tp} \quad (3.8)$$

$$V_{TQa} = v_{tq} \angle \Theta_{tq} \quad (3.9)$$

$$V_{TRa} = v_{tr} \angle \Theta_{tr} \quad (3.10)$$

The flowchart for the synchronisation task is shown in the Figure 3.4. It is apparent that if the data is synchronised, then $v_{tp}=v_{tq}=v_{tr}$ and $\Theta_{tp}=\Theta_{tq}=\Theta_{tr}$ and no action must be taken by the algorithm. If, however, there is a mismatch at any of two ends in relation to a reference one, then although the magnitudes of voltage phasors attained via equations (3.5) to (3.7) would be identical, the phase angles would nonetheless be different. It is then a matter of shifting the data at the unsynchronised end(s) by an appropriate number of samples of voltages and currents (based on the difference of the phase angles $\Theta_{tp}, \Theta_{tq}, \Theta_{tr}$) until such time as errors due to non-synchronous sampling at the three ends are minimised.

3.2.2 Fault Inception Time Identification

Since the current and voltage samples include both pre-fault and post-fault data, it is thus necessary to determine the point within the recorded data of voltages and currents at which the fault has occurred.

Faults cause distortions in the current and voltage waveforms. Current and voltage peaks can change in magnitude and/or phase position with respect to pre-fault conditions. Figure 3.5 shows the flowchart for identification of the fault inception time. In this process, the current samples for all the phases at the three ends are compared simultaneously with the corresponding samples, one cycle previously. Any significant change in the magnitudes of the samples between the two cases would constitute the time at which a fault has occurred. However, in order to ensure that the latter has actually happened, the logic within the processor is arranged such that whichever of the nine phase currents registers a change greater than a predefined threshold level for three consecutive samples first, then those samples determine the fault inception time. It should be mentioned that, for the same discrete time, in case the forementioned criteria is not satisfied

for the current samples, the whole process is then applied to the voltage samples.

It is worth mentioning that is not essential to always detect the first sample which corresponds to the fault inception time. Detection at a slightly later time will simply mean a shift in the reference time for all the waveforms without causing any errors.

3.2.3 Extraction of Fundamental Phasors

In order to attain a high degree of accuracy in the location of a fault, it is vitally important to be able to accurately extract the power frequency voltage and current phasors from the post-fault waveforms which can have significant transients ranging from high frequencies down to DC levels. In this respect, although in practice, the transients in primary systems waveforms are attenuated by the transducers, low pass filters, etc, the waveforms as recorded by fault recorders can still contain quite significant transient components before they are processed through the fault locator algorithm; hence the necessity to employ special digital filtering techniques to reject them.

The method used here is based on one cycle of information and the general DFT equation which gives both

magnitude and phase of the fundamental phasor $X_{v,i}(\omega)$ is given as:

$$X_{v,i}(\omega) = (2/N) \sum_{n=0}^{n=N-1} [x_{v,i}(n)\{cos(\omega n\Delta t) - j sin(\omega n\Delta t)\}] \quad (3.11)$$

Where:

N = number of samples in a cycle

Δt = time step length

ω = $2\pi 50$ Hz frequency of the phasor to be extracted

$x_{v,i}(n)$ = sampled voltage or current waveforms

The voltages and currents fundamental post-fault phasors can then be determined at the three ends of the system as:

$$[V'_{Pa,b,c}] = [X_{vpa,b,c}(\omega)] \quad (3.12)$$

$$[V'_{Qa,b,c}] = [X_{vqa,b,c}(\omega)] \quad (3.13)$$

$$[V'_{Ra,b,c}] = [X_{vra,b,c}(\omega)] \quad (3.14)$$

$$[I'_{Pa,b,c}] = [X_{ipa,b,c}(\omega)] \quad (3.15)$$

$$[I'_{Qa,b,c}] = [X_{iqa,b,c}(\omega)] \quad (3.16)$$

$$[I'_{Ra,b,c}] = [X_{ira,b,c}(\omega)] \quad (3.17)$$

Figure 3.6 shows the frequency response of the DFT filter used. An extensive series of studies has shown that the forementioned DFT technique is very effective in rejecting the high frequency components and provides good filtering of the low frequency components, particularly the DC component. However, in order to improve the algorithm accuracy, the first cycle of post-fault data is ignored, since the transients are most prominent during this period.

As mentioned before, the same DFT technique is used in the synchronisation process purely to determine the pre-fault phasors.

3.2.4 Superimposed Components Calculation

A fault occurrence on a transmission line can be considered as equivalent to superimposing a voltage at the point of fault which is equal and opposite to the pre-fault steady state voltage. The post-fault voltage and current components may be considered as made up of the pre-fault steady state components and fault injected components, as follows:

$$V_{post} = V_{pre} + \Delta V_f \qquad (3.18)$$

$$I_{post} = I_{pre} + \Delta I_f \qquad (3.19)$$

Superimposed components ΔV_f and ΔI_f are simply the difference between the total time variation of the signals and a projection of their steady state pre-fault values.

As mentioned earlier, the technique described herein is based on superimposed components. The difference between post-fault and pre-fault phasors is then given as:

$$[V''_{Pa,b,c}] = [V'_{Pa,b,c} - V_{Pa,b,c}] \quad (3.20)$$

$$[V''_{Qa,b,c}] = [V'_{Qa,b,c} - V_{Qa,b,c}] \quad (3.21)$$

$$[V''_{Ra,b,c}] = [V'_{Ra,b,c} - V_{ra,b,c}] \quad (3.22)$$

$$[I''_{Pa,b,c}] = [I'_{Pa,b,c} - I_{Pa,b,c}] \quad (3.23)$$

$$[I''_{Qa,b,c}] = [I'_{Qa,b,c} - I_{Qa,b,c}] \quad (3.24)$$

$$[I''_{Ra,b,c}] = [I'_{Ra,b,c} - I_{Ra,b,c}] \quad (3.25)$$

Again as mentioned before, the employment of superimposed components rather than total values gives added accuracy by virtue of the fact that errors caused by pre-fault loading are virtually eliminated.

3.2.5 Fault Classification

Fault classification is not an essential requisite for the process of fault distance calculation. It is, however, incorporated into the algorithm as an added feature since an identification of the type of fault and faulted phase(s) can facilitate the restoration and maintenance of the line.

As shown in the next section, the technique is based on modal values of voltages and currents rather than phase values. For some configurations, the choice of the appropriate mode (which can be either an Earth or any of the two Aerials), in terms of accuracy, very much depends upon the type of fault, or more specifically, whether the fault in question involves the ground or not. Although in practice, the latter can be very effectively achieved by monitoring the magnitude of the zero sequence current (which rises sharply for faults involving ground), nonetheless the technique described herein also provides a means for the appropriate mode selection.

The method developed here is based on a comparison between the superimposed and zero-sequence fundamental phasors of currents I''_a, I''_b, I''_c and I''_0 at an end and is summarised in reference [23]:

IF	THE FAULT IS:
(i)	
• $I''_b<kI''_a$ and $I''_c<kI''_a$	a to earth fault
• $I''_a<kI''_b$ and $I''_c<kI''_b$	b to earth fault
• $I''_a<kI''_c$ and $I''_b<KI''_c$	c to earth fault
(ii)	
• $I''_c<kI''_a$ and $I''_b \cong I''_a$ and	
- $I''_0>I_{min}$	a to b to earth
- otherwise	a to b
• $I''_a<kI''_b$ and $I''_c \cong I''_b$	
$-I''_0>I_{min}$	b to c to earth
-otherwise	b to c
• $I''_b<kI''_a$ and $I'_a \cong I''_c$	
$-I''_0>I_{min}$	a to c to earth
-otherwise	a to c
(iii)	
• $I''_a \cong I''_b \cong I''_c$	three-phase fault

k is the ratio of unfaulted to faulted phase current and depends upon system configuration. A series of results has shown that for the system studied here, k=0.3 gives correct fault classification for all fault types. In practice it is also necessary to apply a small

threshold I_{min} to the measurements owing to line unbalance, transducer, filtering errors, etc.

The same criteria is applied to all three ends P, Q and R and in every case studied, at least one end contained enough information for the routine to classify correctly the type of fault.

3.2.6 Modal Transformation

As mentioned before, the fault location developed here is based on modal components of voltages and currents rather than phase values as the former allows the three phase system to be treated like three single-phase circuits independent of each other, thus simplifying the calculations very considerably. Basically, the phase values are transformed into three uncoupled modes: an Earth mode and two Aerial modes, using the theory of natural modes [24].

A distributed parameter three-phase transmission line can be described in the frequency domain by the differential equations:

$$\frac{\partial^2 V}{\partial x^2} = [Z][Y]V \qquad (3.26)$$

$$\frac{\partial^2 I}{\partial x^2} = [Y][Z]I$$

Introducing the theory of natural modes, the phase variations are transformed as:

$$V = [Q]\ V_m$$
$$I = [S]\ I_m \qquad (3.27)$$

and the transmission line equations then become:

$$\frac{\partial^2 V_m}{\partial x^2} = [Q^{-1}][Z][Y][Q]\ V_m \qquad (3.28)$$

$$\frac{\partial^2 I_m}{\partial x^2} = [S^{-1}][Y][Z][S]\ I_m$$

The forementioned uncoupled modes are obtained simply by choosing the appropriate transformation matrices [Q] and [S] to diagonalise $[Q^{-1}][Z][Y][Q]$ and $[S^{-1}][Y][Z][S]$. Although for an unbalanced system, the transformation matrices [Q] and [S] are different, however, if perfect transposition is assumed, then they become identical and using Clerk's transformation are given by:

$$[Q] = [S] = \begin{bmatrix} 1 & 1 & 1 \\ 1 & 0 & -2 \\ 1 & -1 & 1 \end{bmatrix} \qquad (3.29)$$

Results have shown that this assumption of perfect line transposition does not add significantly to the inaccuracy. The error is well within the acceptable limits for most practical applications. The big advantage of the forementioned assumption is that the need to calculate the transformation matrices is obviated. More details about transposed and untransposed line eigenvalues and eigenvectors are given in Appendix A.

The forementioned is the approach adopted here, and equations (3.30) to (3.35) show the modal transformation for voltages and currents, using $[Q^{-1}]$ and $[S^{-1}]$, at all three ends P, Q and R:

$$[V''_{P1,2,3}] = [Q^{-1}][V''_{Pa,b,c}] \quad (3.30)$$

$$[V''_{Q1,2,3}] = [Q^{-1}][V''_{Qa,b,c}] \quad (3.31)$$

$$[V''_{R1,2,3}] = [Q^{-1}][V''_{Ra,b,c}] \quad (3.32)$$

$$[I''_{P1,2,3}] = [S^{-1}][I''_{Pa,b,c}] \quad (3.33)$$

$$[I''_{Q1,2,3}] = [S^{-1}][I''_{Qa,b,c}] \quad (3.34)$$

$$[I''_{R1,2,3}] = [S^{-1}][I''_{Ra,b,c}] \quad (3.35)$$

The modal propagation constants and surge impedances simply become functions of the sequence values of series

line impedances (Z_0, Z_1, Z_2) and shunt admittances (Y_0, Y_1, Y_2), as also explained in Appendix A. For an idealised transposed line they are given by:

$$\Gamma_1 = (Z_0 Y_0)^{1/2}$$
$$\Gamma_2 = \Gamma_3 = (Z_1 Y_1)^{1/2} \qquad (3.36)$$

$$Z_{01} = (Z_0/Y_0)^{1/2}$$
$$Z_{02} = Z_{03} = (Z_1/Y_1)^{1/2} \qquad (3.37)$$

3.2.7 Identification of the Faulted Leg

Since the fault location algorithm described here is based on designating the faulted leg end (amongst the three) as the reference end for the fault distance calculation, it is thus important to be able to correctly identify the faulted leg of the tee before determining the distance to fault.

Figure 3.7 shows the flowchart for the identification of the faulted leg. The technique is based on evaluating the voltages at the tee point from a knowledge of the post-fault current and voltage phasors at the three ends (using equations similar to (3.1) to (3.3)). Figure 3.3(b) shows the faulted model with superimposed modal components. With reference to the figure, if for example, the fault is on the leg PT, then the voltage attained at

the tee point using phasors at ends Q and R would be identical whereas that attained from end P would be very different, indicating that the faulted leg is PT. The other faulted legs can be similarly identified. If, however, there is no discernible difference in the voltages attained with data from all three ends, then it can be safely assumed that, if the fault is internal to the protected system, it is at the tee point itself.

Since the V_T quantities (V''_{TP}, V''_{TQ}, V''_{TR}) are complex numbers, a comparison amongst them are made in terms of distances in a complex plane xy. As can be seen from the example given in the Figure 3.8, the distance RQ (having mode 2 as reference) is near zero, but distances PR and PQ are very large, indicating that the faulted leg is PT. If, however, the three distances are close to zero the fault is at the tee point.

3.2.8 Fault Distance Calculation

The final step in the fault calculation technique is to ascertain accurately the actual distance of the fault from the faulted leg terminal. With reference to Figure 3.3(b) if, for example, the fault is on leg PT, then using two-port matrix relationship for the superimposed modal phasors, both the fault point and the tee point

phasors as functions of the phasors at the three ends are given as:

$$[V''_{Fk}] = \cosh(\Gamma_k \chi)\,[V''_{Pk}] - Z_{0k}\sinh(\Gamma_k \chi)\,[I''_{Pk}] \qquad (3.38)$$

$$[V''_{Fk}] = \cosh(\Gamma_k L_{Pk} - \Gamma_k \chi)\,[V''_{Tk}] + Z_{0k}\sinh(\Gamma_k L_{Pk} - \Gamma_k \chi)\,[I''_{PTk}] \qquad (3.39)$$

Where:

$$\begin{bmatrix} V''_{Tk} \\ I''_{QTk} \end{bmatrix} = \begin{bmatrix} \cosh(\Gamma_k L_Q) & -Z_{0k}\sinh(\Gamma_k L_Q) \\ -Y_{0k}\sinh(\Gamma_k L_Q) & \cosh(\Gamma_k L_Q) \end{bmatrix} \begin{bmatrix} V''_{Qk} \\ I''_{Qk} \end{bmatrix} \qquad (3.40)$$

$$\begin{bmatrix} V''_{Tk} \\ I''_{RTk} \end{bmatrix} = \begin{bmatrix} \cosh(\Gamma_k L_R) & -Z_{0k}\sinh(\Gamma_k L_R) \\ -Y_{0k}\sinh(\Gamma_k L_R) & \cosh(\Gamma_k L_R) \end{bmatrix} \begin{bmatrix} V''_{Rk} \\ I''_{Rk} \end{bmatrix} \qquad (3.41)$$

Also, the following relationship is valid at the tee point:

$$[I''_{PTk}] + [I''_{QTk}] + [I''_{RTk}] = 0 \qquad (3.42)$$

where

k = 1 for Earth mode, 2 and 3 for Aerial modes

Γ_k = modal propagation constant

$Z_{0k} = 1/Y_{0k}$ modal surge impedance

χ = fault distance

Manipulating equations (3.38) to (3.42), in order to obtain the fault distance yields:

$$[\chi_k] = arctanh[D_k/C_k]/\Gamma_k \qquad (3.43)$$

Where:

$$A_k = cosh(\Gamma_k L_Q) V''_{Qk} - Z_{0k} sinh(\Gamma_k L_Q) I''_{Qk}$$

$$B_k = -cosh(\Gamma_k L_Q) I''_{Qk} + Y_{0k} sinh(\Gamma_k L_R) V''_{Rk} - cosh(\Gamma_k L_R) I''_{Rk} + Y_{0k} sinh(\Gamma_k L_Q) V''_{Qk}$$

$$C_k = -Z_{0k} I''_{Pk} + A_k sinh(\Gamma_k L_P) - Z_{0k} B_k cosh(\Gamma_k L_P)$$

$$D_k = -V''_{Pk} + A_k cosh(\Gamma_k L_P) + Z_{0k} B_k sinh(\Gamma_k L_P)$$

Although the analysis shown on equations (3.38) to (3.43) are for faults on leg PT, however, the equations are different for faults on any of the other branches QT and RT. The algorithm is designed to take that into account.

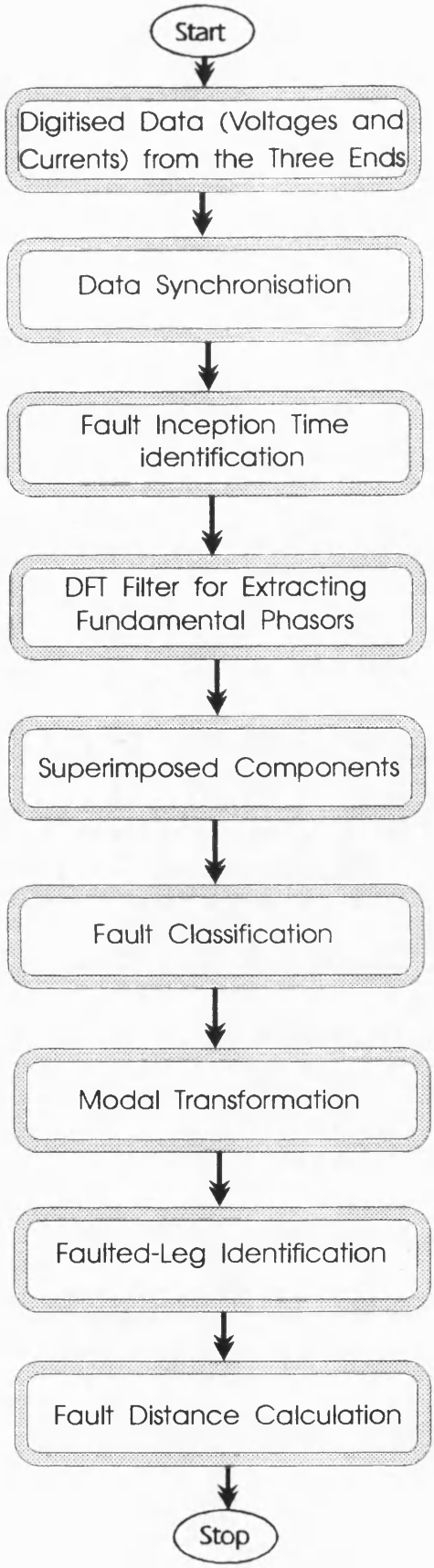

Figure 3.1 A block schematic of the fault locator algorithm

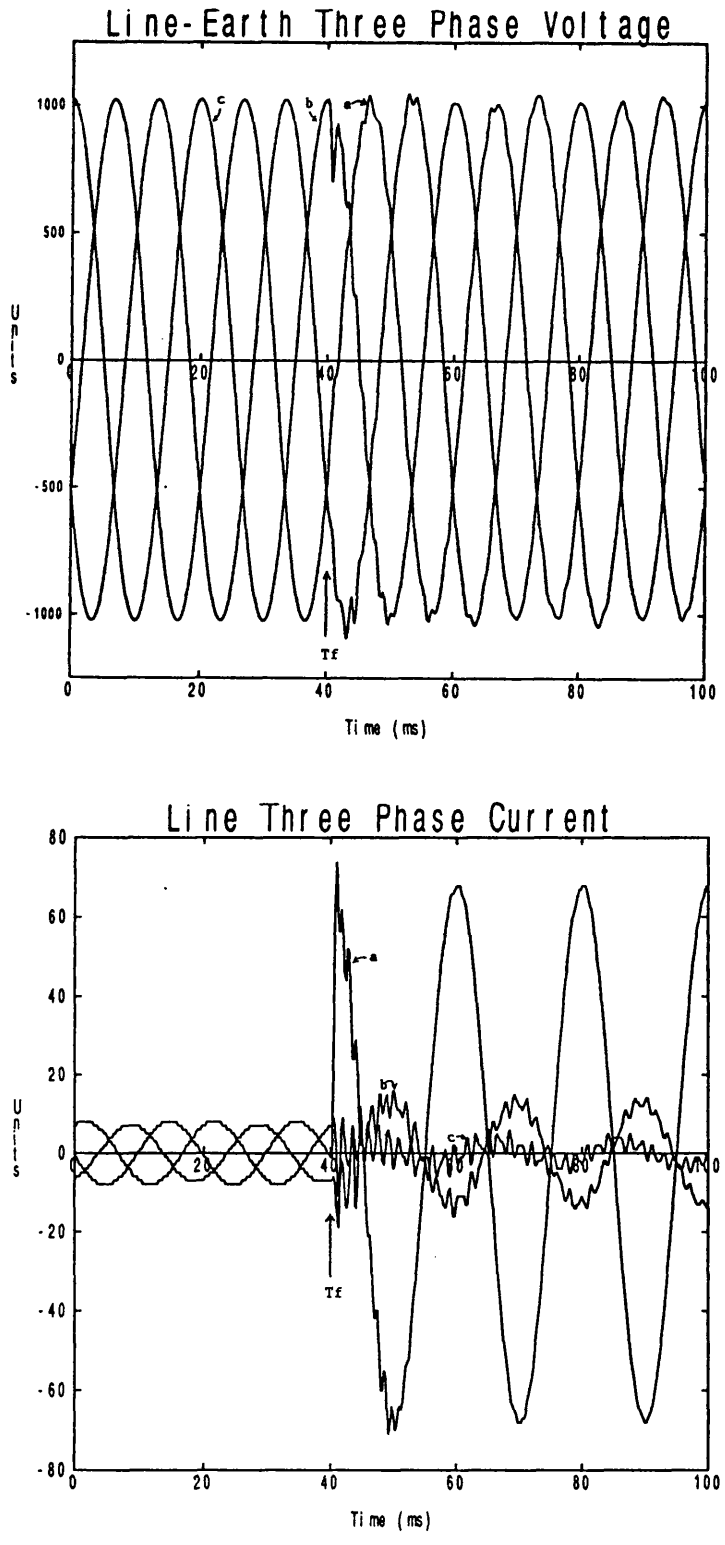

Figure 3.2 Typical voltage and current waveforms (a-earth fault at T-point in Figure 5.1(b) - seen by end P, Tf=fault inception time)

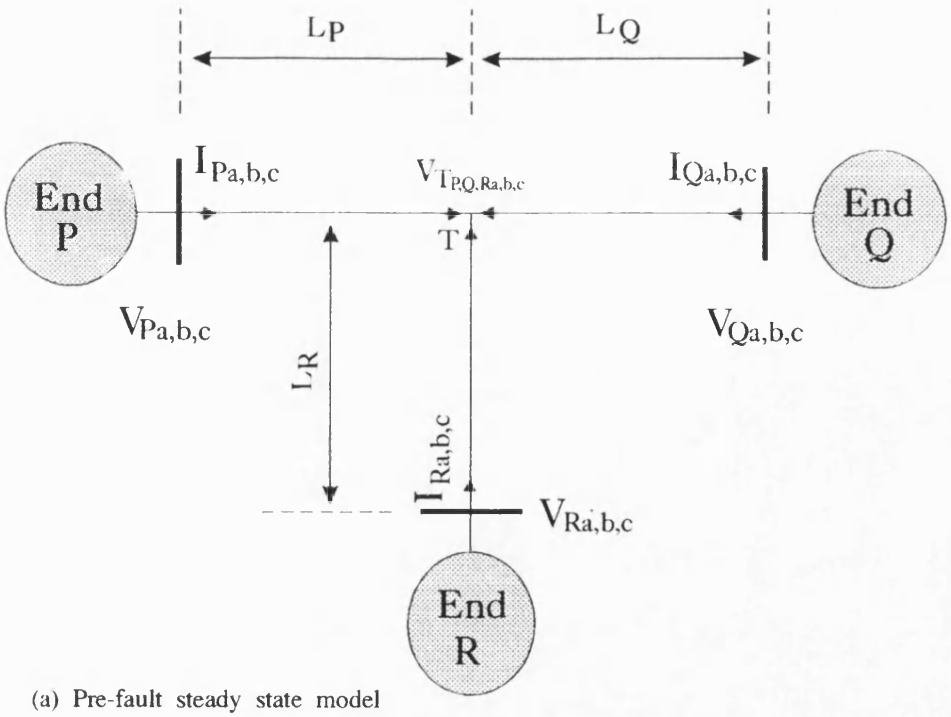

(a) Pre-fault steady state model

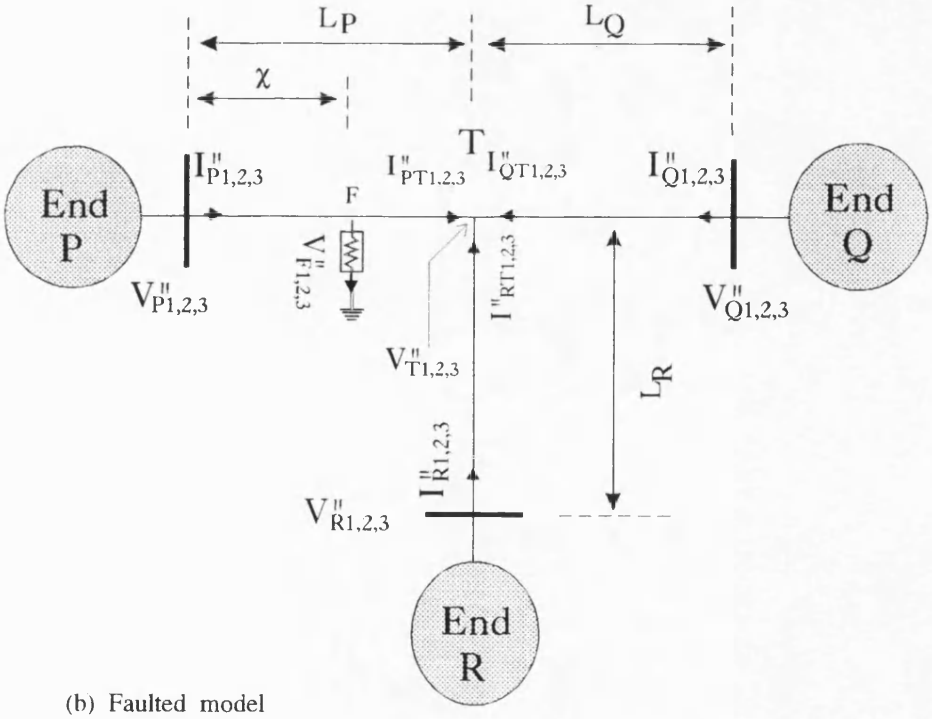

(b) Faulted model

Figure 3.3 Basic teed-feeder model

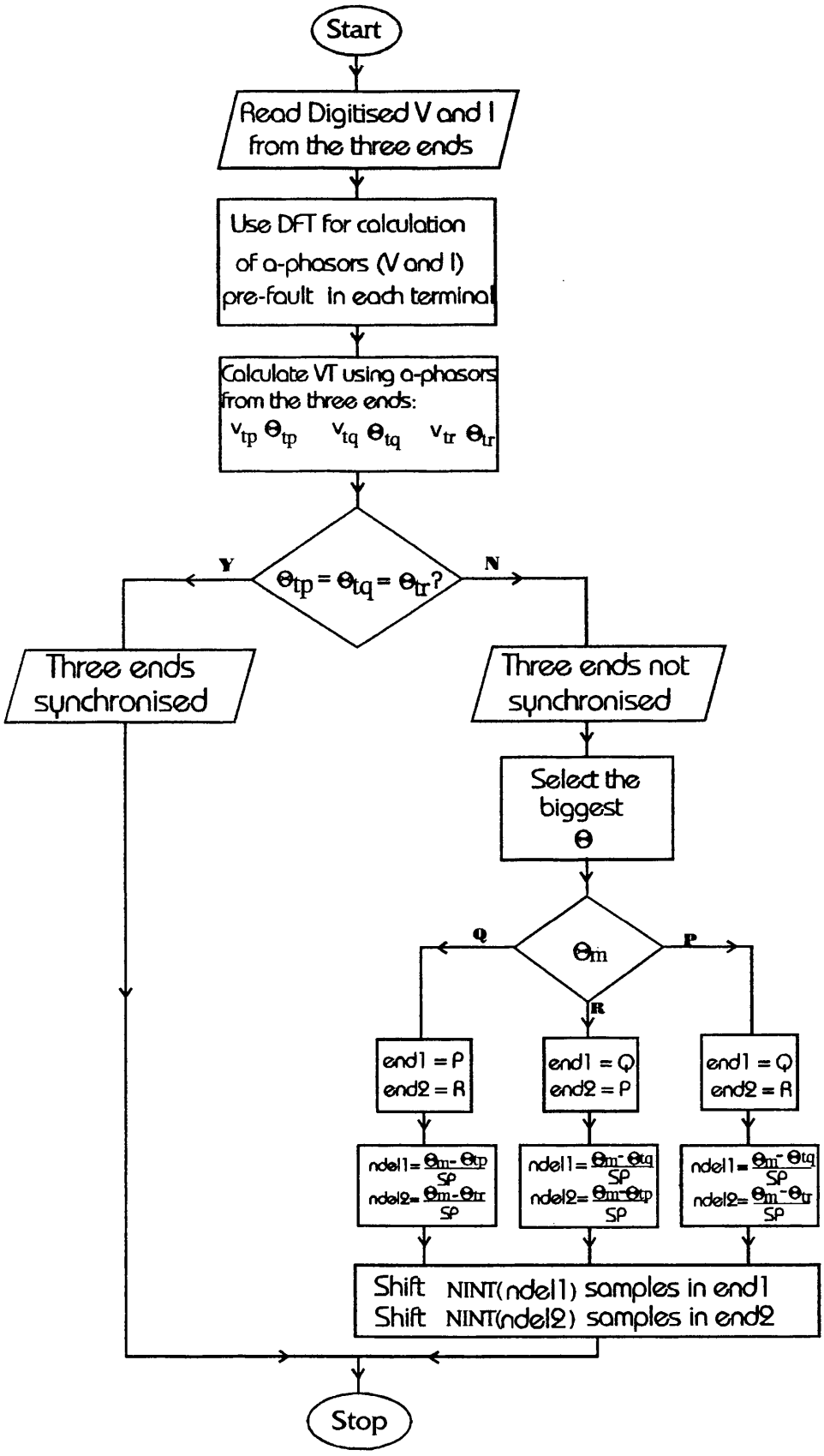

Figure 3.4 Flowchart for the synchronisation routine (SP-sampling interval, NINT(.)-round to nearest integer number)

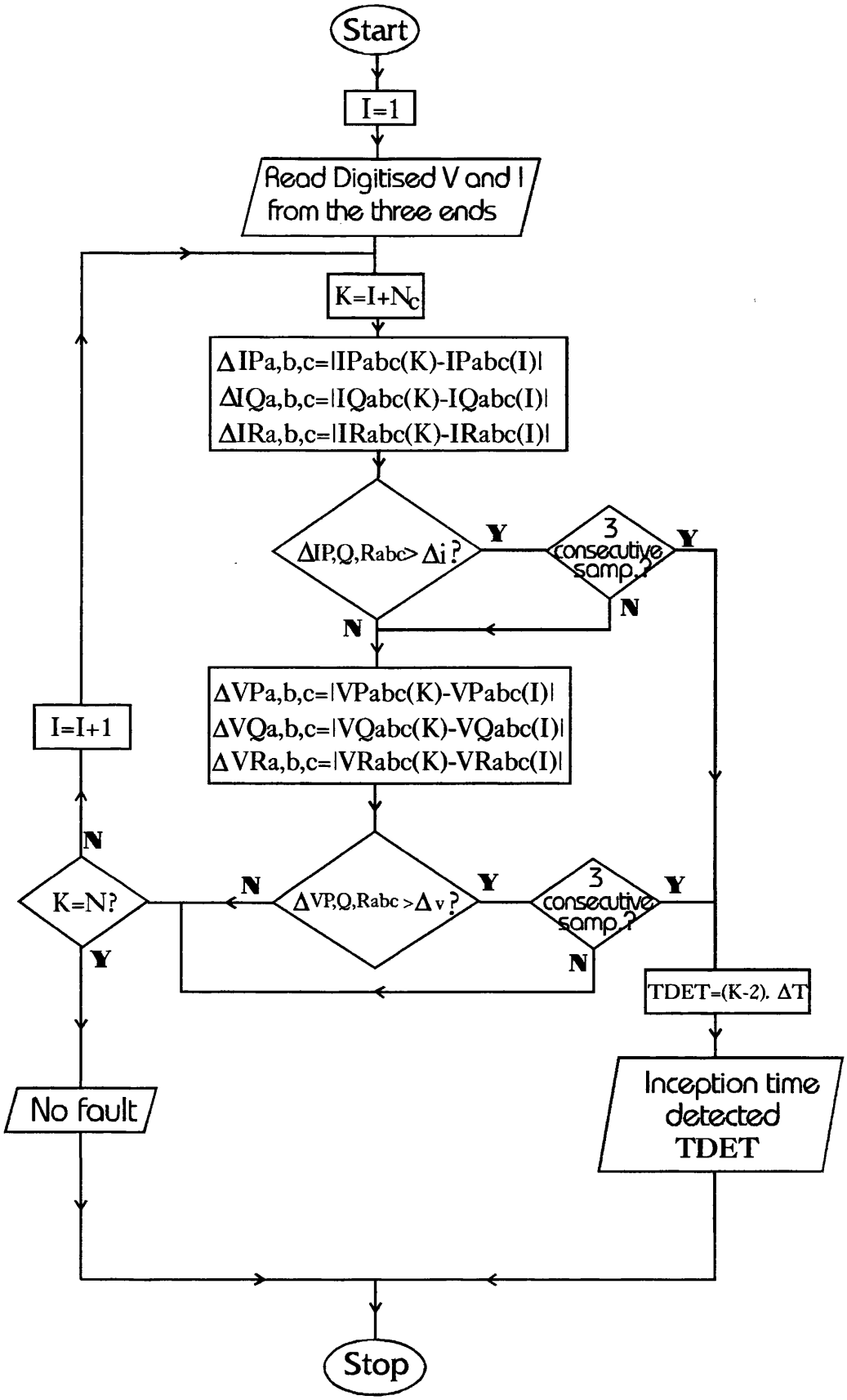

Figure 3.5 Flowchart for fault inception time identification

(N-total number of samples, Nc-number of samples in a cycle Δv, Δi-threshold level for V and I, ΔT-time interval)

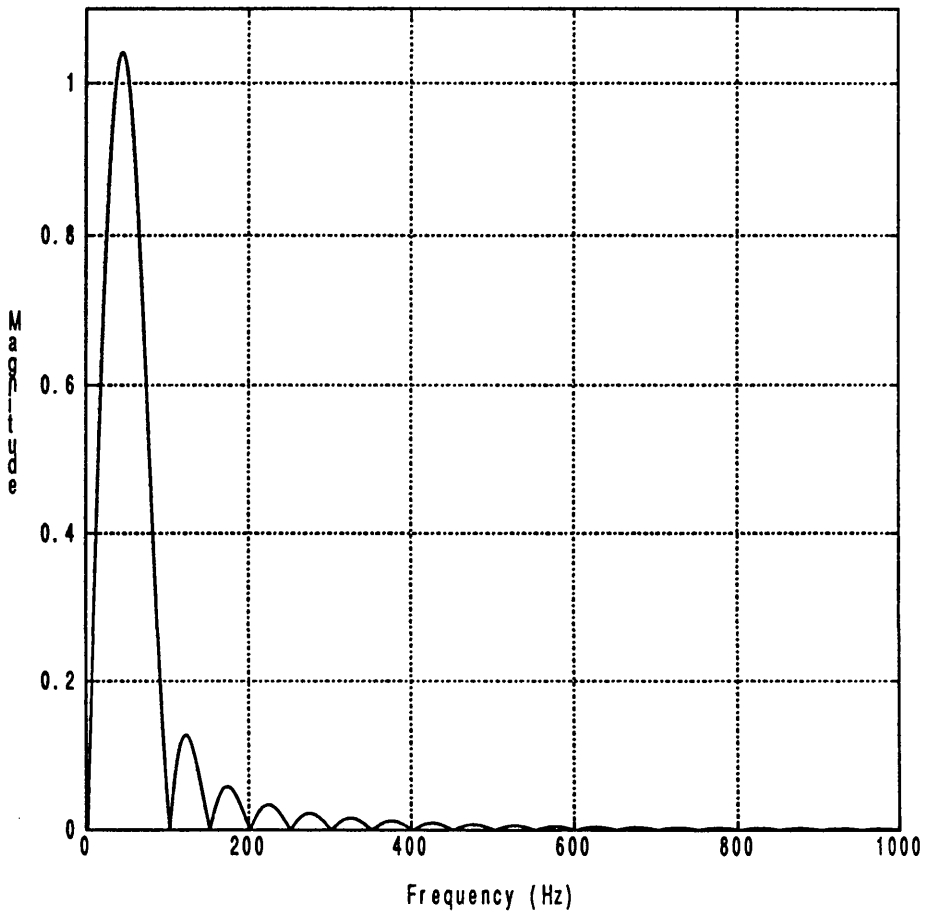

Figure 3.6 Fourier filter frequency response

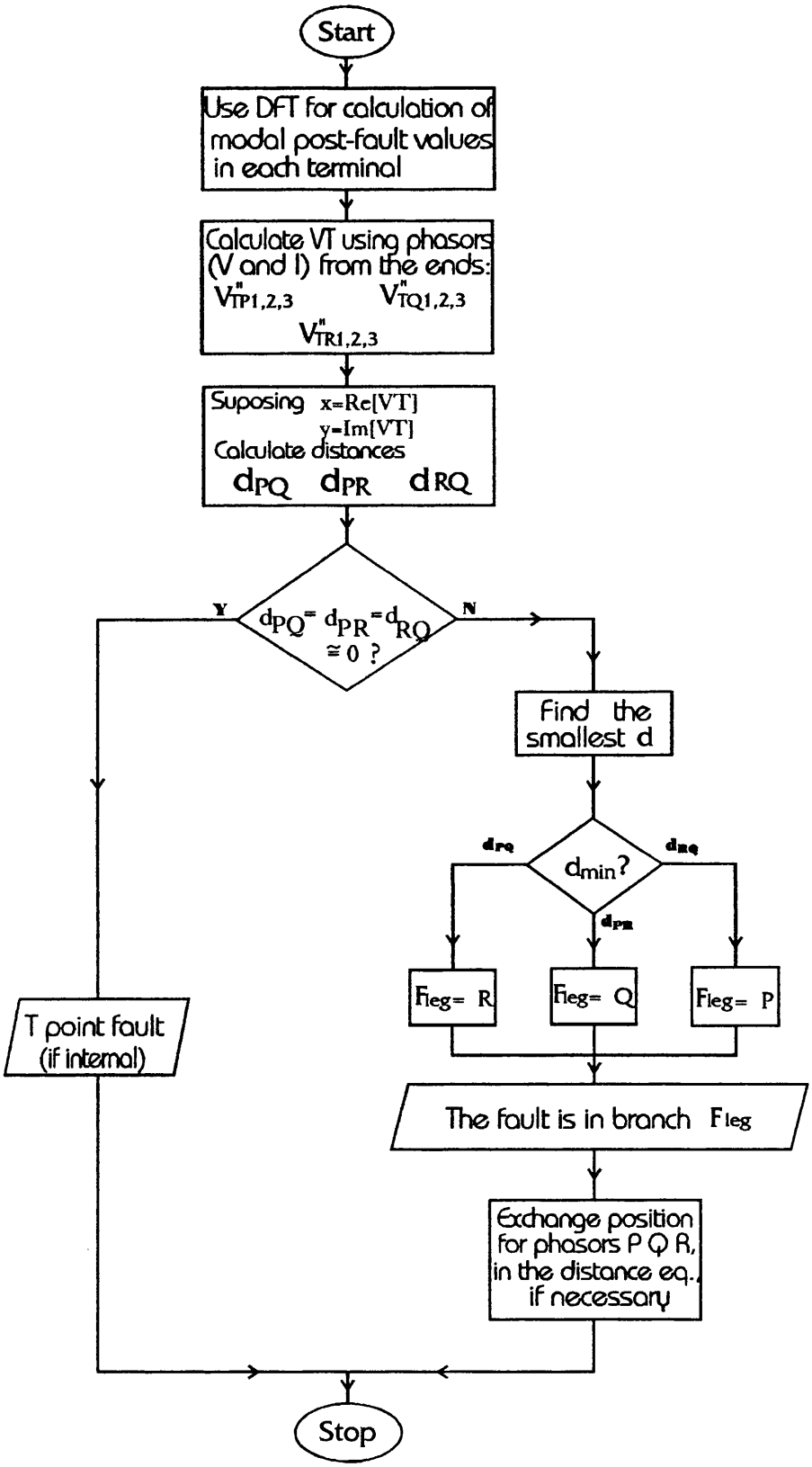

Figure 3.7 Flowchart for the identification of the faulted leg

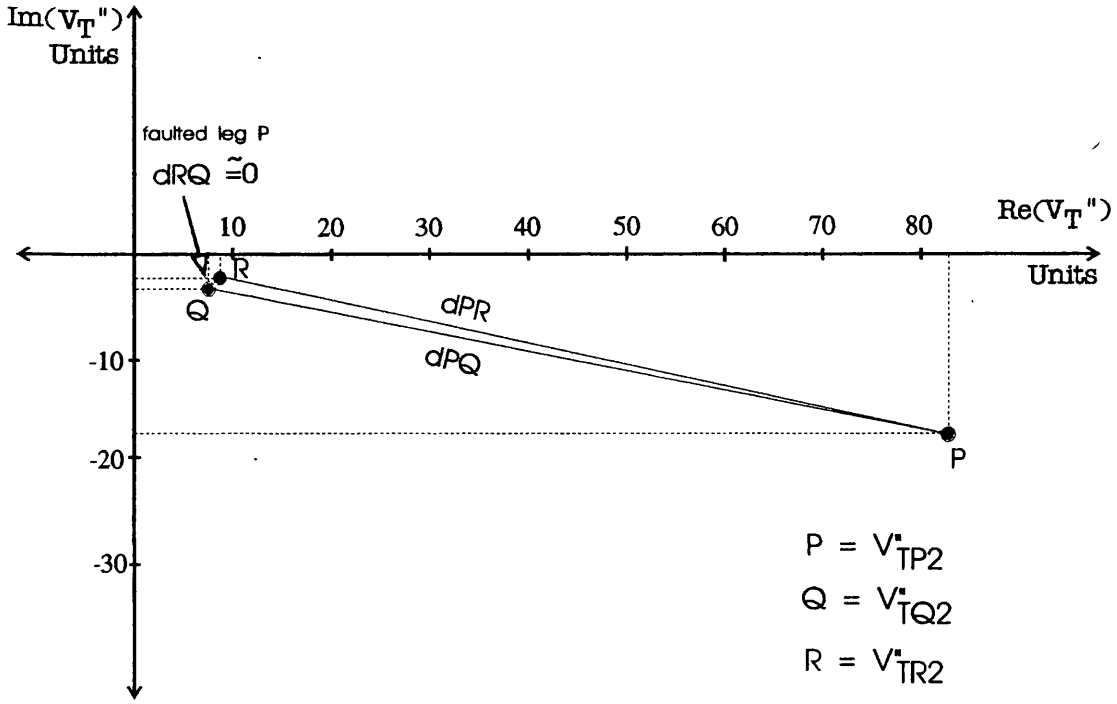

Figure 3.8 An example of the identification of the faulted leg (a-earth fault close to end P - Figure 5.1(a))

CHAPTER 4

PRACTICAL CONSIDERATIONS IN COMPUTER AIDED DESIGN

4.1 INTRODUCTION

It is vitally important that during the performance evaluation of the fault location techniques, the voltage and current waveforms presented to the algorithms are as close as possible to those experienced in practice. In this respect, off line digital simulation of such fault transient waveforms is considered as the most appropriate and economic method. A fault transient simulation package for three terminal lines, developed at University of Bath, is utilised for testing the proposed algorithm. It should be mentioned that although the fault location technique is based on Computer Aided Design (CAD) studies, however, practical considerations such as the effect of transducers, interface modules/analog filters, quantisation, etc, on primary system fault data are also included in the simulation so that the data processed through the algorithm is very close to that attained from actual fault recorders.

The complete fault locator scheme is as shown in Figure 4.1. It represents the various practical stages before the processing of the fault locator algorithm.

4.2 PRIMARY SYSTEM WAVEFORMS

As mentioned before, a fault transient simulation package for both two and three terminal transmission lines, has been developed at University of Bath, with the aim to derive precise current and voltage information of different EHV power system network configurations before and after the fault. A more detailed outline of the principles used in the simulation of the power system is given in Appendix B. In this simulation, modern transmission line theory is used to accurately predict the fault transient behaviour of three terminal EHV overhead lines. The programs are based on the solution of the wave equations using the Superposition and Thevenin theorems. Matrix analysis together with Inverse Fourier Transform techniques are used to transform the solutions from the frequency domain to time domain, in a form suitable for digital computation. The techniques consider the physical arrangement of the conductors, the characteristics of the conductors, the effect of earth return path and the effects of frequency dependant parameters. The various factors such as effect of fault type, differing source capacities at the three ends, unequal line lengths up to the tee point and feed around paths, which influence the transient phenomena, are considered.

The results of this simulation technique have been validated with actual field data. The computer modelling is essentially an extension of that described by Johns and Aggarwal [25] for two terminal lines.

The primary voltage and currents waveforms generated are related to some typical 400 kV and 500 kV three terminal line configurations. The simulation programs are run on a Mainframe computer at a sample rate of 4 kHz.

4.3 CVTs AND CTs

In any fault locator design based on CAD techniques, it is extremely important to take into account the effect of CTs and CVTs (as well as the interface modules/hardware effects) on primary systems waveforms as they can have a significant bearing on the accuracies attained and therefore on any inferences drawn concerning a particular fault locator technique. These effects are incorporated into the simulation via the impulse responses of the elements. Time Domain Convolution techniques based on impulse responses are then applied to the waveforms to produce the expected output.

The primary system waveforms are fed to CTs and CVTs to permit proper insulation level and current-carrying capacity in relays, fault recorders and other instruments. Conventional CVTs have a very low cut-off frequency typically of 600 Hz whereas the CTs have a much

wider bandwidth of typically 10 kHz. For this reason, for the CAD design, the CT is considered ideal. Figure 4.2, represents the frequency and impulse responses for the CVT, which have been generated from frequency tests carried out on practical models of the equipment.

4.4 DIGITAL FAULT RECORDER (DFR)

Disturbance recorders have been used by the power supply industry for many years to continuously monitor sections of power systems to provide a record of fault conditions. These recordings provide data prior to and following the fault incident, referred to as pre-fault and post-fault information. This enables engineering staff to look at conditions leading up to the fault, protection operation and how the control systems on the circuit responded, e.g. breaker operating times, protection carrier channels, etc [26]. There is a growing demand for power utilities world-wide to install fault recorders on power systems, as higher voltages and potential fault current levels have increased.

With the introduction of microprocessors, a new generation of disturbance recorders have been developed. These units offer significant benefits to the user in performance and features, not only presenting the information in a more convenient form, but also having the possibility of further data processing of the

forementioned waveforms. One of the most valuable data processing algorithm that can be implemented is the distance to fault calculation, as the type described in this thesis. As emphasized in the previous chapters, the latter is vital for reliable operation of networks.

4.4.1 Interface Modules

The first step in the DFR is the interface modules. It comprises input transformers for voltages and currents and low pass filters. The transformers convert the outputs from the main line CVTs and CTs into equivalent voltages ($\pm$ 10V). Low pass filters have to be employed to avoid aliasing in voltage and current measurements. A second order Butterworth filter with a cut-off frequency of 1.5 kHz is used, since the sampling frequency is fixed at 4 kHz.

For the CAD design, the voltage transformer is considered ideal, however, a current interface module (CIM) is employed to give a proportional voltage over a specified frequency range which is much less than 10 kHz. The frequency response of the CIM has been generated from tests from a practical model of the equipment whose block diagram and frequency responses are shown in Figure 4.3. The CIM comprises a transformer-reactor (transactor) core which has an air-gap of 5 mm. Since the transactor transfer function is an approximate differential function

plus a single pole, an integrating circuit which has a complementary zero is included in the CIM design. The combined circuit then produces a flat response to within ± 0.5 dB from 2.5 Hz to 1 kHz, as shown by the practical frequency response on Figure 4.3(b). This bandwidth does not impose any limitations on the method since fault current waveforms are generally dominated by low frequency components. Anti-aliasing filter, which is the second order low-pass Butterworth, is also included as part of the CIM [27].

Here again, the effect of interface modules is included via Time Domain Convolution techniques based on impulse responses applied to the waveforms from the main line CVTs and CTs.

4.4.2 Sampling and Analog to Digital Conversion

The three phase voltage and current signals are then fed to six sample and hold devices (4 kHz). The outputs from the devices are then passed through a multiplexer and the analog data is finally converted into binary data by a 12-bit A/D converter that is configured for bipolar analog inputs between ± 10 V.

The CAD technique applied herein takes into consideration the quantisation errors in the fault location process. The data is quantised to a 12-bit resolution before it is processed through the algorithm.

The $\pm 2^{11}$ conversion process leads to a quantisation level of approximately 4.8 mV.

4.4.3 Microcomputer

After the digitisation stage, the voltage and current data is acquired and stored in a circular buffer in the RAM memory before being printed, processed or transmitted.

Usually the microcomputer continuously scans the analog and digital units, storing the data, the oldest information being overwritten. When a fault condition arises, the recorders at all three ends are triggered almost simultaneously and the captured data, as said before, provides a number of cycles of both pre-fault and post-fault data. The data is then transferred to the printer/communications memory. A separate microcomputer can be used to access the printer memory and convert the data into a graphical form for printing. The data from remote ends is then transferred to the local end where the processing is done in order to deduce the distance to fault. Here, it is worth mentioning that unlike the communications requirements for protection schemes, those required for fault location of the type described here, are very modest. Very often manual medium such as disks or relatively simple and cheap automatic means such as a telephone line, suffice.

Figure 4.4 shows the effect of transducer/digital filtering on primary system waveforms. Figure 4.4(a) shows the primary system a-phase voltage and current waveforms (with one cycle pre-fault) for a a-earth fault at 25 Km from one of the ends on a unsymmetrical tee configuration (shown in the next chapter). Figure 4.4(b) shows the voltage and currents waveforms as the output of the DFR or input data into the fault locator algorithm. A comparison between them (Figure 4.4(a) and Figure 4.4(b), graph i) typifies the differences in simulated fault transient data before and after the forementioned transducer/hardware effects have been taken into account in the CAD design. An extensive series of studies have shown that the foregoing approach is justified and accurately emulates both transducer and hardware errors.

Although in practice, the transients in primary systems waveforms are attenuated by the transducers, low pass filters, etc, the waveforms as recorded by the fault recorders (graph i) can still contain quite significant transient components before they are processed through the fault locator algorithm; hence the necessity to employ special digital filtering techniques to reject them. In Figure 4.4(b) (graph ii) is also shown the output of the DFT filter, described in the previous chapter. It can be seen that the latter is very effective in rejecting the high frequency components.

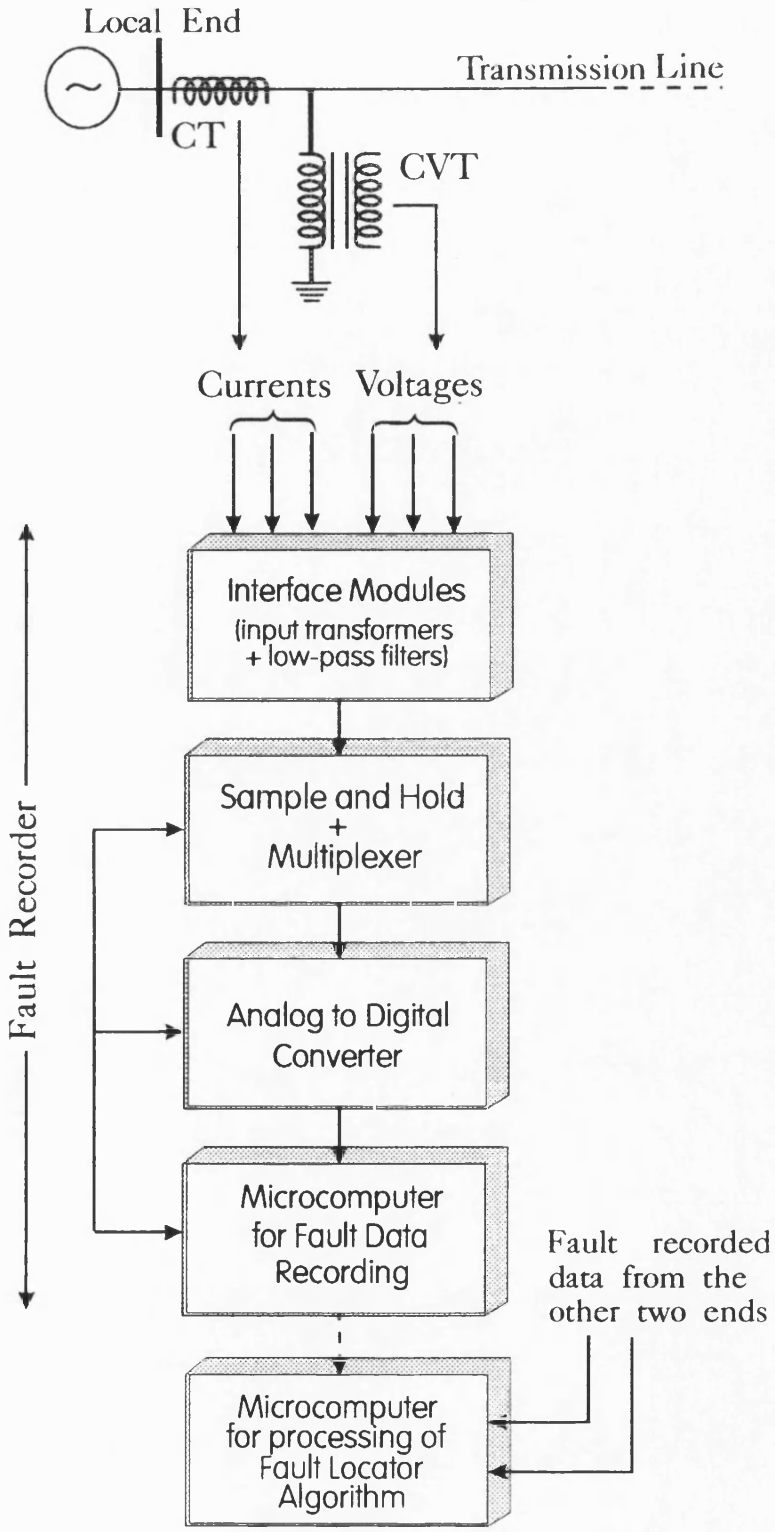

Figure 4.1 A block schematic of the complete fault locator scheme

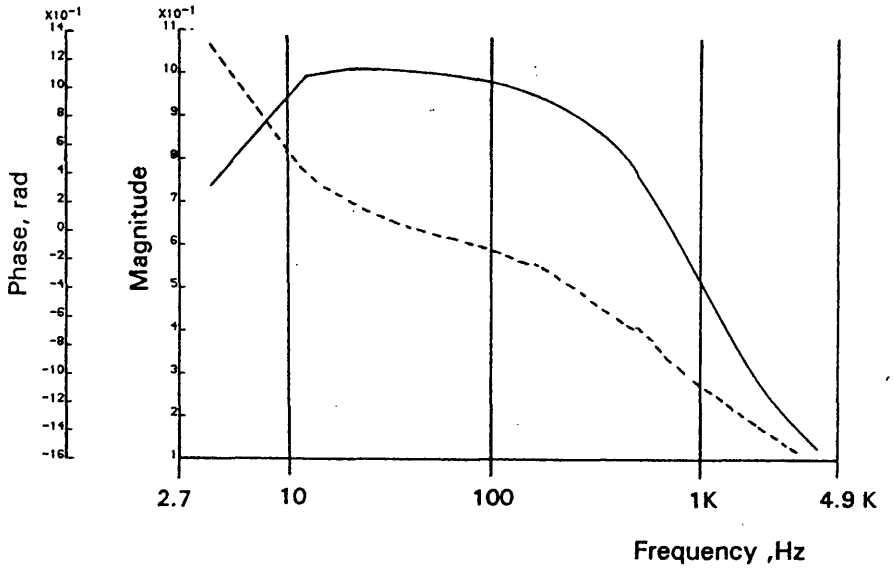

(a) Frequency Response

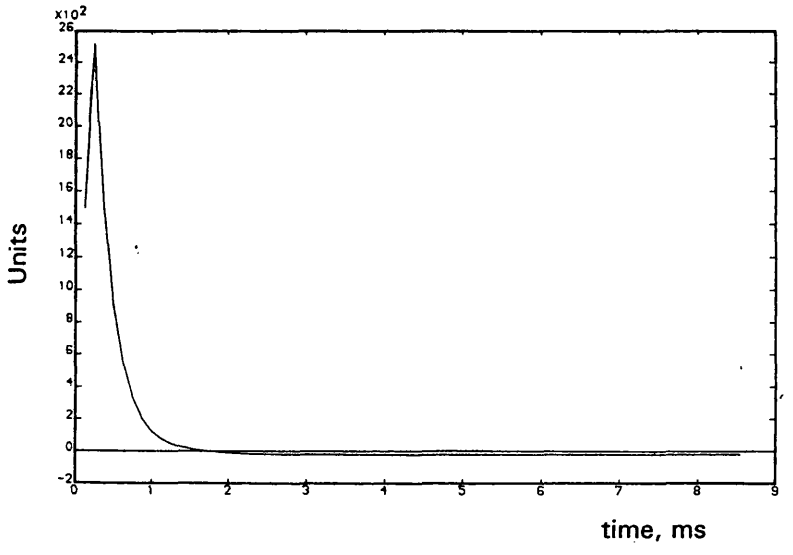

(b) Impulse Response

Figure 4.2 CVT frequency and impulse responses.

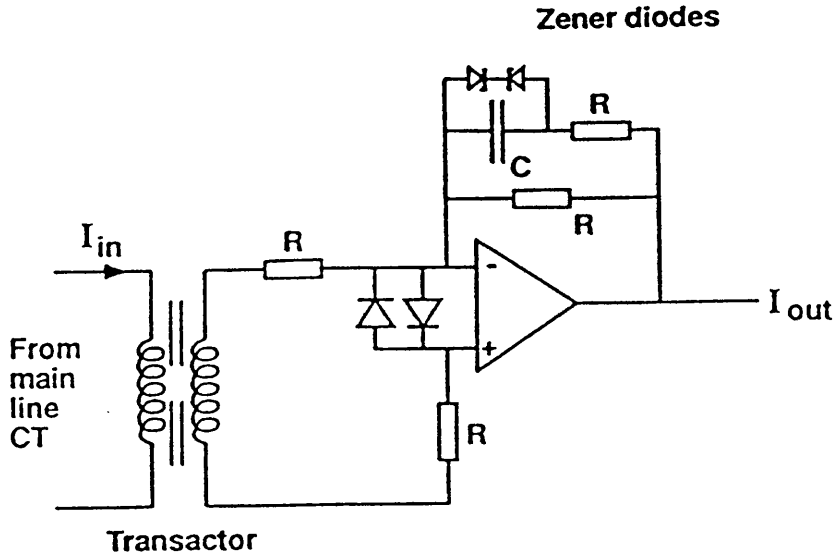

(a) Circuit Diagram

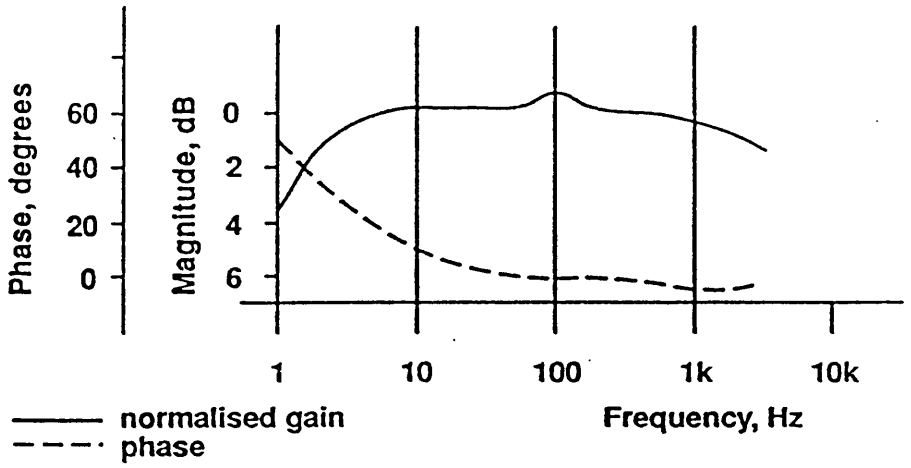

(b) Frequency Response

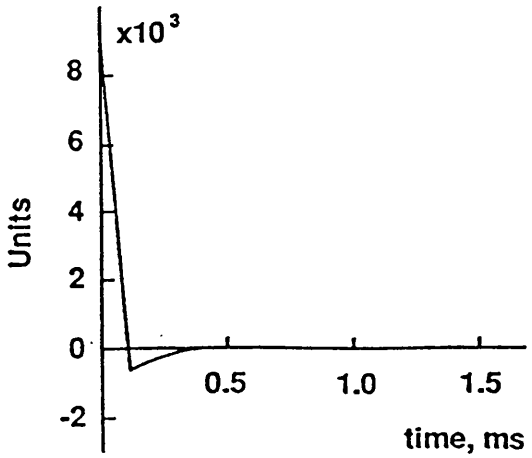

(c) Impulse Response

Figure 4.3 Current input module circuit and response.

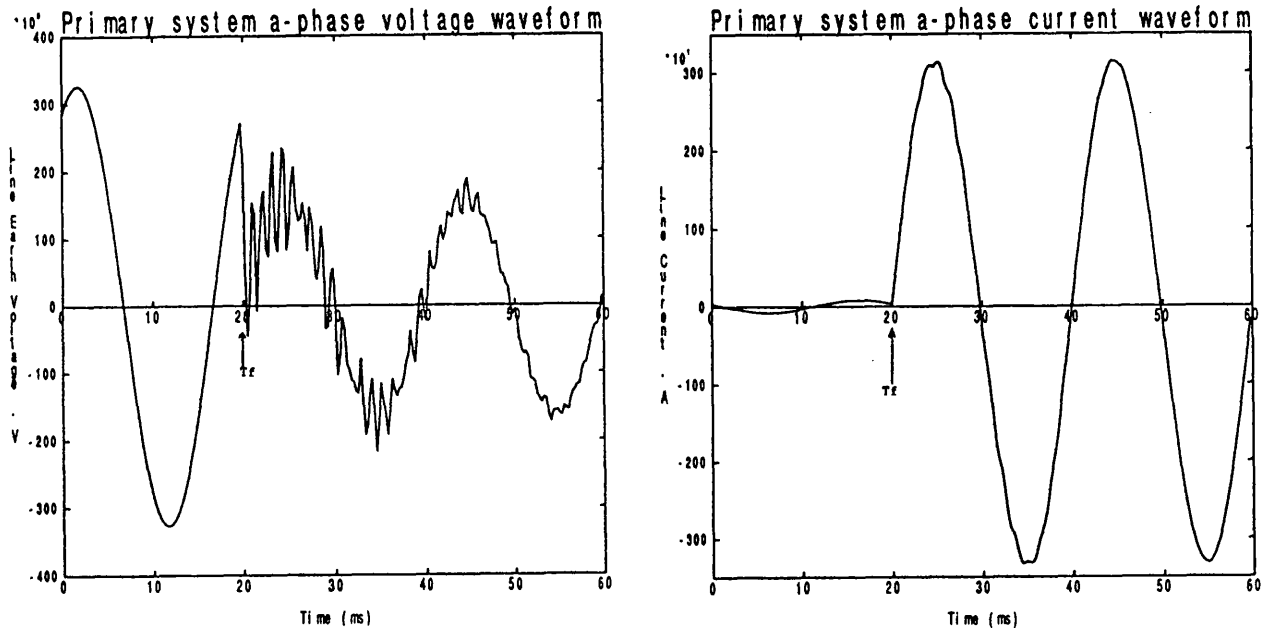

(a)

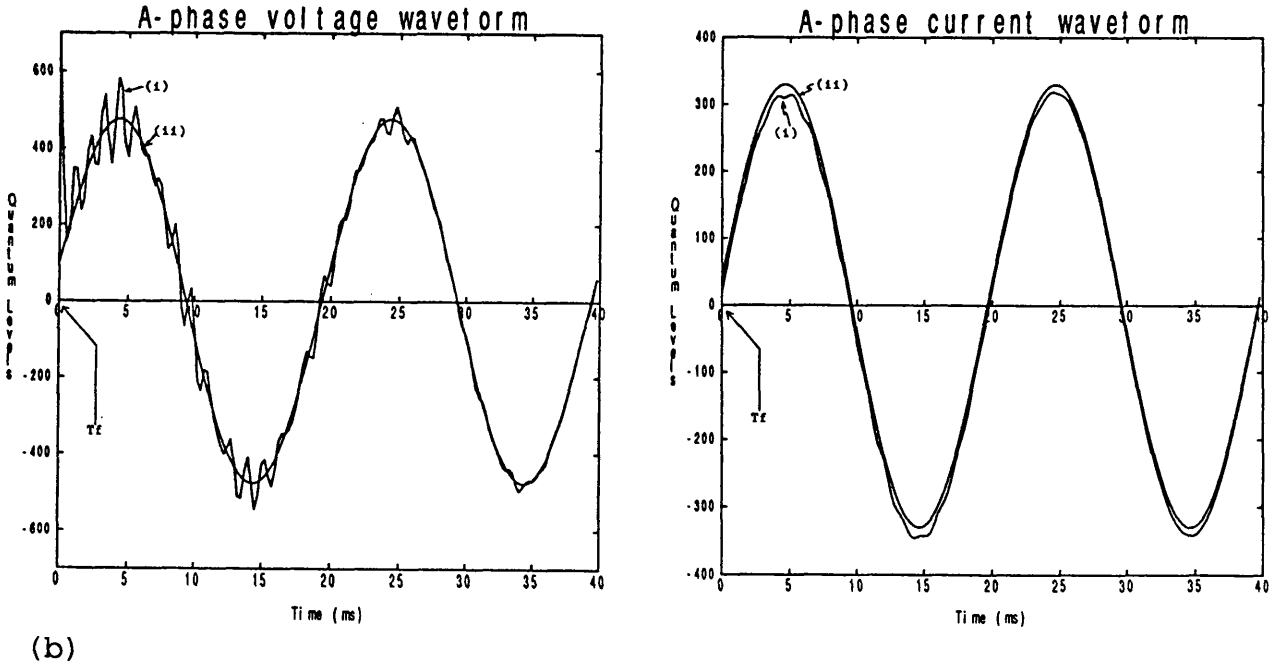

(b)

(i) input data into fault locator algorithm
(ii) output of the DFT filter

Figure 4.4 Effect of transducer/digital filtering on primary system waveforms (a-earth fault at 25 Km from end P on teed config. Figure 5.1(b), Tf=fault inception time)

CHAPTER 5

FAULT LOCATOR ALGORITHM TESTING

5.1 INTRODUCTION

In a complex power network, a multitude of possible circuit configurations can be expected with faults occurring at various positions on the teed circuit. It is by no means possible to demonstrate the fault locator performance for all the different circuit configurations. However, some typical configurations encountered in practice, shown in Figure 5.1 and 5.2, were chosen to show its performance. The first one is a symmetrical tee with equal lengths to the T-point and equal source capacity terminations. In order to demonstrate that the proposed algorithm also gives a reliable and accurate response for a more complicated system, a nonsymmetrical configuration with differing source capacities and line lengths up to the T-point is also presented. The effect of feed-around paths for both the symmetrical and nonsymmetrical systems, which are likely to pose some difficult problems, are also analysed. Finally, the performance of the proposed fault locator for double circuit tees is presented.

Results for different stages of the algorithm, which includes data synchronisation, DFT filtering, fault

classification, faulted leg identification, and fault distance calculation are presented. Although a very extensive series of studies were performed in order to fully test and ascertain the overall performance of the fault locator, however, for brevity only the main results and conclusions are presented here.

5.2 SYSTEM AND FAULT RECORDER INTERFACE MODULES SETTING PARAMETERS

5.2.1 Applications Considered

The results presented in this thesis relate to single and double circuit teed configurations as shown in Figure 5.1 and 5.2, which comprise typical 400 kV vertical construction lines of the type commonly encountered in the United Kingdom. A limited study is also presented for a typical single circuit 500 kV horizontal line commonly used in the USA. Details of the line construction are given in Figure 5.3. The relevant parameters used are:

(i) Earth resistivity (assumed homogeneous) = 100 Ωm

(ii) Source X/R ratio = 30

source sequence impedance ratio Z_{S0}/Z_{S1} = 0.5

(iii) Phase conductor = 4x54/7/0.33 s.c.a. with 0.305 bundle spacing (s.c.a. = steel core aluminium conductor)
earth wire = 54/7/0.33 s.c.a.

(iv) Nominal CVT and CT ratios = 400/0.11 and 2000/1, respectively.

5.2.2 Interface Modules Setting

5.2.2.1 Current Gain, K_i

The current gain is set so that there is no case where current clipping occurs at any end for internal faults. The latter requirement is met by first performing a simple steady state study to determine the maximum fault currents at the three terminals. For example, if for the configurations shown in Figure 5.1, the short circuit levels quoted are the respective absolute maximum levels, then the maximum possible through fault current would occur close to the ends for a solid three phase fault. This would give a maximum current through the CTs of approximately 20 kA. Thus, to ensure that the signals are kept within the ± 10 V range of linearity, K_i is set to the value of:

$$K_i = 10/(20000/2000) = 1.0 \text{ volts per secondary ámpère} \quad (5.1)$$

5.2.2.2 Voltage Gain, K_v

With a standard 63.5 RMS secondary CVT, the maximum input voltage to the voltage/voltage interface, allowing for an over-voltage factor of 2, is:

$$V_{ps} = [2 \times 63.5 \times \sqrt{2}] = 180 \text{ V}$$

To ensure linearity within the ± 10 V, the value of K_v is thus set to:

$$K_v = 10/180 = 0.056 \text{ volts per secondary volt} \qquad (5.3)$$

5.3 TESTING THE PROPOSED SCHEME

The algorithm is tested using the simulation package described in the previous chapter for a variety of conditions for the configurations shown in Figures 5.1 and 5.2. The results shown in this section are concerned with the different stages involved in the fault locating technique presented in Chapter 3.

5.3.1 Synchronisation of Data from the Three Ends

The synchronisation subroutine is the first step in the proposed algorithm. As underlined in Section 3.2.1, it is important to build into the algorithm a mechanism for data synchronisation before evaluating fault distances.

The tests were carried out having one end as a reference and a mismatch in data ranging from 1 to 10 samples respectively for the other two ends. This procedure was repeated by taking in turn each of the three ends as reference. An extensive series of studies have revealed that the data synchronisation subroutine performs to an extremely high degree of accuracy. It should be mentioned that after detecting the mismatch of data amongst the three ends, the subroutine shifts the appropriate number of samples of voltages and currents at each end in order to minimise errors due to nonsynchronisation.

The effect of unsynchronisation on measurement accuracy, in the absence of data synchronisation technique, is discussed in some detail in the next Chapter.

5.3.2 Fault Inception Time Identification

Figure 5.4 shows the current and voltage waveforms on the faulted phase for an a-earth fault at 1 Km from end Q (seen by end Q) for the system shown in Figure 5.1(b), along with the pre-fault waveforms one cycle prior to the fault. As explained in Section 3.2.2, the fault inception time identification is based on changes in magnitude and/or phase angle of the samples of voltages and currents when compared with the previous cycle. Figure 5.4 shows clearly the changes in magnitude in relation to the pre-fault waveform. In this case, the fault inception is detected after one sample at end Q. On the other hand, a phase earth fault at 50 Km from P is detected 2 samples after fault inception at end P. It is also noticed that the fault inception identification is independent of the type of fault. It should be mentioned that it is not always possible to detect the fault inception time at the precise instant the actual fault occurs. However, an extensive series of studies have shown that the maximum delay in the detection of fault inception time is always 4 samples or less. As far as the algorithm is concerned, this delay is of no consequence on the measurement accuracy.

5.3.3 DFT Filter

Figure 5.5 to 5.7 show the voltage and current waveforms before and after the DFT filter is applied for an a-earth fault at 1 Km from end Q on teed configuration shown on Figure 5.1(b), seen by ends P, Q and R respectively. The figures show the waveforms immediately after fault inception.

Figure 5.8 to 5.10 show a double phase (a-b) fault at the same position and for the same configuration considered above, again seen by ends P, Q and R respectively. In both cases, the fault inception angle is 90° with reference to the a-phase voltage waveform.

It can be seen that the filtering technique proposed is very effective in the extraction of the fundamental frequency component from post fault data.

5.3.4 Fault Classification

As mentioned before (Section 3.2.5), the method for fault classification is based on a comparison between the superimposed and zero-sequence fundamental current phasors for the phases a, b, c and the zero component. Figures 5.11 to 5.14 show the results for the fault classification subroutine for the different types of fault at different locations on leg PT of configuration

shown in Figure 5.1(b). The values for the phasors $I"_a$, $I"_b$, $I"_c$ and $I"_0$ are normalised to the phase that has the largest phasor value. Thus using the factor K=0.3, as described in Section 3.2.5, phasors smaller than 0.3 are considered to be healthy and the phasors greater than 0.7 are considered to be faulted. The decision whether the fault involves ground or not, is made based on the existence of the zero sequence component. Again, as mentioned before, a small threshold I_{min}=0.1 is necessary to be applied so as to cater for measurement errors due to line unbalance, filtering errors, etc.

The tests were carried out for faults on configurations shown in Figure 5.1 and 5.2 and an extensive series of different fault conditions studied showed that the fault classification subroutine was able to correctly classify the type of fault for all the cases.

5.3.5 Identification of the Faulted Leg

The identification of the faulted leg is performed after the phase quantities have been transformed into modal components. As described in Section 3.2.7, the method of identification of the faulted leg is based on a comparison of the values d_{PQ}, d_{PR} and d_{QR} in a complex plane xy. Figures 5.15 to 5.18 show the results for the faulted leg identification subroutine for the

unsymmetrical teed configuration represented in Figure 5.1(b). Figures 5.15 and 5.16 represent the identification of the faulted leg PT for an phase-earth fault and a double phase to earth fault respectively, at different fault positions. As explained before, the near zero value identifies the faulted leg. In these two cases $d_{QR} \cong 0$ indicates that the faulted leg is PT. Figure 5.17 shows the identification of the faulted leg RT for a three phase-earth fault on the same configuration, for different fault positions. This time $d_{PQ} \cong 0$ indicates that the fault is on leg RT. It is important to note that for a fault at 100 Km from R end, i.e. T-point, the values $d_{PQ}=d_{PR}=d_{QR} \cong 0$, confirming that the fault is at the T-point itself.

Figure 5.18 shows the identification of the faulted leg QT (double-phase fault) for the same unsymmetrical configuration. It is worth mentioning that leg QT (10 Km) is much shorter than the other two legs PT and RT (each 100 Km). This effectively means that although the values d_{PR} (for a fault on leg QT) comes out to be greater than zero, however, its magnitude when compared to values d_{PQ} and d_{PR} is still very significantly smaller and the correct decision concerning the faulted leg is still retained.

Again, an extensive series of tests involving different fault positions were performed on the configurations shown on Figures 5.1 and 5.2 and the

results showed that the algorithm identified the faulted leg correctly for all fault cases studied.

5.3.6 Fault Distance Calculation

Having identified the faulted leg, the fault distance calculation part of the algorithm is then finally executed. The error for this calculation is expressed as a percentage of the length of a particular leg of the tee and is given as:

$$\% \text{ error} = \frac{(\text{estimated location} - \text{actual location})}{\text{length of the leg of tee}} \times 100 \quad (5.4)$$

For the results presented in this section the % error in the fault distance calculation is usually plotted against actual fault distance expressed as a percentage of the faulted line length, for a variety of different systems and fault conditions. In the majority of cases, results for faults on all the three legs of the system are represented in the same figure using, as said before, the faulted leg end as reference for the distances estimated. Effect on measurements accuracy due, for example, to such factors as type of fault, transposed and untransposed lines, feed around path, etc is analysed for the teed configurations shown in Figures 5.1 and 5.2.

5.3.6.1 Faults on a Symmetrical Tee

The performance of the fault locator proposed is discussed in this section for a symmetrical tee, i.e. equal line lengths up to the T-point. Figures 5.19 to 5.23 typifies the results attained for different types of fault on the symmetrical teed configuration shown in Figure 5.1(a), based on a 400 kV vertical construction single-circuit line of the type described in Figure 5.3(a).

(a) Type of Mode Selection

Figures 5.19 and 5.20 show the fault location error (modes 1, 2 and 3) for the symmetrical and transposed teed configuration, considering an a-earth fault and a-b-earth fault respectively. Figure 5.21 and 5.22 show the same situation for the same system, but considering the lines untransposed. It should be mentioned that the performance considering the three different legs PT, QT and RT are absolutely identical, which makes the curves relating to them in the Figures 5.19 to 5.23 to be coincidental.

Considering faults involving earth, it is thus apparent that a higher degree of accuracy is attained when using Earth-mode (mode 1) based signals rather than the two Aerial modes (modes 2 and 3). A series of studies

have shown that this is always the case for single-circuit vertical construction lines (including the unsymmetrical tee presented in the next section). It is generally found that the asymmetry associated with vertical construction lines manifests itself into causing larger errors when utilising Aerial-mode rather than Earth-mode based signals.

It should be mentioned that for faults clear of ground or three phase faults, fault location has to be based on Aerial modes due to the absence of the Earth mode for such faults. This effectively means that in the forementioned applications the fault locating algorithm would be applied to all three modes, the presence of a significant level of residual current being used to identify the existence of a fault involving earth. The latter is obtained from the fault classification subroutine.

(b) Line Transposition

The transformation matrices [Q] and [S], used in the algorithm for obtaining the modal values, can be evaluated at power frequency for any configuration from a knowledge of the line geometry. This would include the effects of line untransposition. However, as mentioned in Chapter 3, in order to considerably simplify the processing, perfect line transposition has been assumed

when setting the parameters into the fault locator described herein. In this case, irrespective of the line geometry, the transformation matrices take the simplified form given in equation (3.29) (Chapter 3) for any transmission line configuration. It is thus important to ascertain as to what extent the accuracy for faults on untransposed lines is affected by this assumption.

Comparing Figure 5.19 and 5.20 with Figure 5.21 and 5.22 which are for transposed and untransposed lines respectively, both with assumed transposed parameters, it is apparent that there is a small improvement (considering the earth mode) in the measurement accuracy attained for the transposed case. This would be expected for the reasons stated above, but the important point to note is that the accuracy is not unduly affected by untransposition. As said before, the error is well within the acceptable limits for most applications. Another example is given in the next section for the unsymmetrical tee configuration.

(c) Type of Fault

Figure 5.23 shows a comparison of the accuracies attained for different types of faults on the symmetrical tee configuration with untransposed lines (Figure 5.1(a)). First of all, it is worth mentioning that in

general, the maximum error is attained for faults close to ends P, Q and R for all types of fault.

When comparing faults involving earth, it is apparent from Figure 5.23 that the error for multi-phase earth faults is greater than that for the corresponding single-phase-earth faults. The error tends to be accentuated for three phase and pure phase-phase faults, the maximum error attained for the latter being approximately 1.5 % for a close-up fault. The Earth modes were chosen for faults involving earth and Aerial modes for the others.

For the extensive series of tests realised, with different configurations, the best accuracies were always found for single-phase to earth faults when compared to other types. It should be mentioned that phase earth are the most common type of faults which can occur on a transmission line in practice.

For untransposed lines of the type described in this section, similar types of faults on different phases give slightly different measurement accuracies. However, results showed that the differences in accuracies attained for the three phases were less than about 0.5% of each other for all types of fault. For brevity only the a-earth, a-b and a-b-earth were chosen to be presented in this chapter.

(d) Nonsymmetrical Source Capacities

Figures 5.24 to 5.26 show the accuracy for a untransposed symmetrical system of the type shown in Figure 5.1(a) with the source capacity at end R dropping from 20 GVA to 5 GVA. It is interesting to note that the performance for the three different legs are no longer identical for that case. Comparing Figure 5.24 with 5.23 for an a-earth fault, it is apparent that the accuracy attained for the leg RT is much worse than for the case with symmetrical sources and that the accuracies attained for the legs PT and QT remain roughly the same.

Figures 5.25 and 5.26 show the accuracy for the system with different source capacities at end R for an a-b fault and three-phase fault respectively. Again the performance for leg RT is much worse than for the other two. It can be also seen that, as mentioned in the previous section, the algorithm gives the best performance for an a-earth fault when compared with the other types.

Studies have shown that the difference in performance attained for leg RT is not only due to the asymmetry caused by a reduction in the source capacity, but also by the fact that RT is now connected to a weaker source. These two factors will cause a deterioration in the algorithm performance for that particular leg. The effect

of source capacity is further discussed in the next chapter.

5.3.6.2 Faults on an Unsymmetrical Tee

The performance of the fault locator discussed in the previous section has been in relation to a symmetrical tee. Although this type of system is one amongst a large number of different tee configurations encountered in practice, it nevertheless very usefully illustrates some of the salient features of the locator, particularly in its ability to retain a high degree of accuracy under a number of different practical situations. However, it is also vitally important to examine the performance for an unsymmetrical tee since very often a major cause of error is due to the unequal lengths of a teed feeder. Figures 5.27 to 5.30 typify the performance of the locator for faults on a teed configuration of the type shown in Figure 5.1(b).

Figures 5.27 and 5.28 show the results attained for an a-earth fault on the unsymmetrical teed configuration, based on a 400 kV vertical construction single-circuit line of the type shown in Figure 5.3(a) for a transposed and untransposed line respectively. The effect of untransposition for a unsymmetrical system can be observed comparing the two cases. It is also apparent from the Figures that the percentage error for the

unsymmetrical system is greater than that attained for the symmetrical system considered previously, under similar faults. The unsymmetrical tee performance can be attributed to a significant increase in unbalance caused by the unequal lengths of the tee. In teed circuits, the degree of unbalance due to untransposition very much depends on the level of asymmetry i.e. on line lengths relative to each other and its effect on accuracy attained is then shown. The Figures also show that the worst performance is attained for faults on leg QT which is substantially shorter than the other two. Figure 5.29 shows the performance for an untransposed and unsymmetrical system for an a-b fault. As expected, the algorithm accuracy attained for this type of fault is worse than that attained to an a-earth fault and this can be attributed to the fact that aerial modes signals have to be used for the former.

It should be mentioned that although the teed circuit has some line loading, however, this is of little consequence as far as the measurement accuracy is concerned, since the employment of superimposed rather than total components of modal signals virtually eliminates any errors caused by line loading.

(a) Horizontal Construction

Although 400 kV vertical construction lines are commonly encountered in the United Kingdom, 500 kV horizontal construction lines of the type described in Figure 5.3(b) are also quite common in other parts of the world. It is thus important to examine the performance of the algorithm for faults on such configurations. Figure 5.30 typifies the accuracy for the unsymmetrical configuration presented in Figure 5.1(b) for an a-earth fault on an untransposed single-circuit horizontal line using transposed line parameters. It is evident that the degree of accuracy attained for such lines is higher than that for the vertical construction, as shown in Figure 5.28. An extensive series of studies have shown that this is always the case for all types of fault and is essentially due to the greater symmetry associated with the former.

5.3.6.3 The Effect of a Feed-Around Path

In teed circuits, it is fairly common to have tenuous feed-around paths as shown in Figure 5.1(c) and 5.1(d).

For certain internal fault conditions, a feed around path can result in an over-distance calculation, particularly in conventional impedance measurement techniques and this is particularly so in unsymmetrical

teed configurations of the type shown in Figure 5.1(d). Considering the teed circuit configuration shown in Figure 5.1(d), simulation studies shown that there is a reversal in the polarity of the phase current at end R only, as the fault, which is an a-earth fault at voltage maximum, moves from the T-point to a location close to end P. This is due to the current fed to end R via the feed-around path becoming stronger as the fault moves closer to end P [27]. This effect is illustrated in Appendix B.

Figures 5.31 and 5.32 show the accuracies for the circuits in the presence of the feed-around path for an a-earth fault. Figure 5.31 typifies the results attained for the symmetrical configuration with feed-around path as shown in Figure 5.1(c) on an untransposed single-circuit vertical line . Figure 5.32 show the accuracy for an unsymmetrical configuration with feed-around path, as shown in Figure 5.1(d), also for the vertical construction. Comparing Figure 5.31 with Figure 5.24 and Figure 5.32 with 5.28, it can be seen that the fault locator algorithm described here interestingly gives a performance that is better than that attained in the absence of an outfeed, particularly for faults on the legs PT and RT which are the two legs connected via the outfeed.

5.3.6.4 Faults on a Double Circuit Line

The fault locator algorithm of the type described in this thesis is general and, therefore, can be used for any multi-phase system, including a double circuit line. It is normal practice in double circuit lines to assume that there is a fault locator working independently on each of them. However, it is important to ascertain how the mutual coupling between the two circuits, for a fault on one circuit, would affect the measurement accuracies attained.

The performance of the fault locator is presented, in the next two sections, for the configurations shown in Figure 5.2(a) and 5.2(b) for a 400 kV vertical construction double circuit line of the type shown in Figure 5.3(c). The lines are untransposed and assumed transposed parameters are used.

(a) Type of Mode Selection

Figures 5.33 to 5.36 present the accuracy for the double circuit of the type shown in Figure 5.2(a) for different types of fault. Figures 5.33 and 5.34 typify the accuracy, for modes 1, 2 and 3, for an a-earth fault and a-b-earth fault respectively. It is apparent that, unlike the single circuit line, better accuracy is achieved when employing Aerial mode (mode 2) rather than Earth mode (mode 1) signals. It is important to mention

that mode 2 could not be defined for some types of fault. In this case mode 3 must be used instead. Studies have shown that one of the Aerial modes will always be present.

A large number of tests for the untransposed systems have shown that Aerial modes (mode 2 or 3 (in special cases)) are always more accurate than Earth mode for a double tee circuit of the type shown in Figure 5.2(a). This effectively means that by employing the Aerial modes, any chance of a false indication of the fault on a healthy circuit due to mutual coupling between the faulted and healthy circuits is minimised since this coupling is primarily associated with Earth mode signals.

Figure 5.35 show the accuracy (mode 2) for the three legs PT, QT and RT at different locations for an a-earth fault. Here again it is apparent that, like the results for the single circuit line, the shortest leg QT presents the worse performance when compared with the other two. Figure 5.36 shows the measurement accuracy (mode 2) at different locations for different types of fault. A series of studies have also shown that the degree of accuracy attained for double circuit lines is generally higher than that for the single circuit lines for the same types of fault.

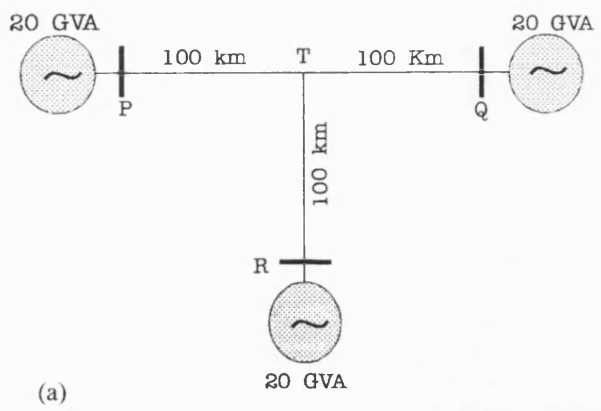

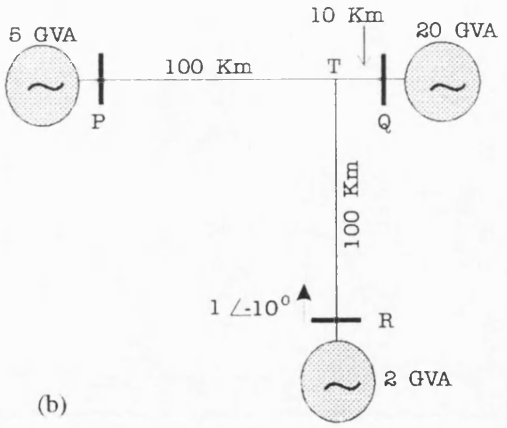

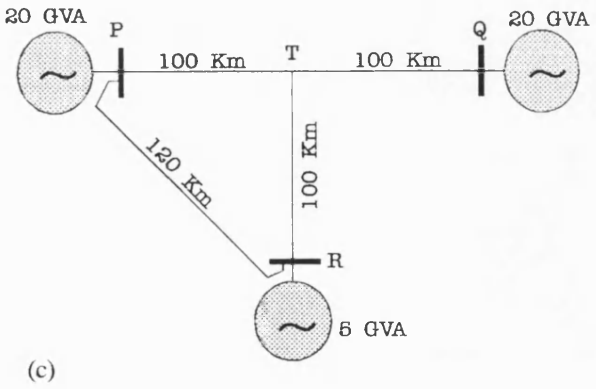

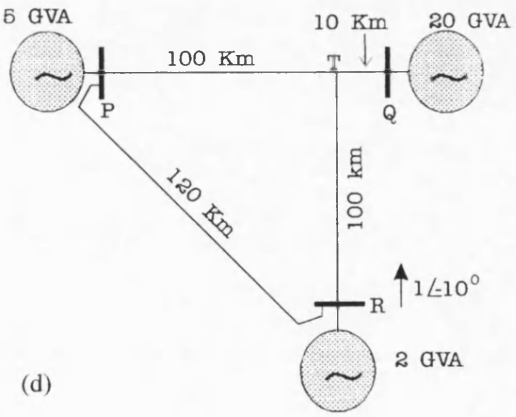

Figure 5.1 Single teed configurations studied

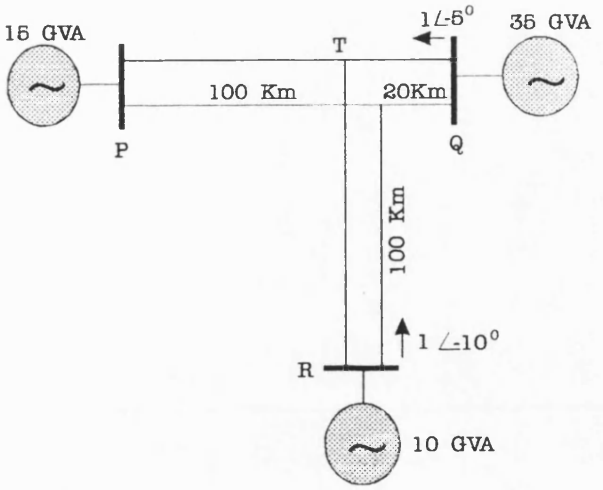

(a)

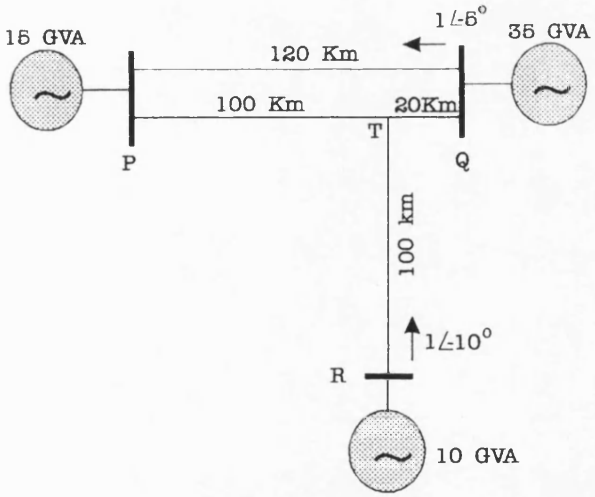

(b)

Figure 5.2 Double teed configurations studied

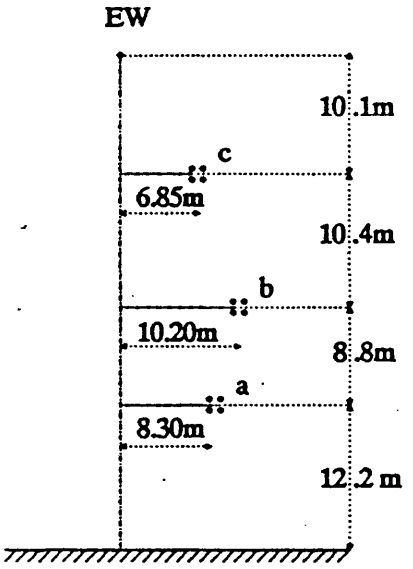

(a) Vertical single-circuit line

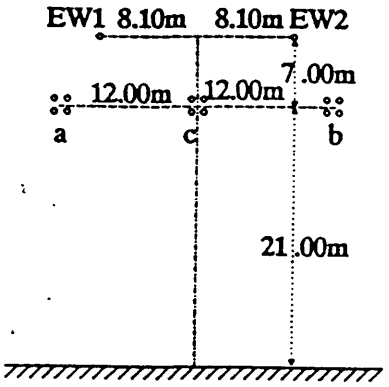

(b) Horizontal single-circuit line

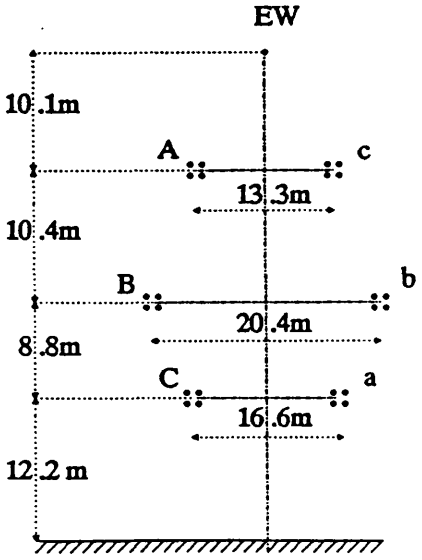

(c) Double-circuit line

Figure 5.3 Line constructions studied.

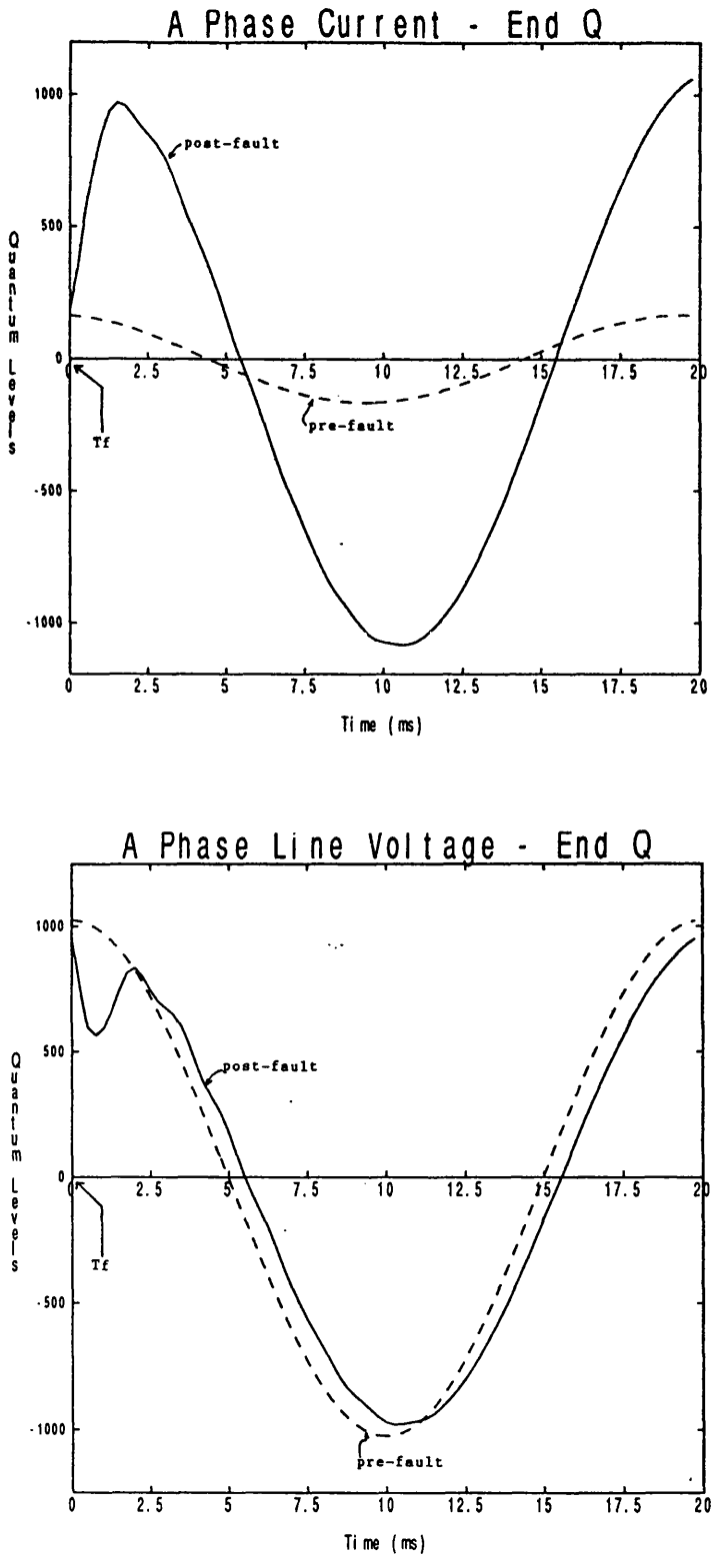

Figure 5.4 Current and voltage waveforms immediately after the fault and one cycle prior to the fault occurrence (Tf=fault inception time, Rf=30Ω).

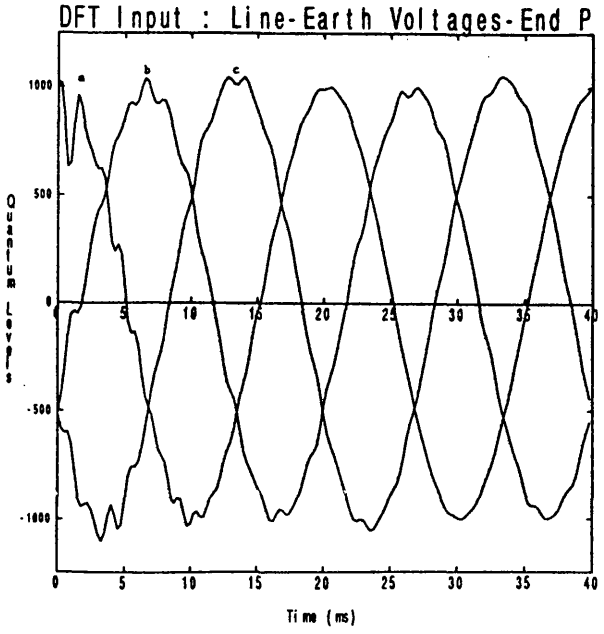

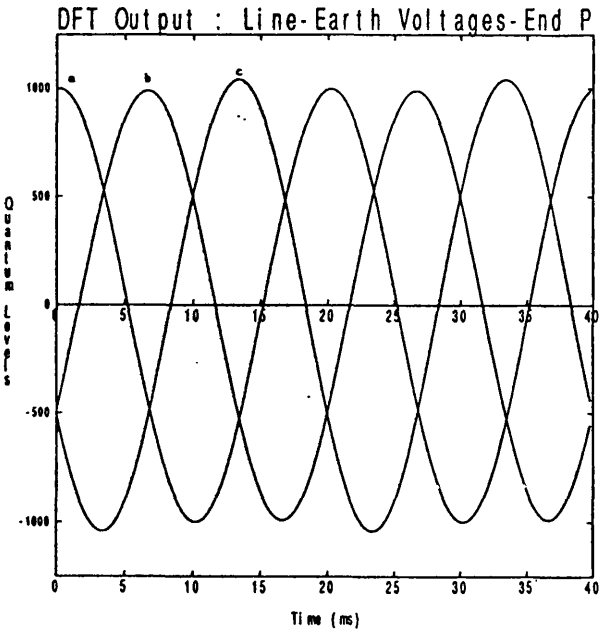

(a) Voltage Measurements

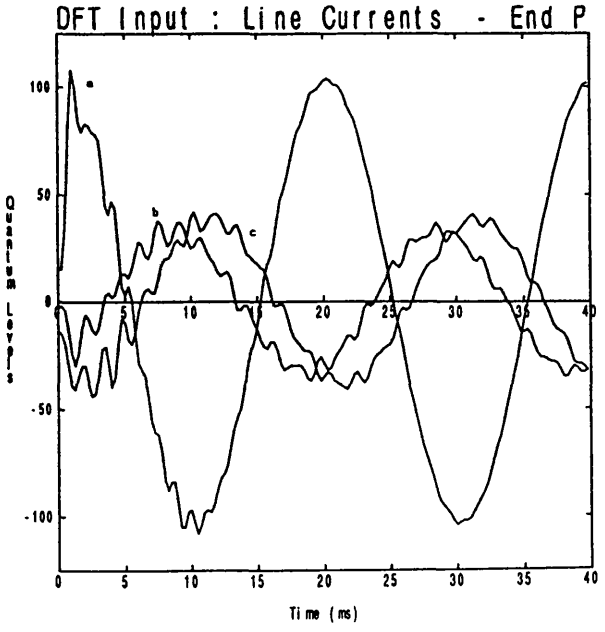

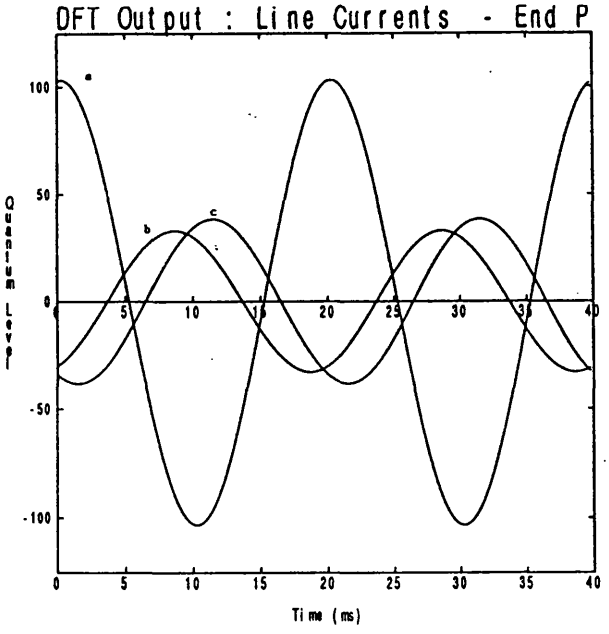

(b) Current Measurements

Figure 5.5 Input and Output of the DFT filter - End P (a-earth fault, Rf=30Ω)

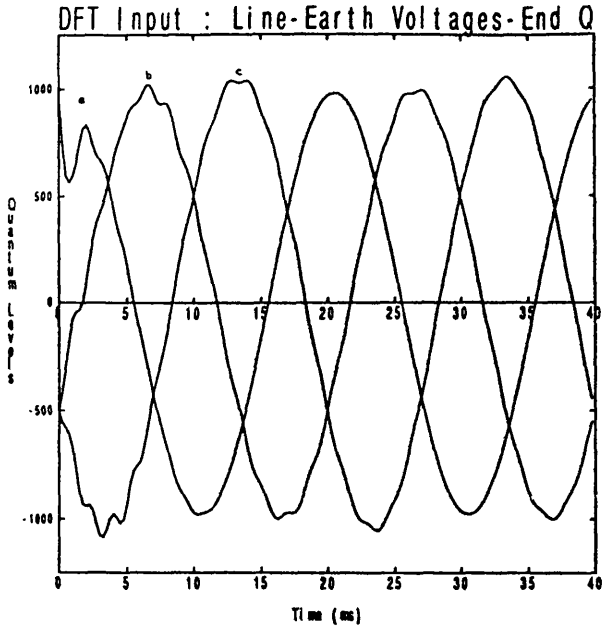

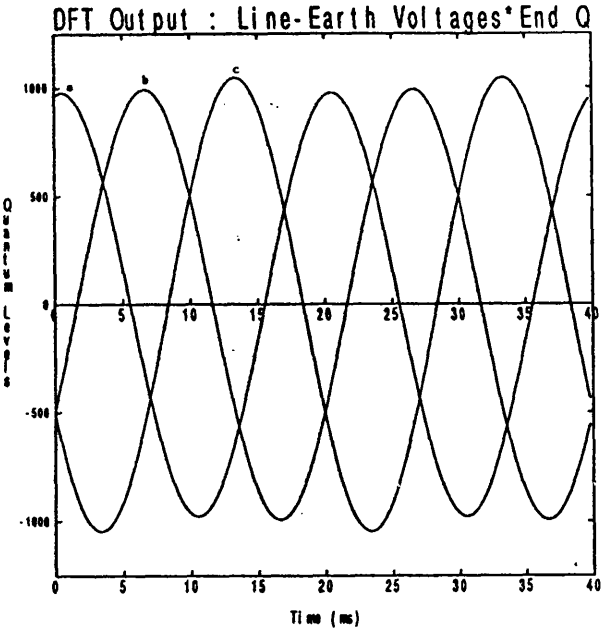

(a) Voltage Measurements

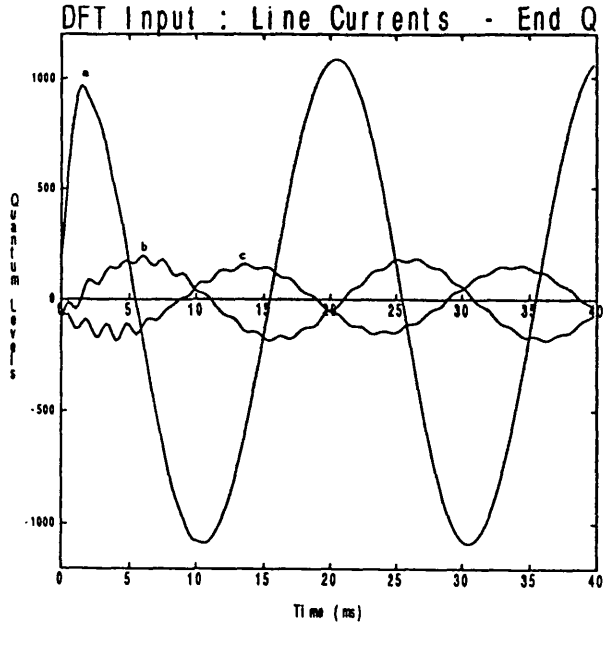

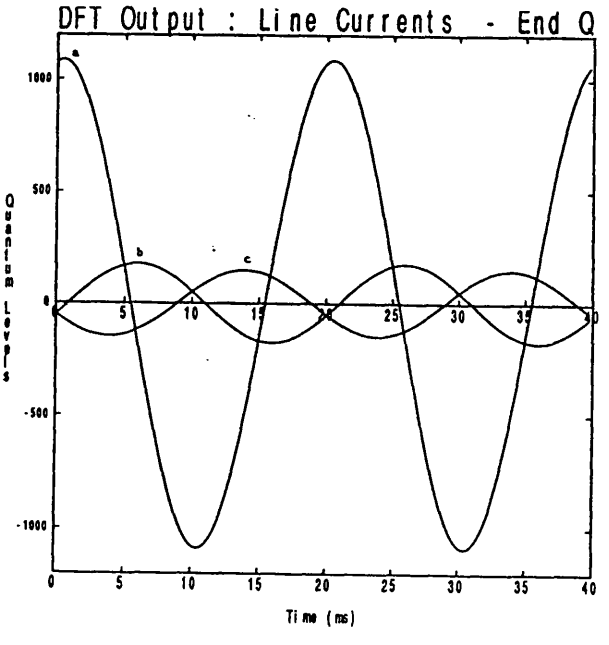

(b) Current Measurements

Figure 5.6 Input and Output of the DFT filter - End Q (a-earth fault, Rf=30Ω)

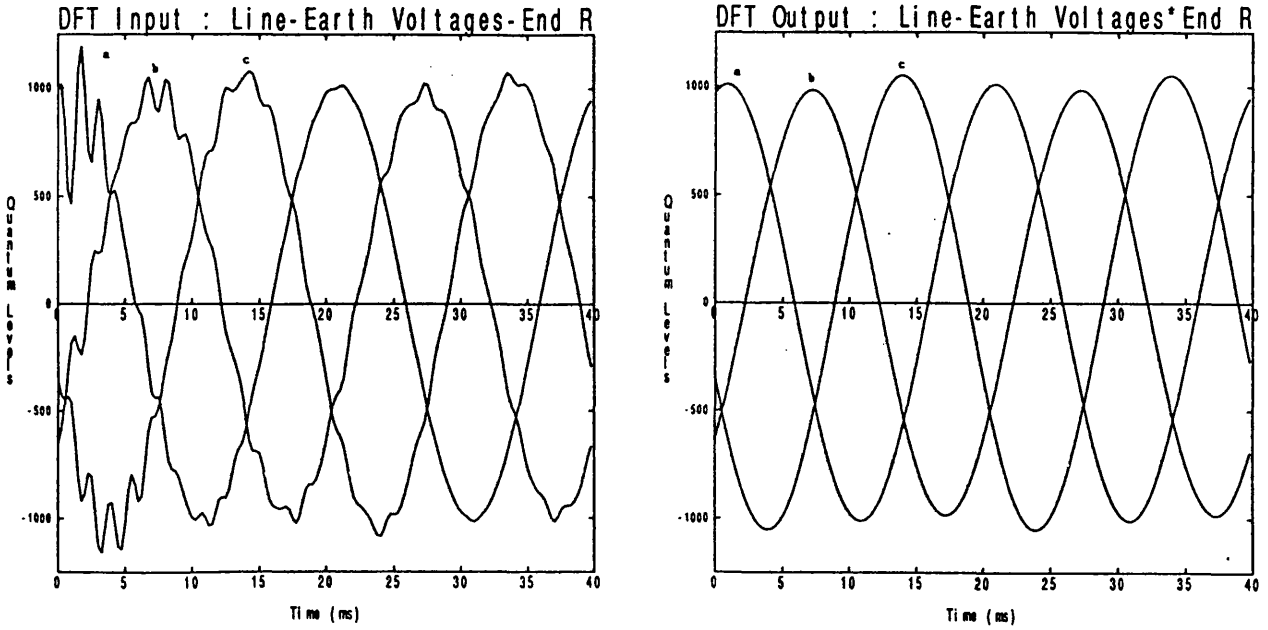

(a) Voltage Measurements

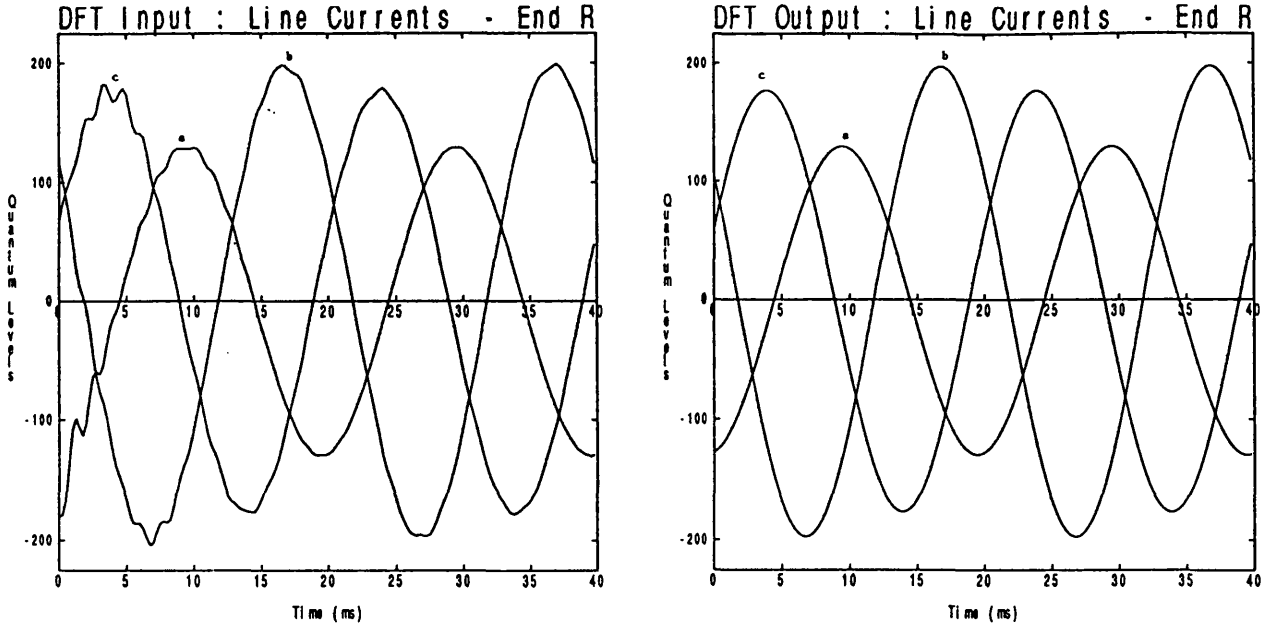

(b) Current Measurements

Figure 5.7 Input and Output of the DFT filter - End R (a-earth fault, Rf=30Ω)

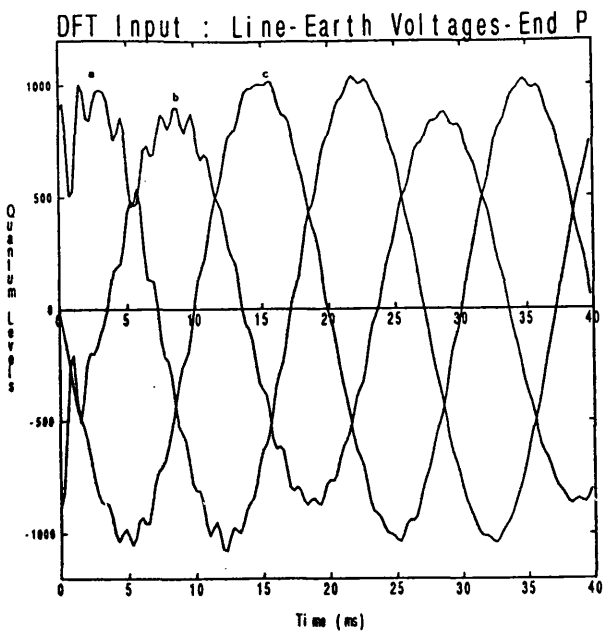

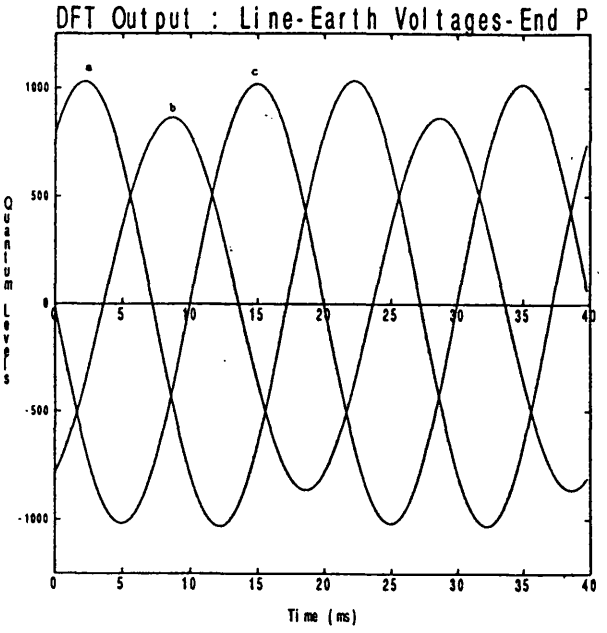

(a) Voltage Measurements

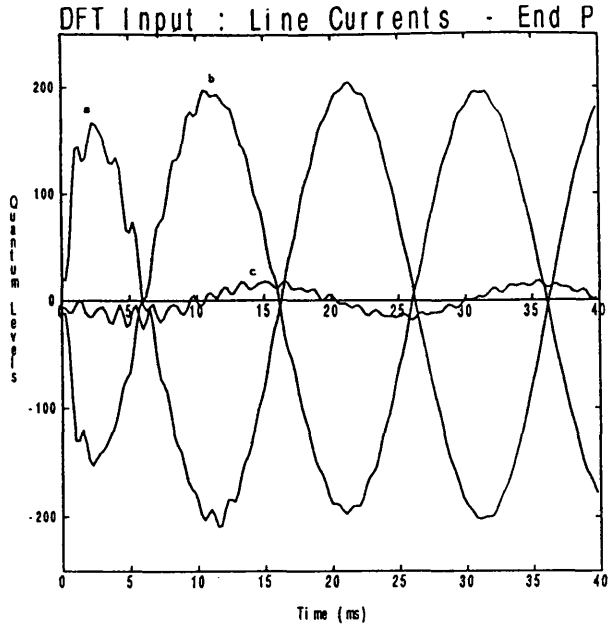

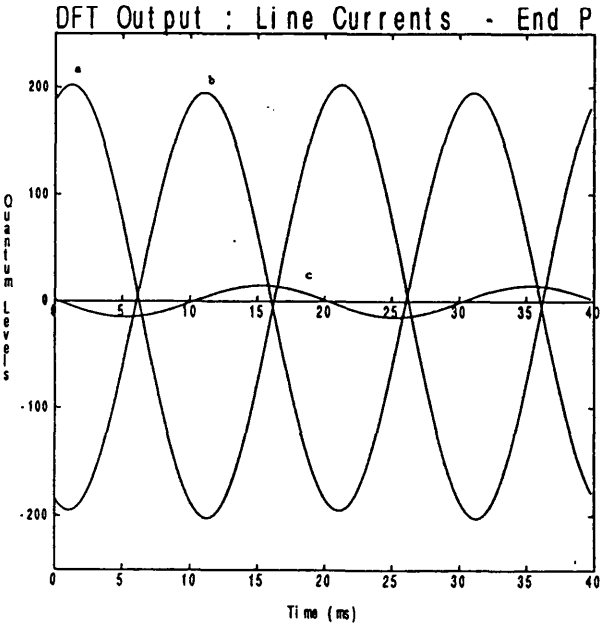

(b) Current Measurements

Figure 5.8 Input and Output of the DFT filter - End P (a-b fault, Rf=30Ω)

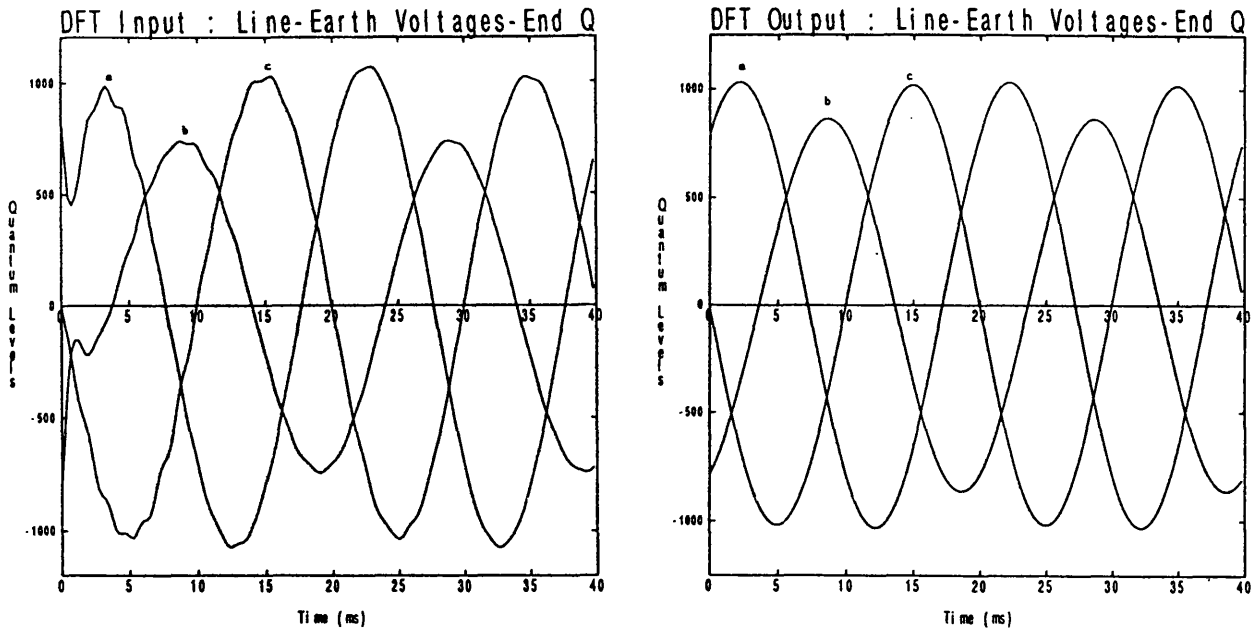

(a) Voltage Measurements

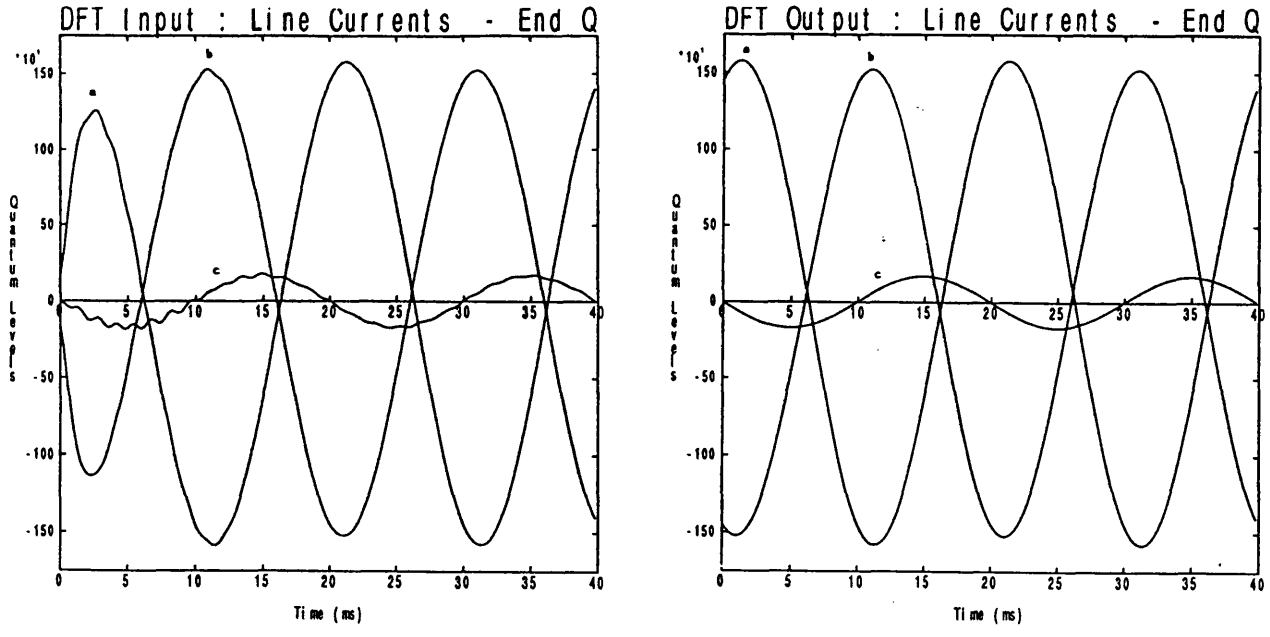

(b) Current Measurements

Figure 5.9 Input and Output of the DFT filter - End Q (a-b fault, Rf=30Ω)

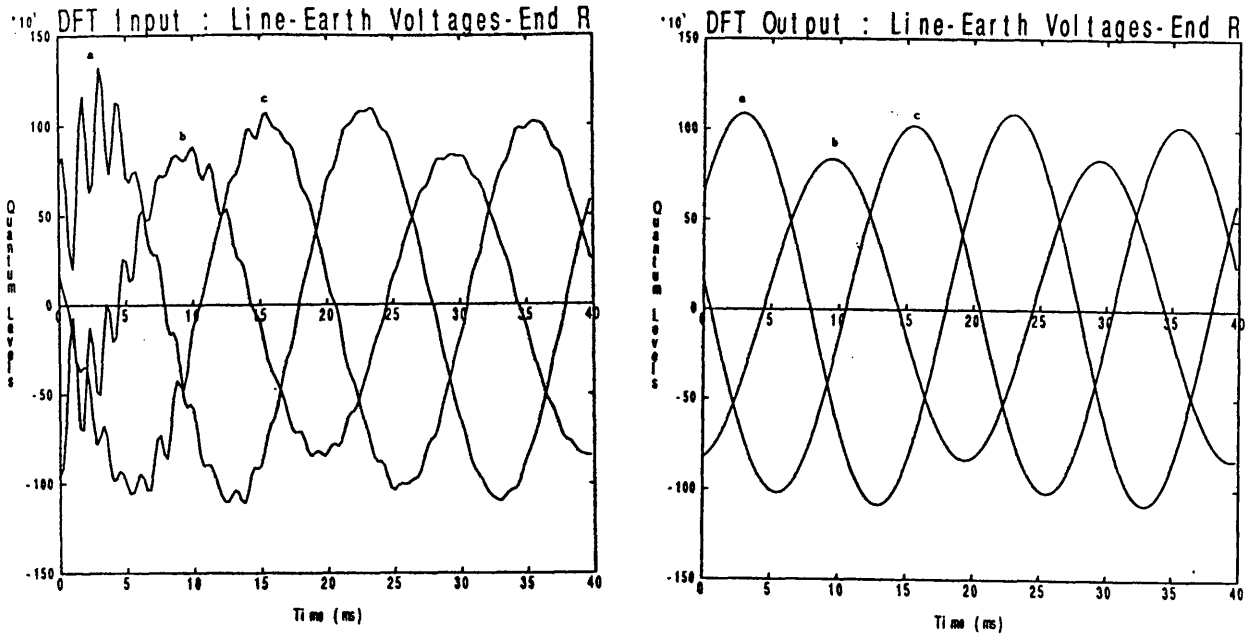

(a) Voltage Measurements

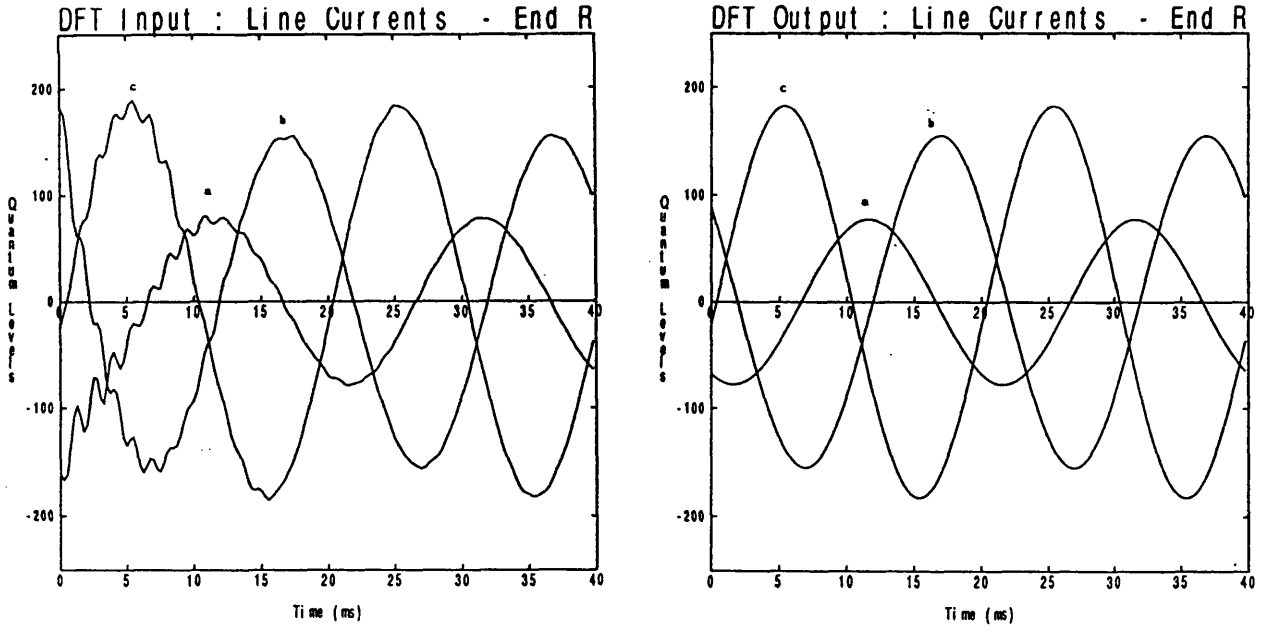

(b) Current Measurements

Figure 5.10 Input and Output of the DFT filter - End R (a-b fault, Rf=30Ω)

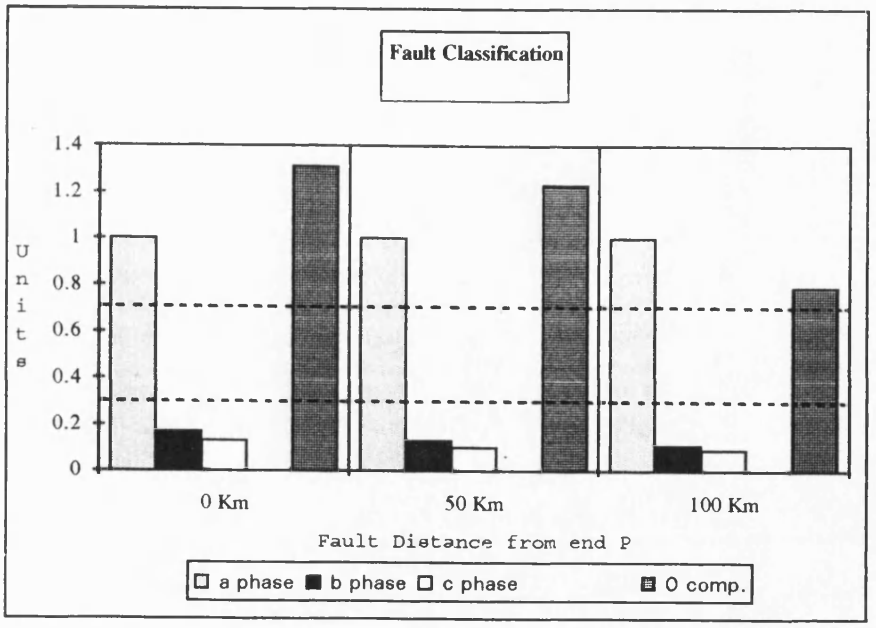

Figure 5.11 Fault classification for phase a-earth fault on leg PT (unsymmetrical system)

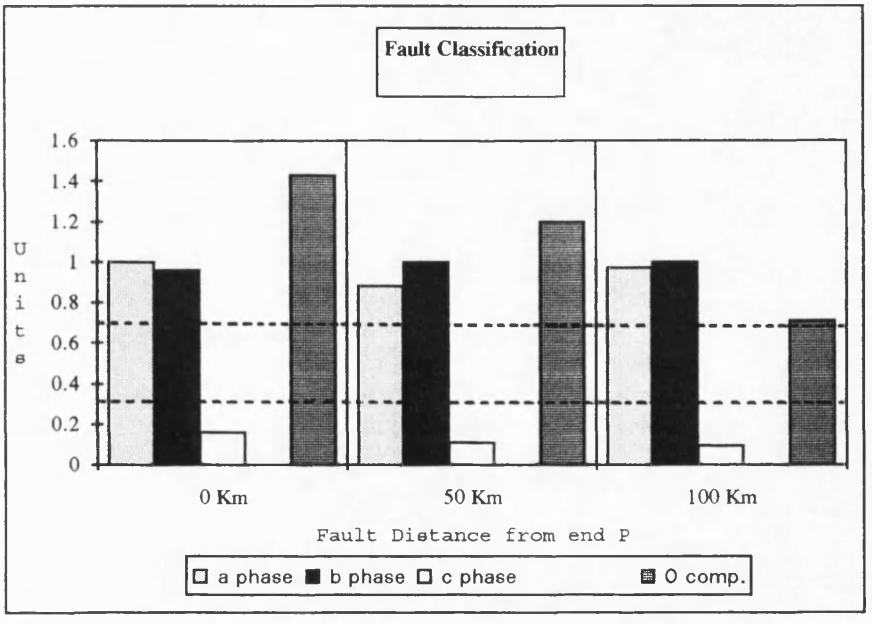

Figure 5.12 Fault classification for an a-b-earth fault on leg PT(unsymmetrical system)

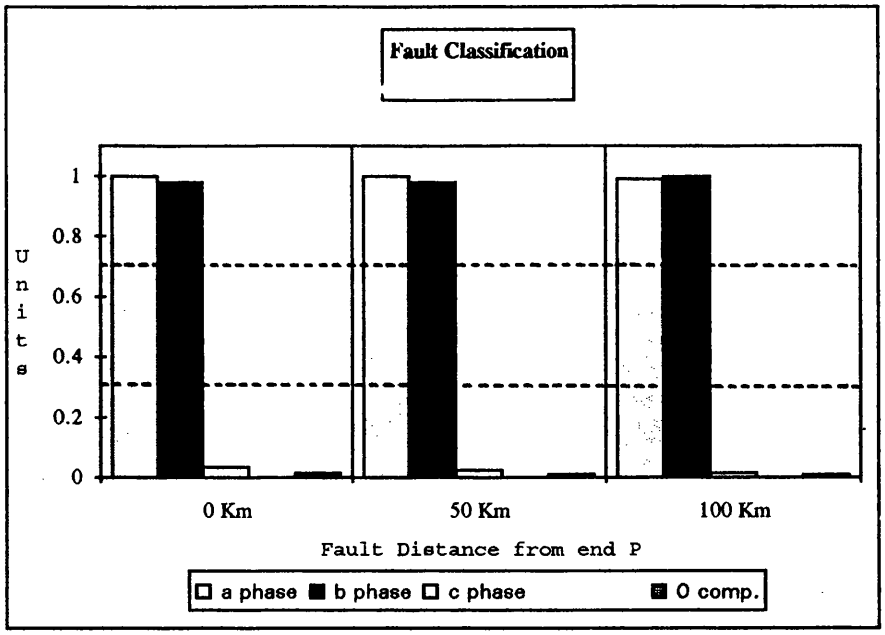

Figure 5.13 Fault classification for phase a-b fault on leg PT (unsymmetrical system)

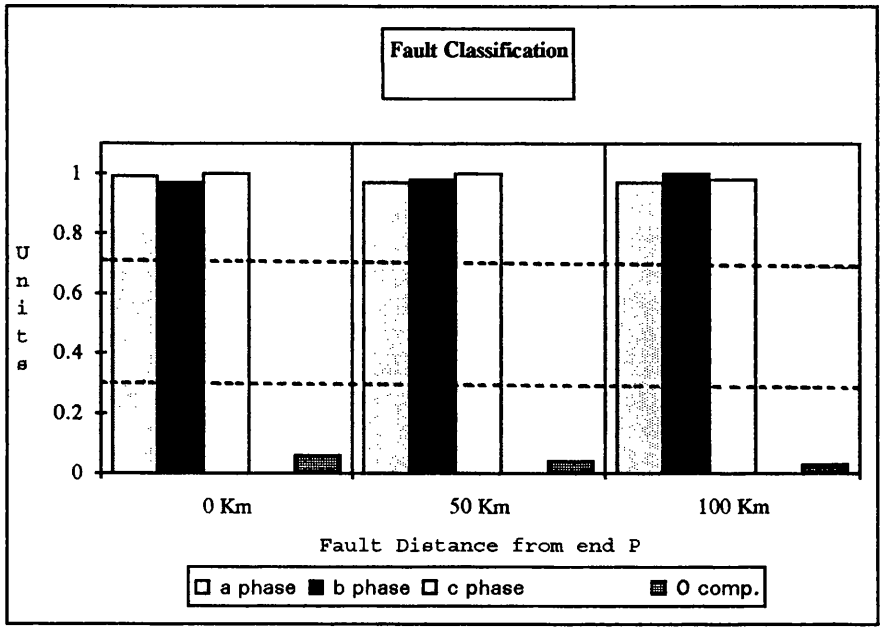

Figure 5.14 Fault classification for a three-phase fault on leg PT(unsymmetrical system)

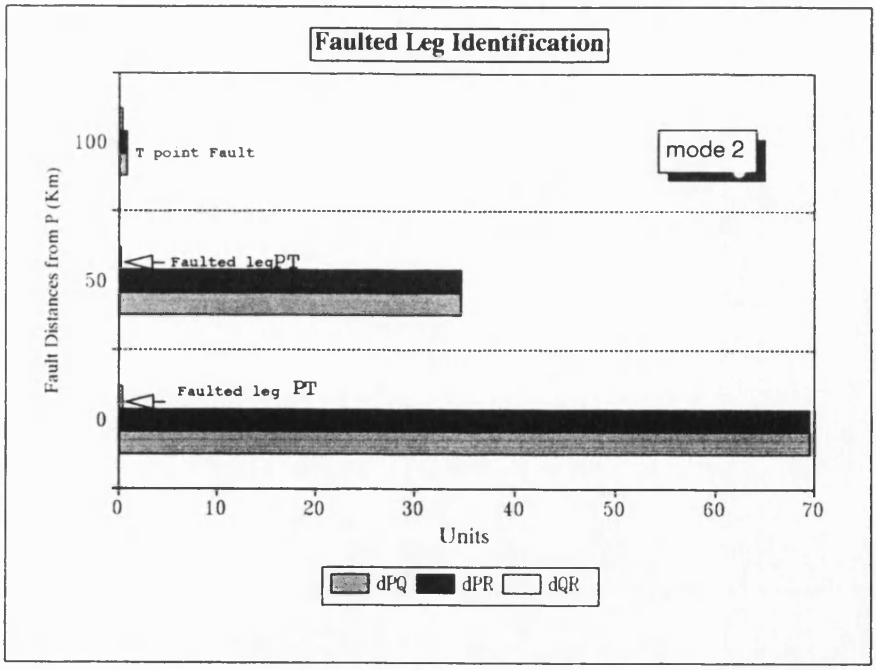

Figure 5.15 Identification of the faulted leg PT for the unsymmetrical system (phase-earth fault)

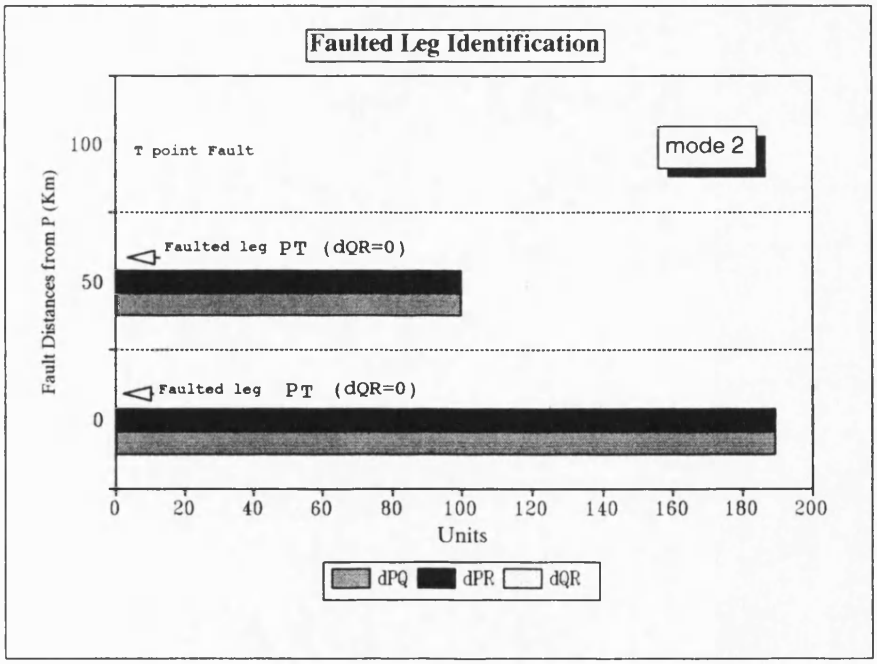

Figure 5.16 Identification of the faulted leg PT for the unsymmetrical system (double-phase earth fault)

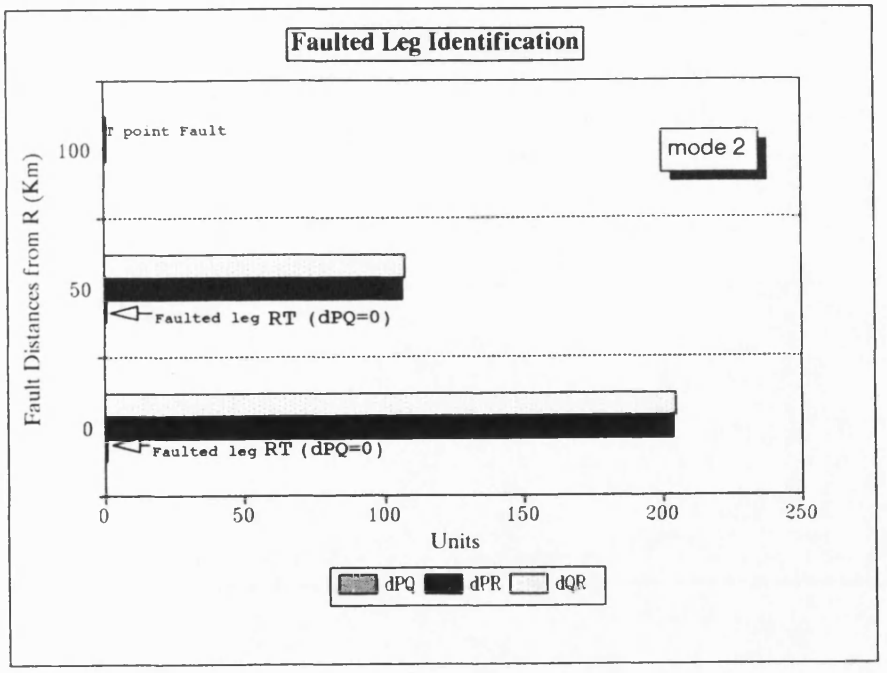

Figure 5.17 Identification of the faulted leg RT for the unsymmetrical system (three-phase fault)

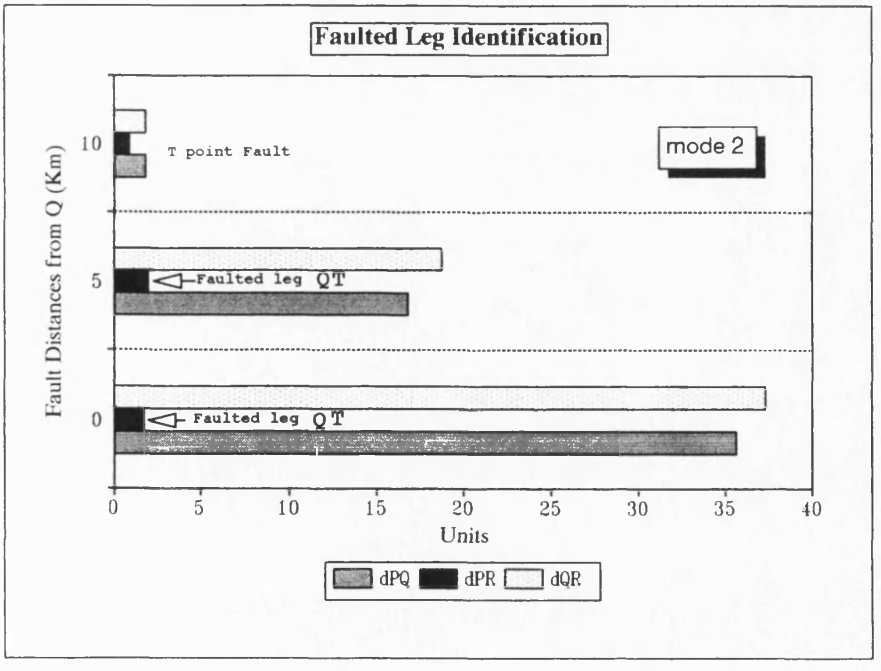

Figure 5.18 Identification of the faulted leg QT for the unsymmetrical system (double-phase fault)

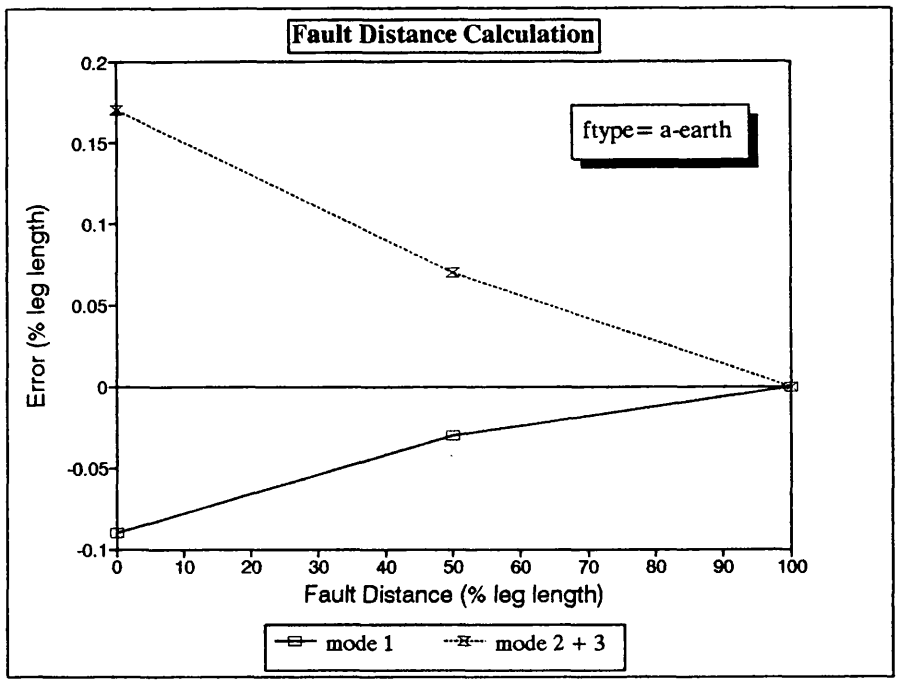

Figure 5.19 Results for an a-earth fault on a symmetrical and transposed vertical teed configuration. (Rf=10 Ω)

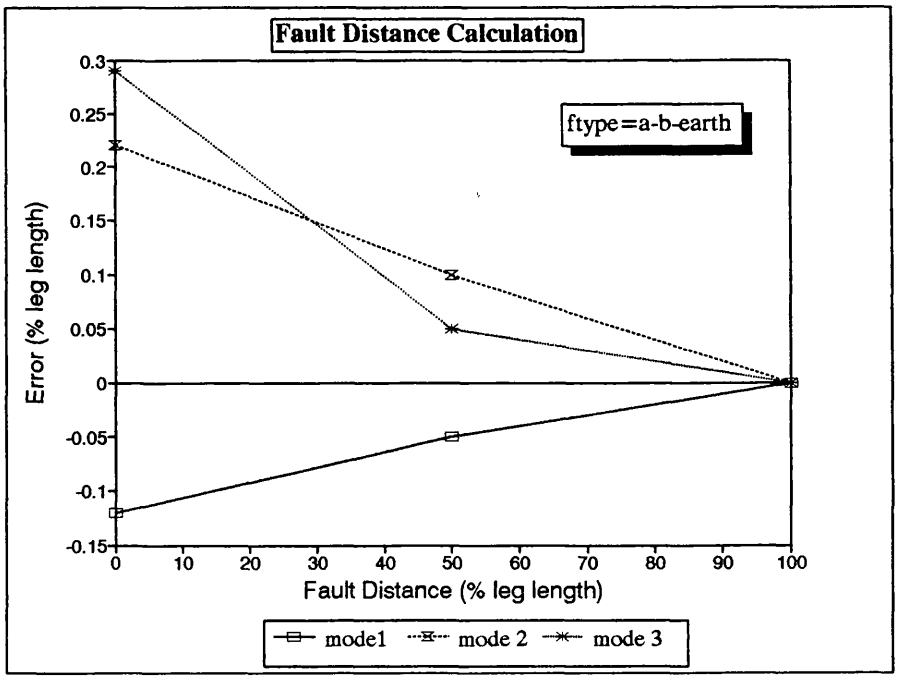

Figure 5.20 Results for an a-b-earth fault on a symmetrical and transposed vertical teed configuration. (Rf=10 Ω)

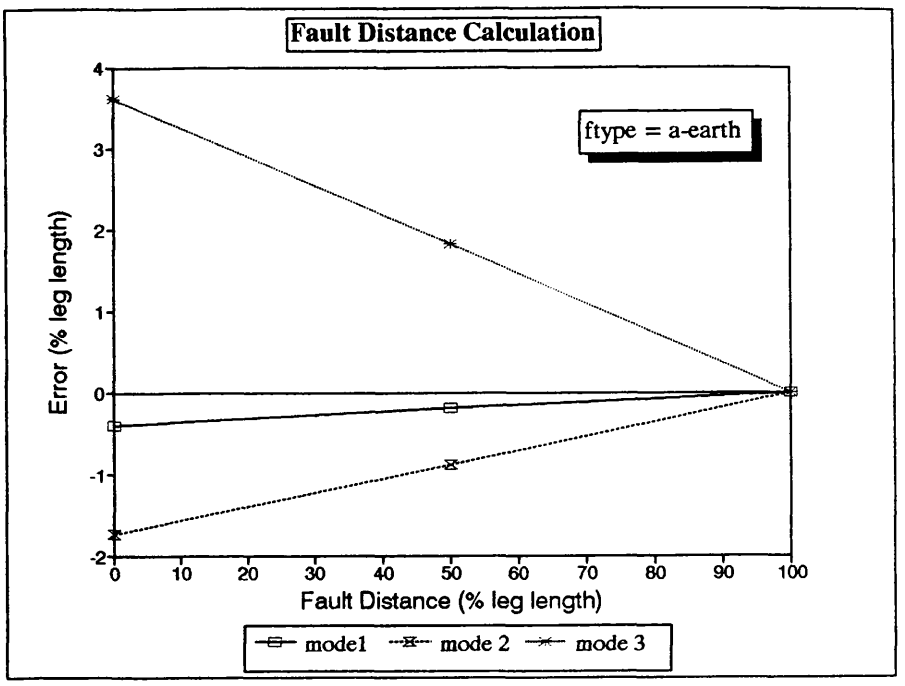

Figure 5.21 Results for an a-earth fault on a symmetrical and untransposed vertical teed configuration, using transposed line parameters. (Rf=10 Ω)

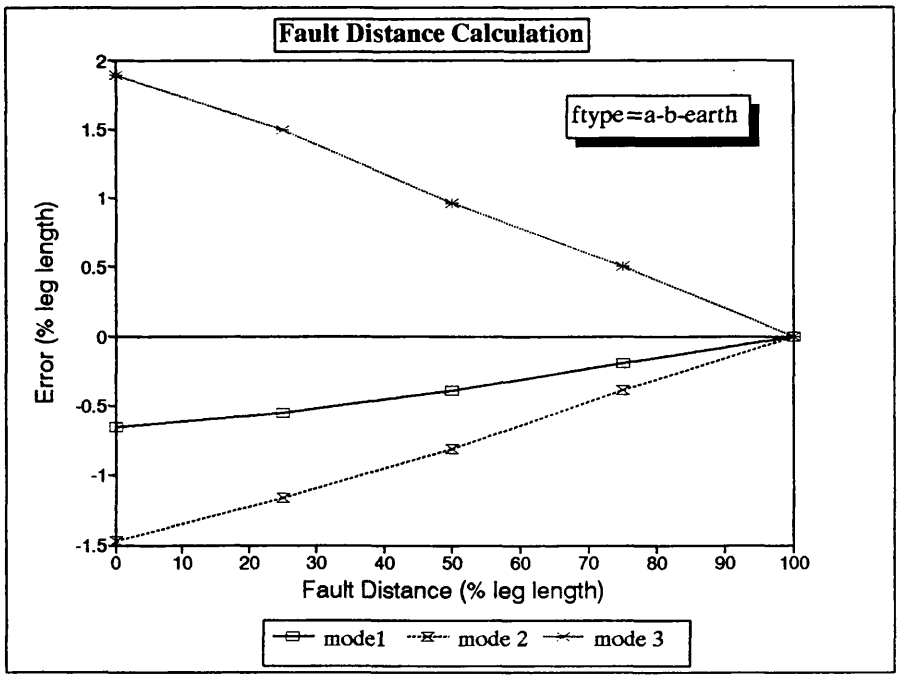

Figure 5.22 Results for an a-b-earth fault on a symmetrical and untransposed vertical teed configuration, using transposed line parameters. (Rf=10 Ω)

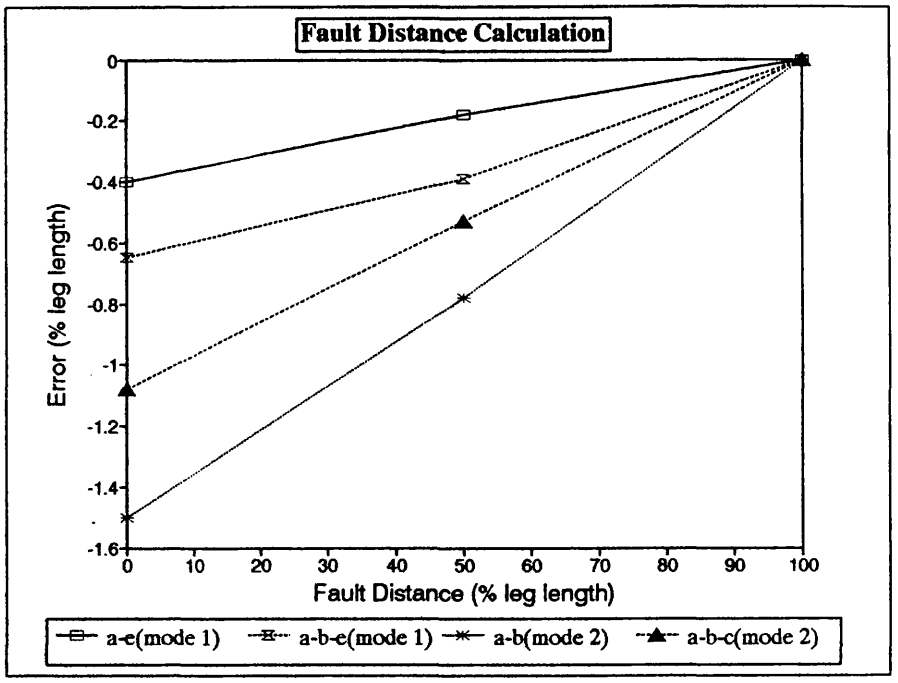

Figure 5.23 Results for different types of fault on a symmetrical and untransposed vertical teed configuration. (Rf=10 Ω)

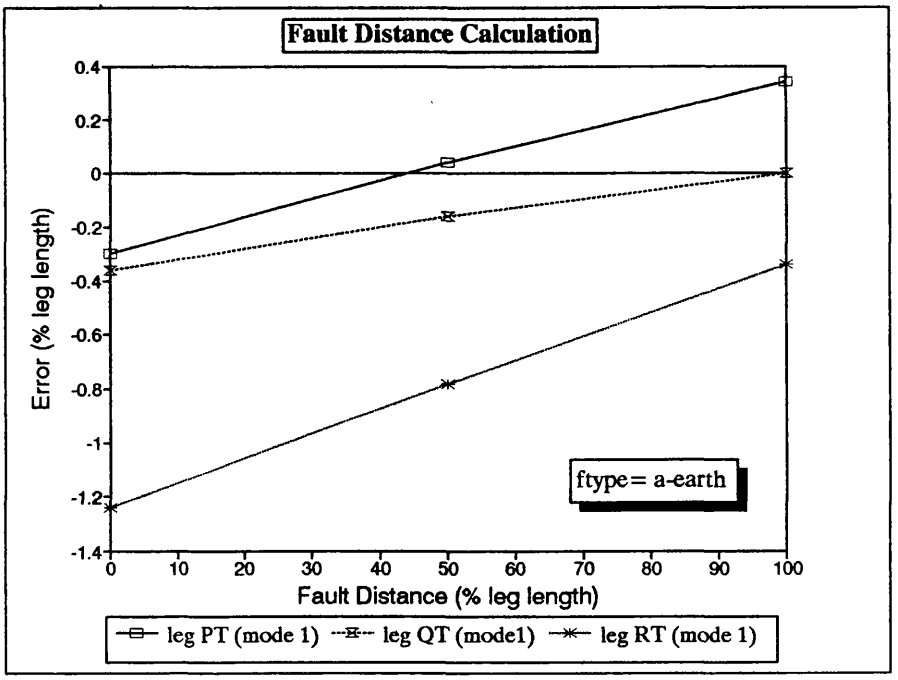

Figure 5.24 Results for an a-earth fault on a symmetrical and untransposed vertical teed configuration, with nonsymmetrical source capacities. (Rf=10 Ω)

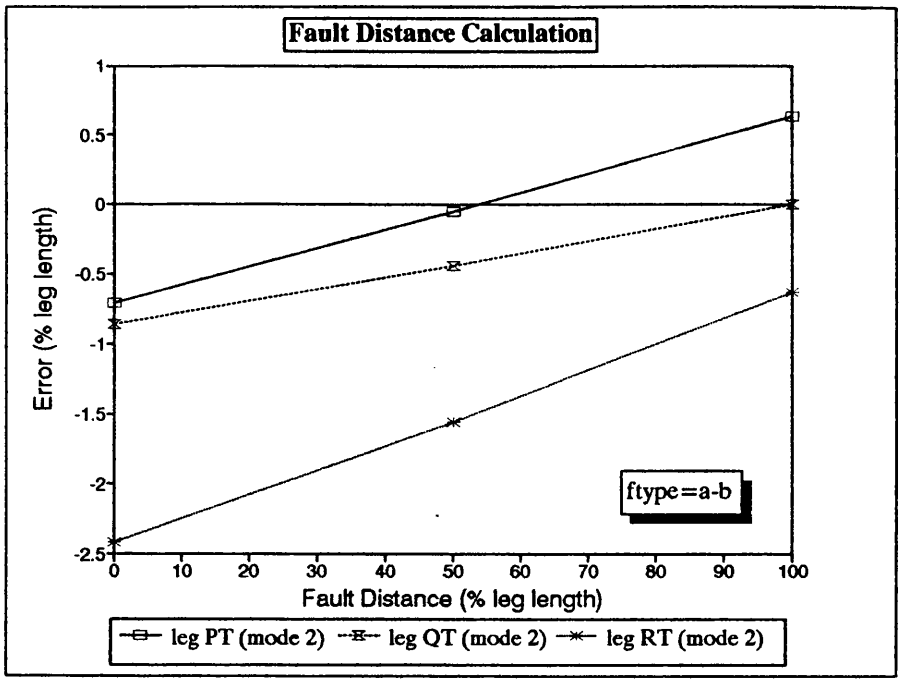

Figure 5.25 Results for an a-b fault on a symmetrical and untransposed vertical teed configuration with nonsymmetricalsource capacities. (Rf=10 Ω)

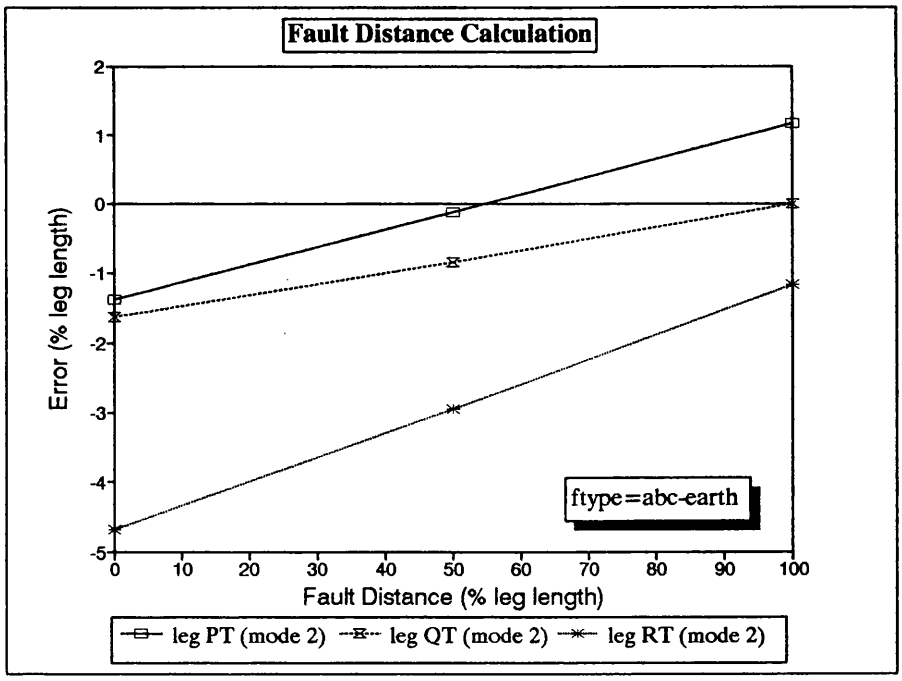

Figure 5.26 Results for a three phase fault on a symmetrical and untransposed vertical teed configuration with nonsymmetrical source capacities. (Rf=10 Ω)

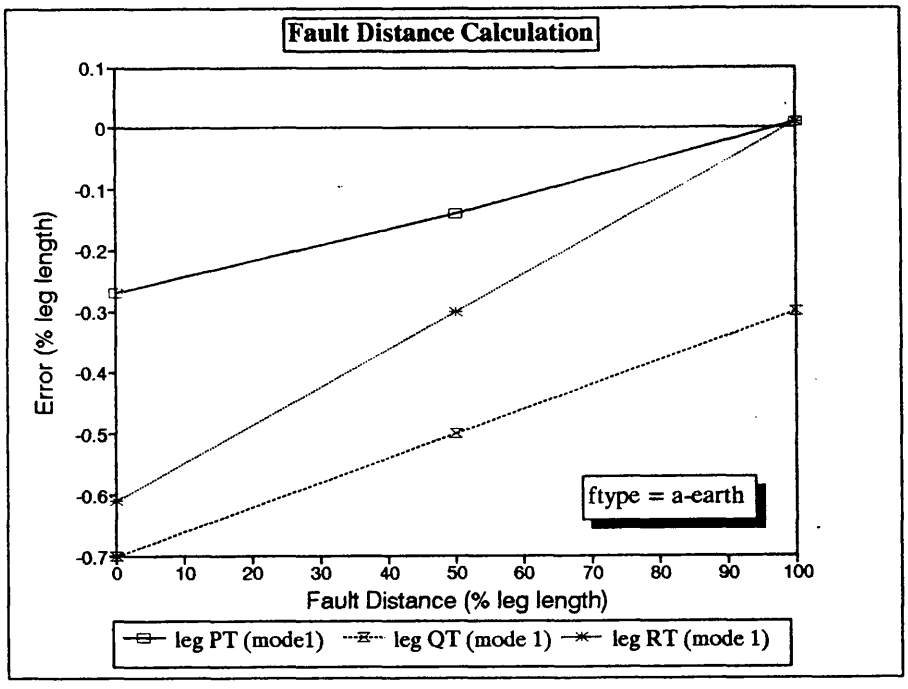

Figure 5.27 Results for an a-earth fault on an unsymmetrical and transposed vertical teed configuration . (Rf=60 Ω)

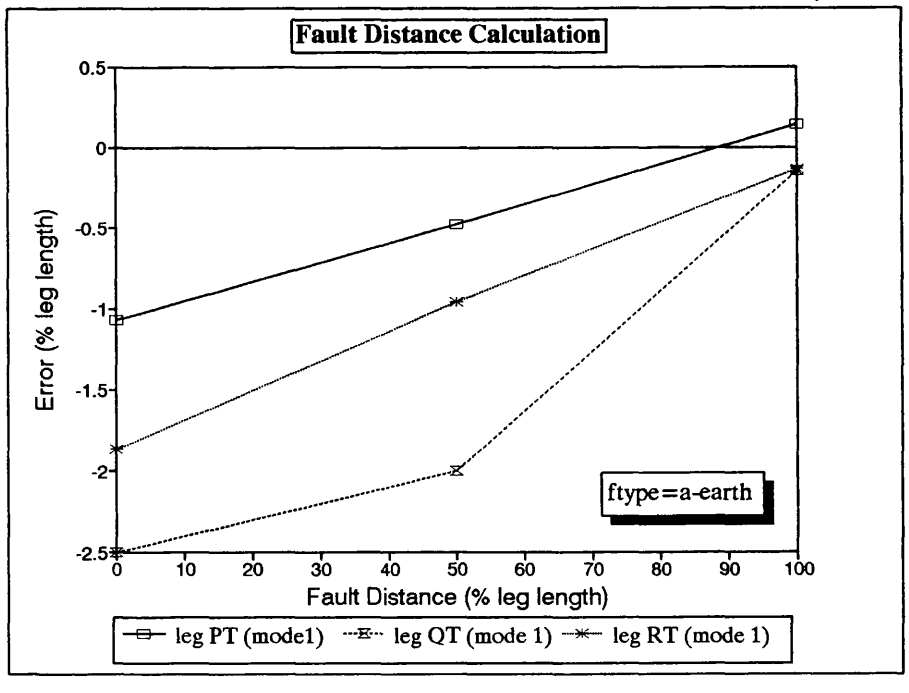

Figure 5.28 Results for an a-earth fault on an unsymmetrical and untransposed vertical teed configuration . (Rf=60 Ω)

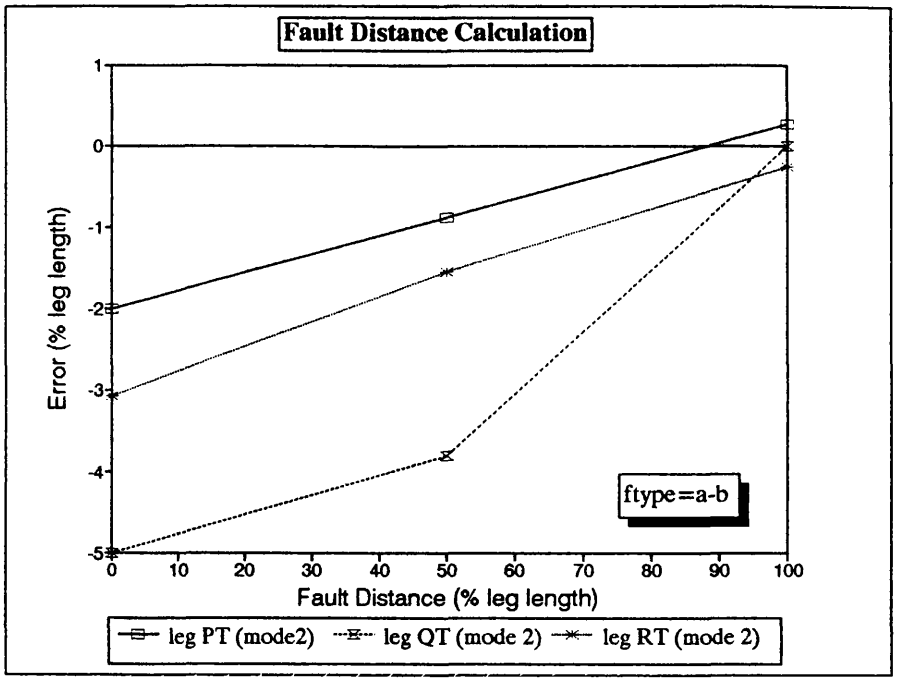

Figure 5.29 Results for an a-b fault on an unsymmetrical and untransposed vertical teed configuration. (Rf=60 Ω)

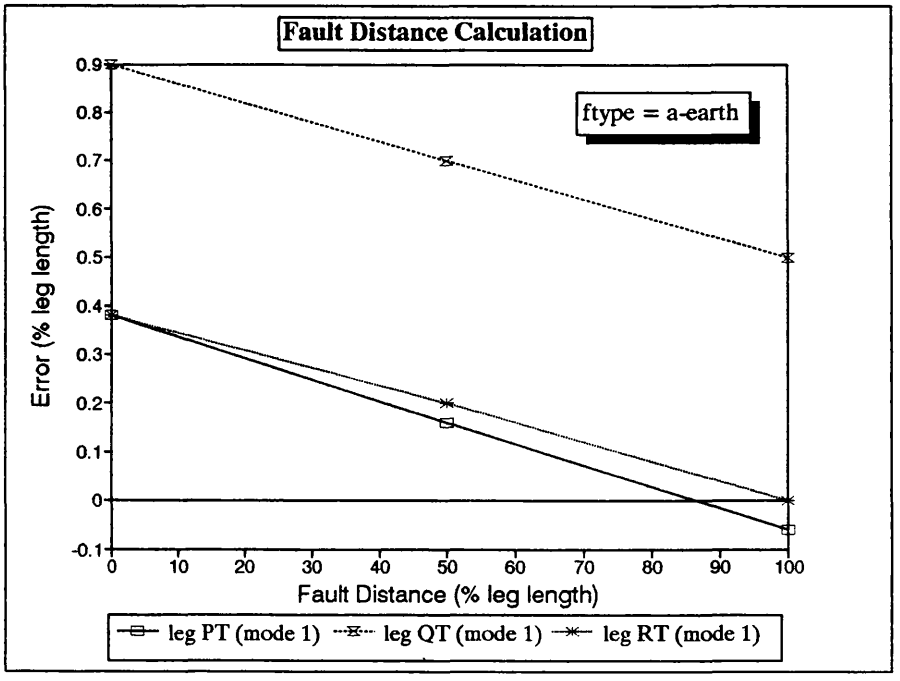

Figure 5.30 Results for an a-earth fault on an unsymmetrical and untransposed horizontal teed configuration. (Rf=60 Ω)

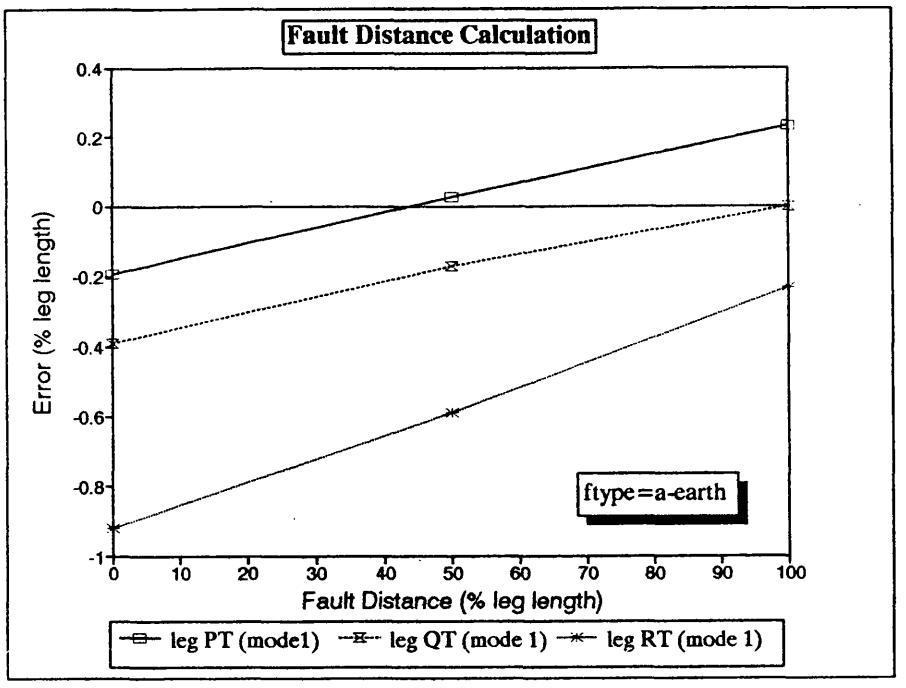

Figure 5.31 Results for an a-earth fault on a symmetrical and untranposed vertical teed configuration with feed-around path.(Rf=10 Ω)

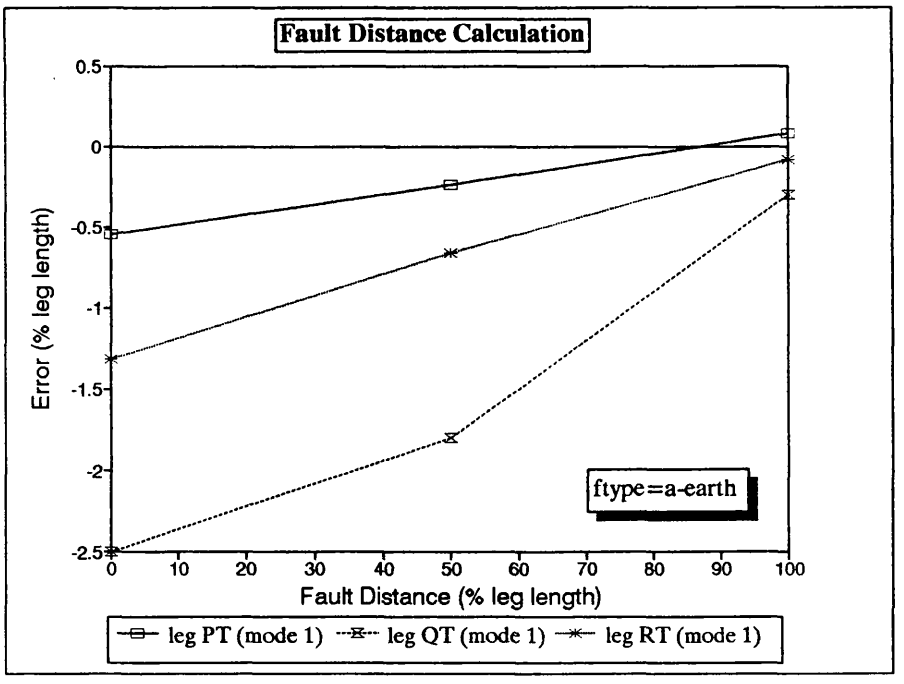

Figure 5.32 Results for an a-earth fault on an unsymmetrical and untransposed vertical teed configuration with feed-around path.(Rf=60Ω)

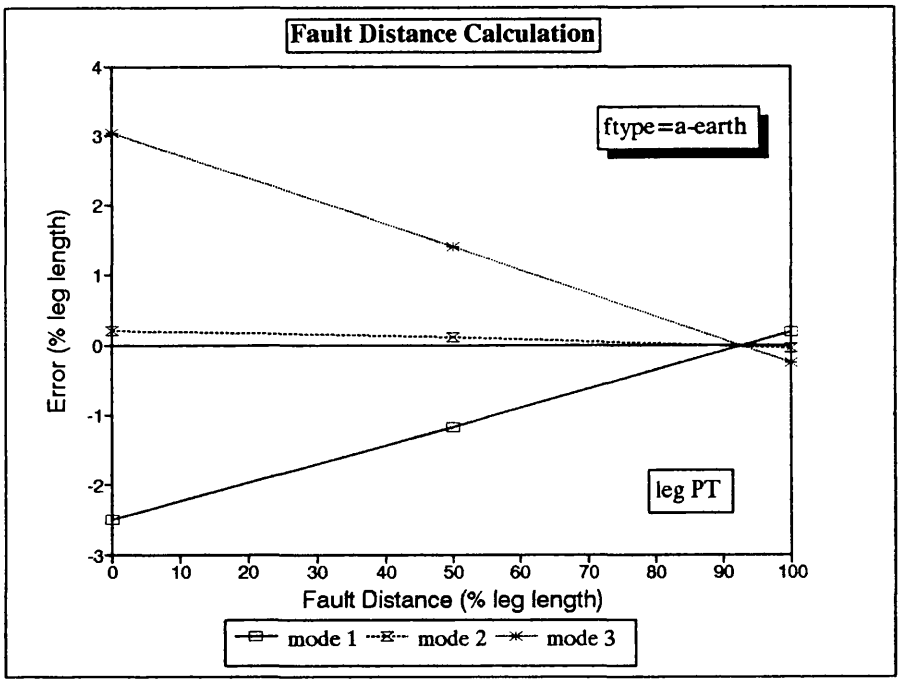

Figure 5.33 Results for an a-earth fault on an untransposed double circuit. (Figure 5.2(a), Rf=30 Ω)

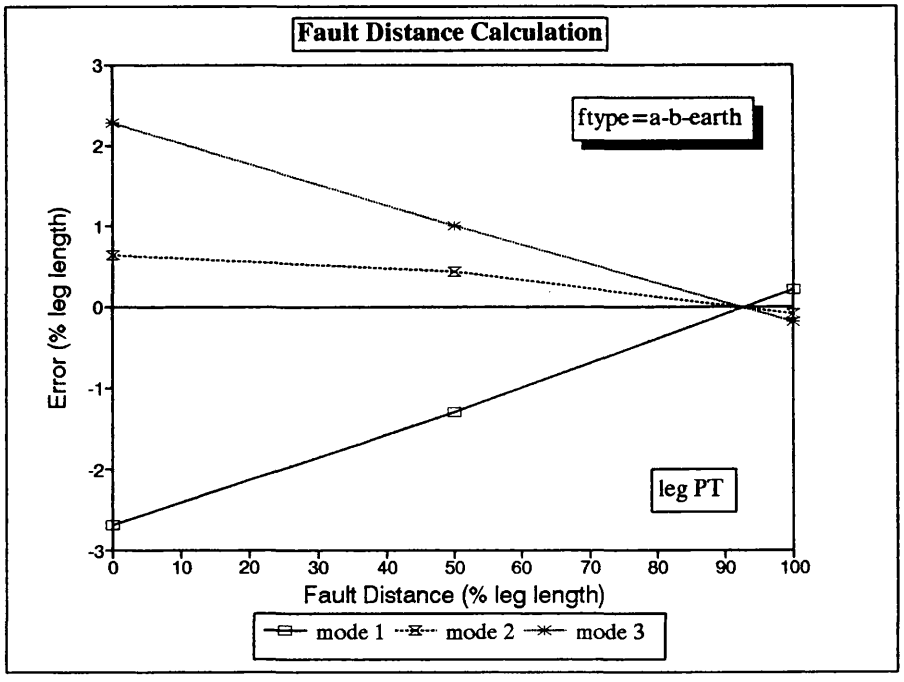

Figure 5.34 Results for an a-b-earth fault on an untransposed double circuit. (Figure 5.2(a), Rf=30 Ω)

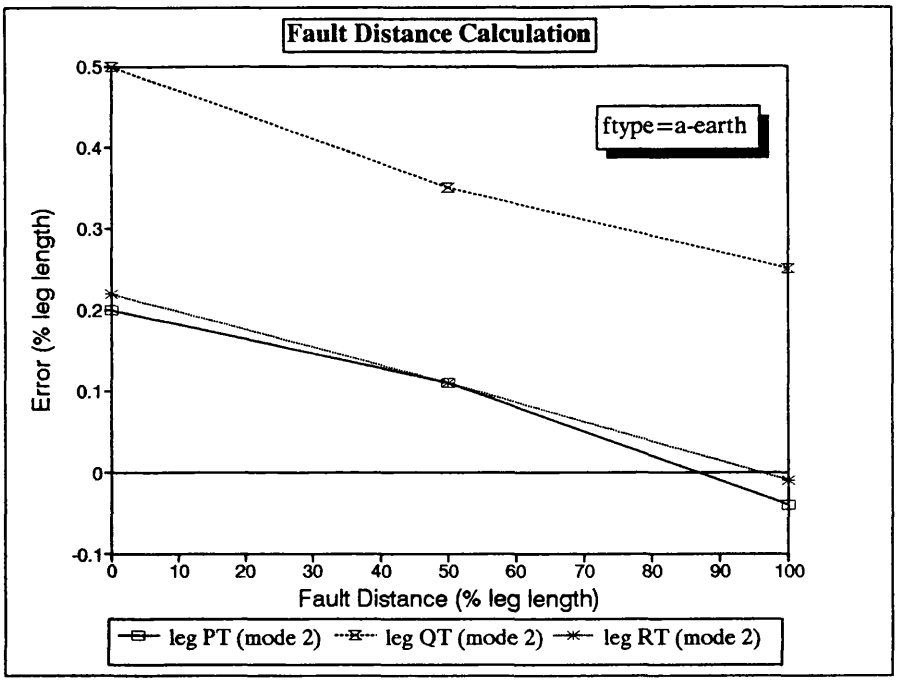

Figure 5.35 Results for an a-earth fault on an untransposed double circuit. (Figure 5.2(a), Rf=30 Ω)

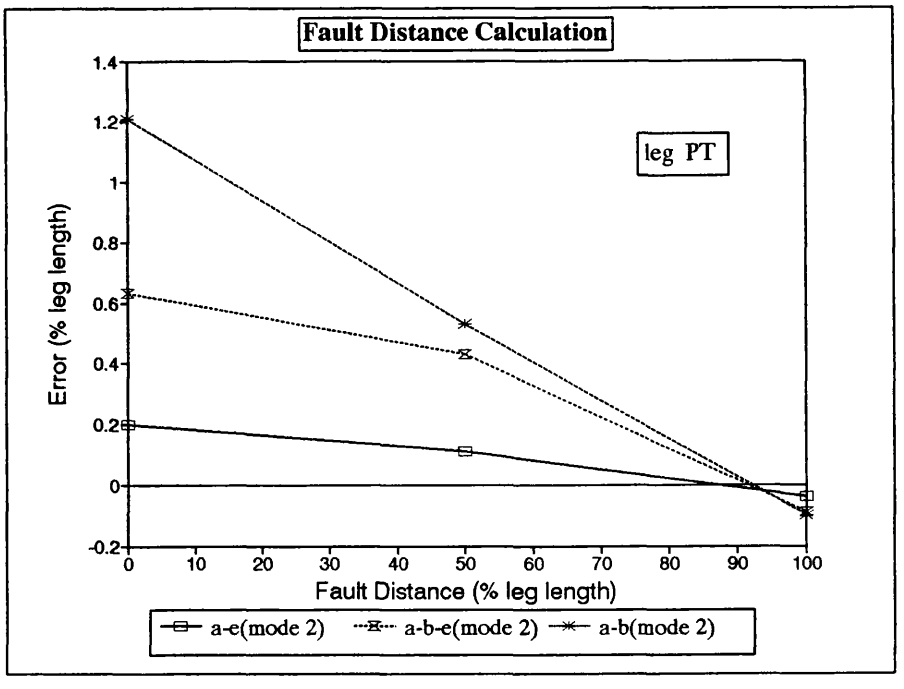

Figure 5.36 Results for different types of fault on an untransposed double circuit. (Figure 5.2(a), Rf=30 Ω)

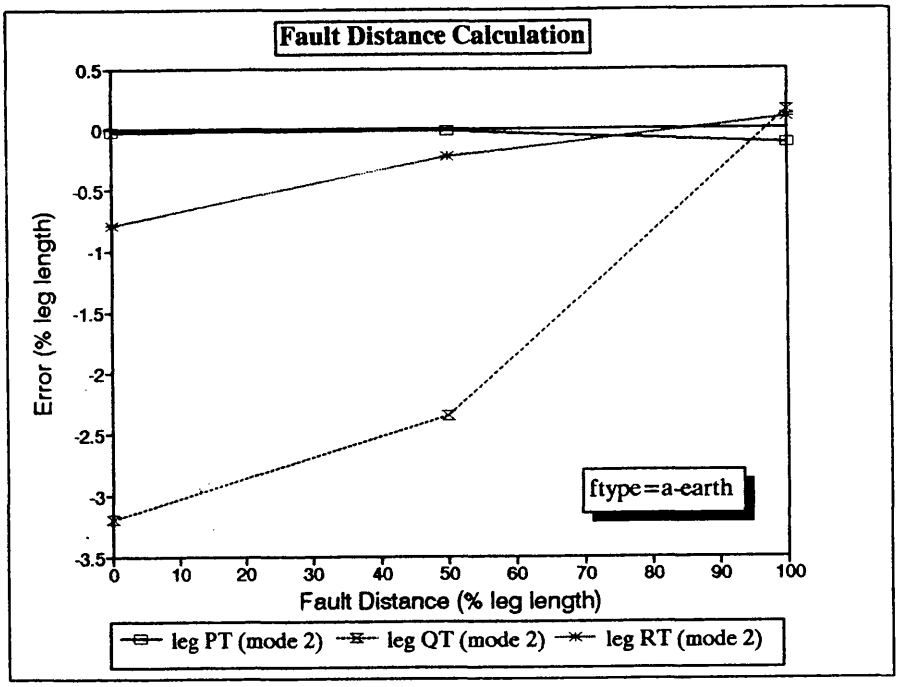

Figure 5.37 Results for an a-earth fault on an untransposed double circuit. (Figure 5.2(b), Rf=30 Ω)

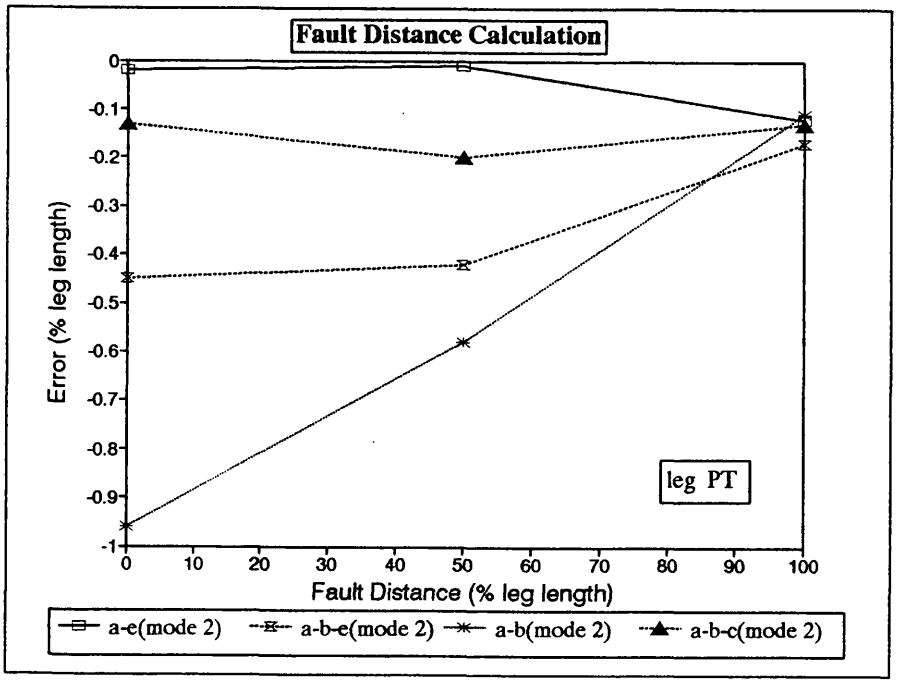

Figure 5.38 Results for different types of fault on an untransposed double circuit. (Figure 5.2(b), Rf=30 Ω)

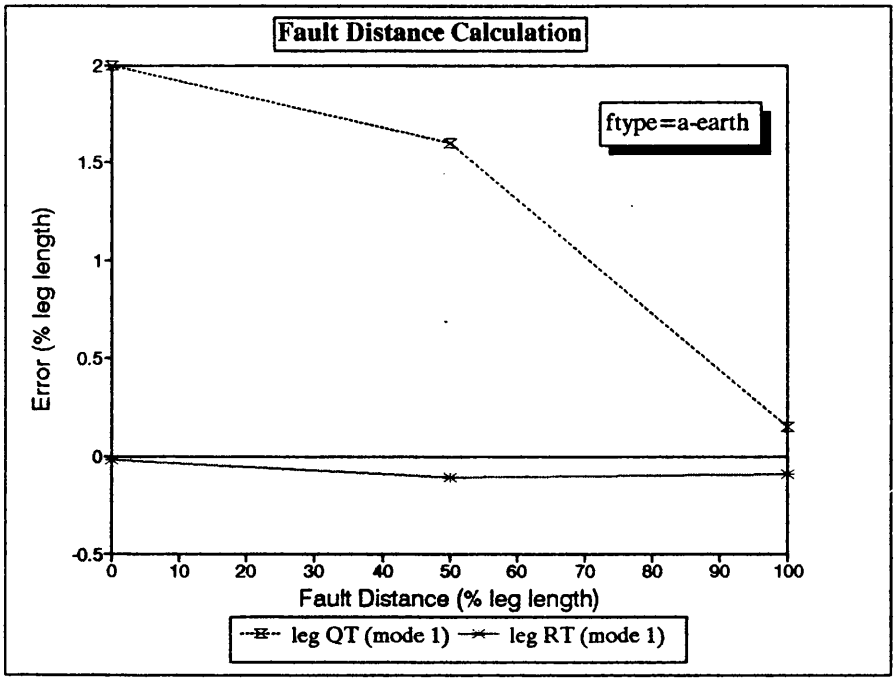

Figure 5.39 Results for an a-earth fault on an untransposed double circuit for legs QT and RT, considering mode 1.(Figure 5.2(b), Rf=30 Ω)

CHAPTER 6

PERFORMANCE EVALUATION AND SENSITIVITY ANALYSIS OF THE FAULT LOCATOR ALGORITHM

6.1 INTRODUCTION

This chapter has been divided into two main parts. The first part is concerned with presenting the performance evaluation of the proposed algorithm. The effect of data unsynchronism, differing source capacities, fault resistance, fault inception angle, etc on accuracy are examined. The system configurations considered for this purpose are of the vertical construction type, as shown in Figure 6.1. They are essentially the same as the symmetrical and unsymmetrical configurations studied in the previous chapter with a variation in some of the parameters. The second part of the chapter is wholly devoted to a sensitivity analysis of the fault locator algorithm. Non-algorithmic errors, introduced for example, by incorrect setting parameters, are then investigated. For the latter purposes, the same system configurations are used to illustrate such effects.

It should be mentioned that, like the results in the previous chapter, for the purpose of brevity, the results presented in this chapter have been selected from an extensive series of tests and they attempt to represent,

in the best way, the general performance of the algorithm for the different situations described above.

6.2 PERFORMANCE EVALUATION

This section presents the performance evaluation of the fault locator algorithm under different system and fault conditions. It should be mentioned that for tests carried out in this section, the symmetrical and unsymmetrical systems represented in Figure 6.1 were considered with untransposed lines but with transposed parameters set into the algorithm.

6.2.1 Effect of Data Unsynchronism

As emphasised in Section 3.2.1 and 5.3.1, the input data to the fault locating algorithm, derived from the three ends of the line, must be related to a common time reference in order to avoid errors caused by unsynchronisation. The technique developed to minimise such errors is described in some detail in Section 3.2.1. However, it is interesting to establish what levels of unsynchronism can be tolerated by the algorithm, if such a technique is not utilised, without unduly affecting the accuracy.

Figures 6.2 to 6.5 show the effect of nonsynchonised data from the three ends of the symmetrical system shown in Figure 6.1(a) for an a-earth, a-b-earth, a-b and three phase fault, respectively. The faults are applied at different fault locations on leg PT. It is evident from the figures that taking end P as reference, if there is a mismatch in data at ends Q and R of 1 and 2 samples respectively, then there is a slight deterioration in accuracy attained (curve ii) comparing with that for perfectly synchronised data (curve i), but is still well within the acceptable limits. However, if for some abnormal reasons, the data at end R is in unsynchronism by a large number of samples, say 5, then there is a significant increase in error (curve iii), again as shown by the figures. This clearly identifies a need for building into the algorithm a mechanism for data synchronisation before evaluating fault distances.

As mentioned in Section 5.3.1, the data synchronisation subroutine implemented in the technique described herein performs to a high degree of accuracy. For the data unsynchronised examples considered in Figures 6.2 to 6.5, the subroutine detects the mismatch of data and shifts the appropriate number of samples of voltages and currents at each end, restoring the accuracy attained to approximately the same level as that attained for the perfectly synchronised data as shown by curve (i).

6.2.2 Effect of Source Capacity

Although the actual fault location algorithm is independent of source capacities, however, it was shown in Section 5.3.6.1(d) that there is a deterioration in performance in terms of accuracy attained when a particular leg of the teed circuit is connected to a weak source. It is thus important to verify the effect of source capacity on the performance of the proposed algorithm.

The source parameters, particularly their capacities, significantly affect the fault transient waveforms. For a fault on a leg connected to a large source, the local busbar voltage is held nearly constant with little distortion. On the other hand, in the case of a small source capacity, very considerable waveform distortion occurs and the corresponding line current is significantly smaller compared with the latter, for the same type of fault. This effect is illustrated in Appendix B.

Figures 6.6 and 6.7 show the effect of source capacity on the accuracies attained for the symmetrical system shown in Figure 6.1(a). Figure 6.6 illustrates the measurement accuracies attained when the source capacity at end P is varied from a large value to a very small value. It can be clearly seen for the faults considered

(a-earth and a-b faults at 50 Km from end P) that, although the algorithm still retains an accurate evaluation of fault position, there is a clear deterioration in accuracy at low capacities, more so for the phase-phase fault. The same effect can be observed in Figure 6.7, where an a-b fault is applied at different locations of leg PT, having the source capacity at end P at 0.5 GVA, 10 GVA and 20 GVA respectively.

A weak source capacity termination, particularly for faults clear of ground, is a condition not particularly conducive to the performance of the proposed algorithm. The latter is for two main reasons:

- The magnitude of the current signals become quite low for weak source terminations. A direct consequence of this is that the effect of quantisation errors, relative to the signals, is accentuated.

- The level of distortion, particularly in the voltage waveform, as mentioned, is much higher when a line is terminated in a weak source than in a large capacity source. In this respect, it should be mentioned that although the DFT technique (as described in Section 3.2.3) is very effective in accurately extracting the fundamental phasors from the distorted waveforms, however, in the case of highly distorted waveforms, larger errors in the extracted components are inevitable.

6.2.3 Effect of Fault Resistance

It is vitally important to ascertain if the fault location estimation is significantly influenced by changes in fault resistance. A series of tests were thus realised with the proposed fault locator algorithm to examine its sensitivity to different fault resistances. Again, the simulation package described in Appendix B was used for this purpose. The fault resistance arrangements used by the simulation package for each type of fault, is also shown in Appendix B.

Table 6.1 shows the effect of fault resistance on the accuracies attained for the unsymmetrical system of the type shown in Figure 6.1(b) subjected to an a-earth and a-b-earth fault respectively, at 50 Km from end P. Table 6.2 illustrates the same effect for a three phase-earth fault at the T-point. The tests were carried out varying the fault resistance from 0 to 400 Ω for one particular type of fault. The effect of fault resistance is not studied for phase-phase faults because in practice the fault resistance for such type of faults rarely ever exceeds about 1 Ω. It is clearly evident from the tables that the fault locator gives an inherently accurate evaluation of fault position that is largely independent of the fault resistance. An extensive series of tests have shown that this is the case for all types of fault

involving a fault resistance. This is a very significant advantage over conventional techniques, particularly those based on impedance to fault measurements, which tend to produce excessive errors when dealing with resistive faults.

6.2.4 Effect of Fault Inception Angle

For the results presented hitherto, the faults have been applied either at an instant corresponding to voltage maximum or at zero voltage in the faulty phase or phases. The former of the two is the worst case from the point of view of travelling wave distortion. The other extreme, i.e. when the fault is applied at zero voltage, distortion is extremely small because there is not a large and sudden voltage change at the point of fault. The well known offset nature of the current waveforms is, however, observed [25].

It is thus important to verify the algorithm behaviour for faults at different inception angles to those studied previously. This section analyses the effect of the fault inception angle variation on the accuracies attained. Tests were performed for around-the-clock different fault inception angles ranging from 0° to 360°, in steps of 30°. Figure 6.8 shows the degree of accuracy attained for the symmetrical tee illustrated in Figure 6.1(a). The faults applied are mid-point a-earth,

a-b-earth, a-b and three phase fault respectively, on leg PT. Likewise, figure 6.9 shows the degree of accuracy attained for mid-point a-earth faults on legs PT, QT and RT respectively, for the unsymmetrical tee configuration shown in Figure 6.1(b). In common with the previous study, the results clearly show that the algorithm maintains a high degree of accuracy which is almost independent of the fault inception angle. This feature is important since in practice, faults can occur at any point on wave i.e. the fault inception angle cannot be defined in advance. The studies thus clearly demonstrate the near immunity of the fault locator algorithm to errors caused by either high frequency transients or DC offsets. This feature can be primarily attributed to the effectiveness of the DFT technique in rejecting such transients.

6.2.5 Effect of Fault Cycle

As described in Section 3.2.3, the DFT technique ignores the first cycle of post fault data for the series of tests realised hitherto, since the transients are most prominent during this period. It should be mentioned, however, that in some cases, due to extremely fast relay clearance time of the faults, only the first cycle of fault recorded information is available for the purpose of deducing the fault location. It is thus important to ascertain the algorithm behaviour for such cases.

Tables 6.3 shows the accuracies attained for different types of fault at different locations on leg PT, for the system illustrated in Figure 6.1(a), using the first and second cycle of data respectively. It is evident from the table that the global accuracies attained remain roughly the same. However, it is interesting to note that, for a three phase-earth fault, the accuracies attained are significantly better when using the first cycle of data.

6.2.6 Effect of Sample Rate

As mentioned in Section 4.4, the three phase voltage and current signals are sampled at 4 kHz at the three ends of the system. Although this sample rate can be relatively easily implemented in practice since the digital hardware to do so is readily available, nonetheless, it is interesting to verify the accuracies attained, if lower sampling frequencies of 2 kHz and 1 kHz are chosen, respectively. Tables 6.4 and 6.5 illustrate the effect of sample rate on the accuracies attained using the unsymmetrical configuration shown in Figure 6.1(b).

Table 6.4 shows the accuracies attained for an a-earth fault at different locations of leg PT for the sample rate of 4 kHz, 2 kHz and 1 kHz, respectively. Table 6.5 shows the same effect but for different types of fault

applied at the T-point. It is clearly evident that the accuracies attained for the two lower sample rates of 2 kHz and 1 kHz are little different from those attained for the higher rate of 4 kHz. This is an added advantage of the proposed algorithm since in certain applications, lower sampling rates are desirable for economic reasons due to a saving in expensive hardware.

6.2.7 Effect of Using Superimposed Components

Under normal steady-state operation, there will generally be a power flow on the line prior to a fault. This will result in the voltage sources at each end of the line being out of phase with respect to the others and consequently will affect the fault current distribution.

It has been emphasised in the previous chapters that the technique described in this thesis, makes use of superimposed components of voltages and currents rather than total values in order to eliminate errors caused by line loading. It is, therefore, interesting to verify to what degree is the accuracy affected, if total values rather than superimposed values are employed. Figures 6.10, faults on legs PT and RT, and 6.11, faults on leg QT, show the accuracies attained using total and superimposed components respectively, for an a-earth fault at different positions of the configuration shown

in Figure 6.1(b). The configuration has a significant power flow between ends. As expected, the accuracies attained using superimposed components are significantly better than those attained using total components, particularly for faults on legs QT and RT. It should be mentioned that improved performance associated with superimposed components can be wholly attributed to the fact that the steady-state power flow component responsible for the rather large errors when employing total components, is virtually non-existent in the superimposed components.

6.2.8 Performance Under External Faults

In a fault locator, although a high accuracy for internal faults is the primary concern, nonetheless, it should also be stable under external faults. For the fault locator described herein, an external fault produces an estimation which is consistently very much higher than that expected for an internal fault, results shown in Table 6.6 being a typical example. Judging from the results, it is evident that when the algorithm indicates such abnormally high values, then it can be safely assumed that the fault is external. Studies have shown that the forementioned is the case for all practically encountered external faults.

6.3 EFFECT OF SETTING PARAMETERS ON THE PROPOSED ALGORITHM

As emphasised in Chapter 4, although the proposed technique is based in Computer Aided Design (CAD) studies, practical considerations such as effect of transducers, interface modules/analog filters, quantisation, digital filtering, etc are included in the fault location process, so that the fault data processed through the algorithm is very close to that encountered in practice. With regard to the setting procedures, however, exact system data, particularly in terms of line impedance, line lengths, etc have been assumed. In practice, this will not be the case and some non-algorithmic errors due to incorrect setting are therefore inevitable.

It is thus important to determine as to what extent the proposed algorithm is sensitive to such factors. The setting parameters considered in this section are the line impedance matrix and the line lengths of the tee configuration. Tests were then carried out by deliberately introducing a ± 5% error into the forementioned parameters. A brief comment about the source capacity setting is also made.

6.3.1 Source Capacity Setting

In conventional fault locating techniques, particularly those based on impedance to fault measurements, a major source of errors in accuracy is the dependence of the algorithm on source capacity setting and therefore source impedance. In practice, this is undesirable since capacities constantly change according to changing load conditions. With regard to the technique described herein, it is very important to emphasise that the proposed algorithm, however, does not require any source impedance setting. The source independence of this method is therefore a very significant advantage over other techniques.

6.3.2 Effect of Line Impedance Matrix Error

Investigations will be carried out in this section concerning the sensitivity of the algorithm subjected to setting errors in the line impedance matrix [Z] only. The line admittance matrix [Y], that represents the effect of shunt capacitance, has a much smaller effect on accuracy (this is so because the line lengths considered here are fairly short) and the setting errors associated with this parameter will therefore be not considered here. The results are presented by introducing a deliberate ± 5% error into the magnitude and the argument of the [Z]

matrix elements and the combined effect of these two errors on the accuracy are considered.

Tables 6.7 and 6.8 show the results of [Z] matrix errors for the configuration illustrated in Figure 6.1(a) for transposed and untransposed lines respectively, subjected to an a-earth fault. The results for exact parameters, i.e. zero error case, is also shown for comparison purposes. It is clearly evident that for all the cases the fault location algorithm maintains its high degree of accuracy. This is a very important finding since as mentioned before, in practice it is never ever possible to have a precise knowledge of the line impedances.

When considering the effect of setting error on an untransposed line, it is again evident from Table 6.8 that the levels of accuracy attained are very high, but as would be expected, the errors are slightly higher than the corresponding results attained for the transposed line case. However, it should be mentioned that the additional errors introduced by the [Z] matrix setting are approximately the same for the transposed and untransposed case, being up to 0.23% for the cases shown.

It should also be mentioned that the accuracies achieved in the synchronisation, fault classification and identification of the faulted leg techniques are

matrix elements and the combined effect of these two errors on the accuracy are considered.

Tables 6.7 and 6.8 show the results of [Z] matrix errors for the configuration illustrated in Figure 6.1(a) for transposed and untransposed lines respectively, subjected to an a-earth fault. The results for exact parameters, i.e. zero error case, is also shown for comparison purposes. It is clearly evident that for all the cases the fault location algorithm maintains its high degree of accuracy. This is a very important finding since as mentioned before, in practice it is never ever possible to have a precise knowledge of the line impedances.

When considering the effect of setting error on an untransposed line, it is again evident from Table 6.8 that the levels of accuracy attained are very high, but as would be expected, the errors are slightly higher than the corresponding results attained for the transposed line case. However, it should be mentioned that the additional errors introduced by the [Z] matrix setting are approximately the same for the transposed and untransposed case, being up to 0.23% for the cases shown.

It should also be mentioned that the accuracies achieved in the synchronisation, fault classification and identification of the faulted leg techniques are

maintained in the presence of the setting errors in the [Z] matrix.

6.3.3 Effect of Line Length Setting Errors

The effect of line length errors on the accuracy attained is analysed in this section. Line lengths up to the T-point (L_P, L_Q and L_R) are subjected to a ± 5% error and a combination of such setting errors are fed into the algorithm. Tables 6.9 illustrates the results of the line length setting errors for the symmetrical configuration shown in Figure 6.1(a) with transposed lines, subjected to an a-earth fault at 1 Km, 50 Km and 100 Km from end P respectively. Table 6.10 show the same effect for the unsymmetrical configuration shown in Figure 6.2(b) with untransposed lines.

It can be seen from the tables that the algorithm is significantly affected by the line length setting errors. However, it is evident that the errors are more prominent for a fault at the T point, introducing up to ± 5% error in the fault locator estimation . On the other hand, for faults at 1 Km from end P, only up to approximately ± 0.8% error is introduced, considering the transposed and untransposed cases for the two configurations. It is thus apparent that as the fault position moves from that close to end P to the T-point, the measurement accuracies

attained become progressively worse, the error reaching a high of 5% for the T-point.

Once again, accuracies attained by synchronisation, fault classification and identification of the faulted leg techniques are not affected.

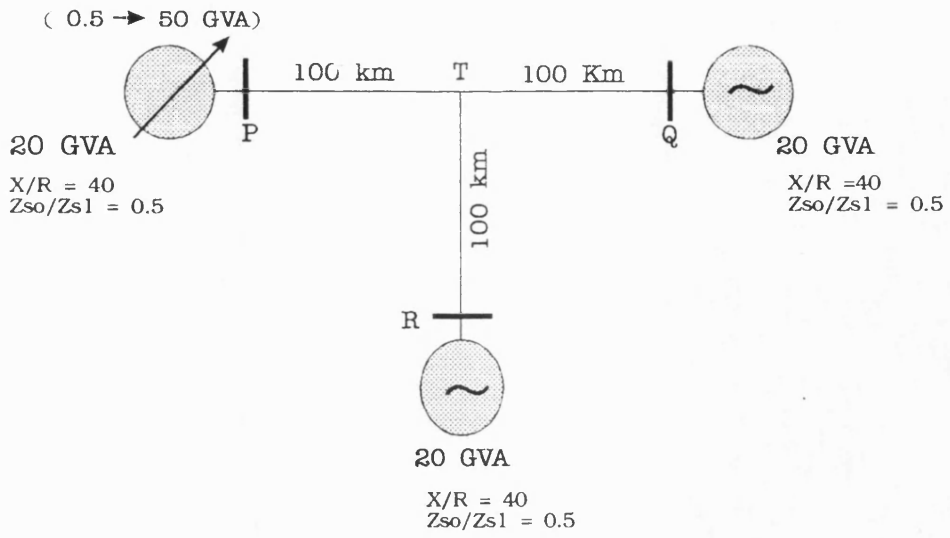

(a)

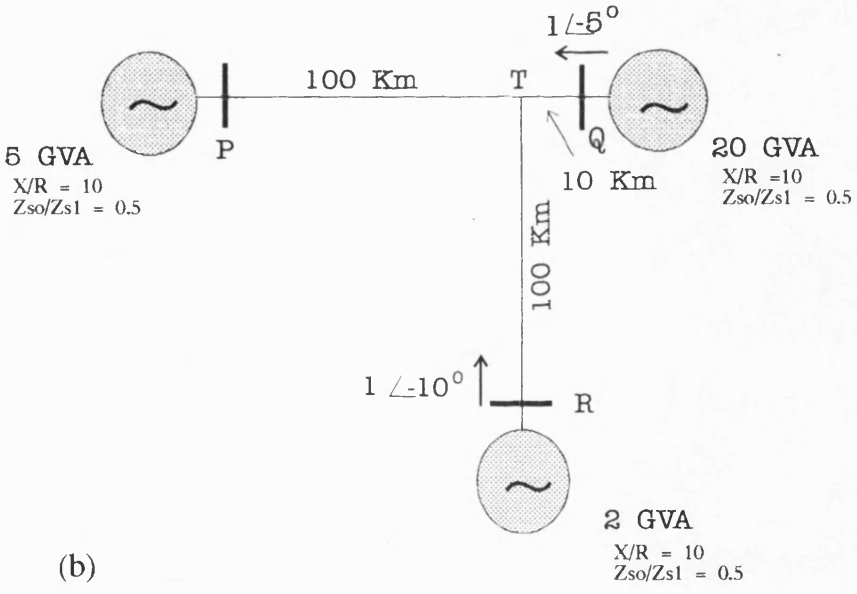

(b)

Figure 6.1 Teed configurations studied

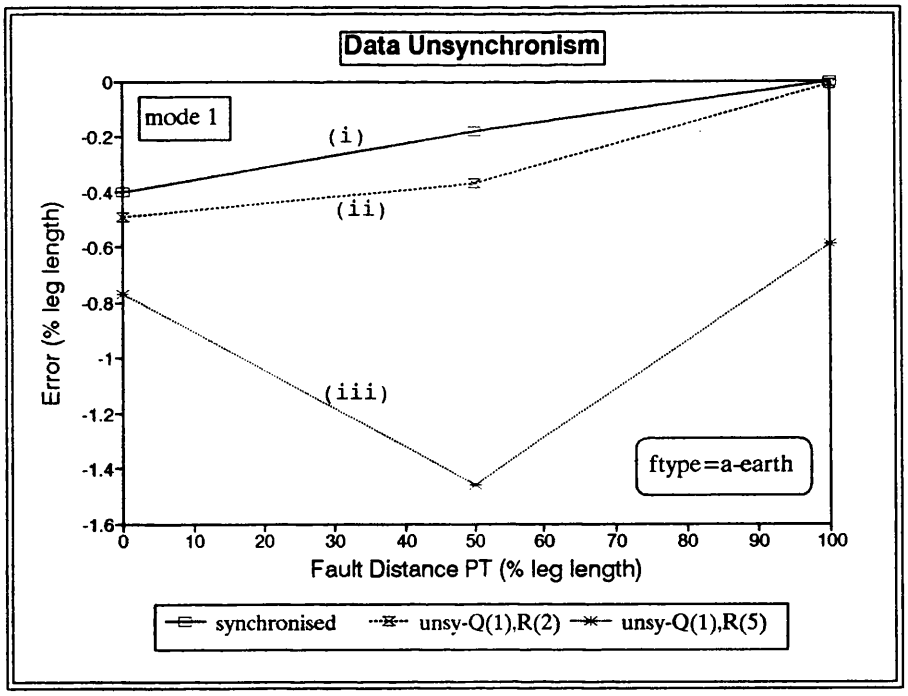

Figure 6.2 Effect of data unsynchronism on the locator's accuracy for a symmetrical system, subjected to an a-earth fault.(Rf=10 Ω)

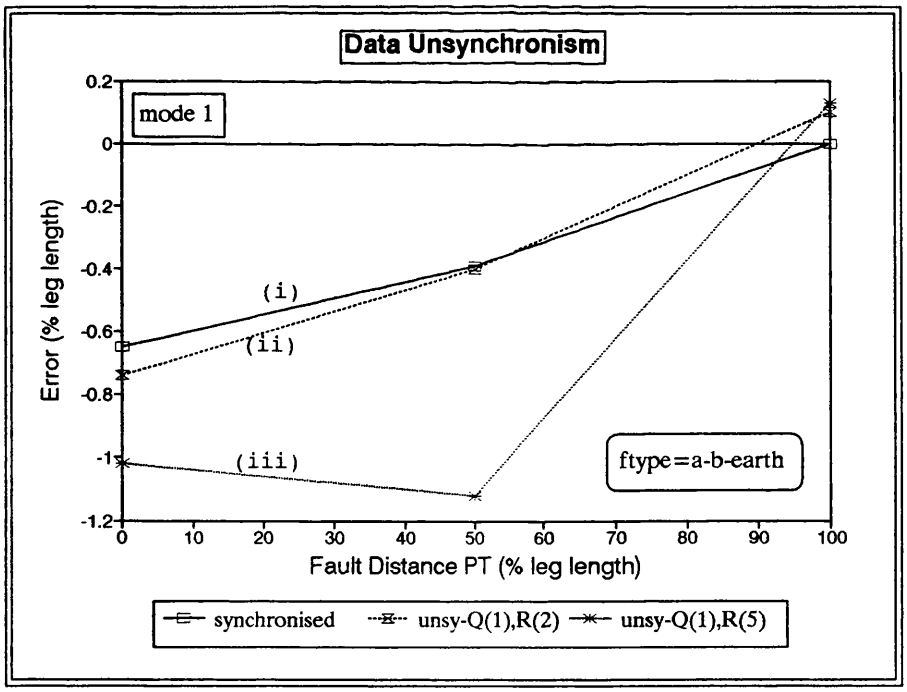

Figure 6.3 Effect of data unsynchronism on the locator's accuracy for a symmetrical system, subjected to an a-b-earth fault.(Rf=10Ω)

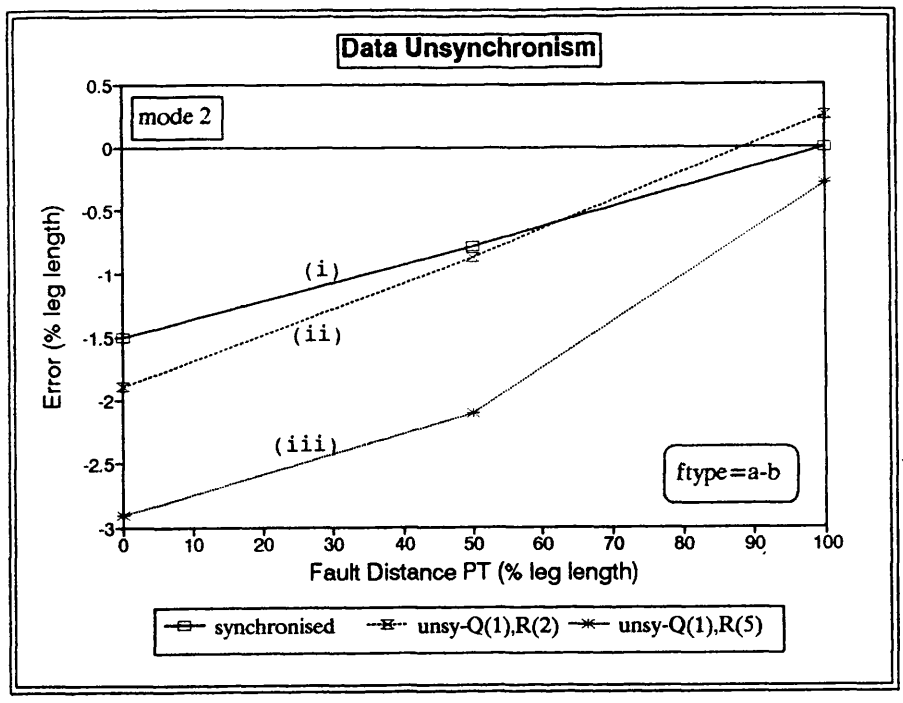

Figure 6.4 Effect of data unsynchronism on the locator's accuracy for a symmetrical system, subjected to an a-b fault.(Rf=10 Ω)

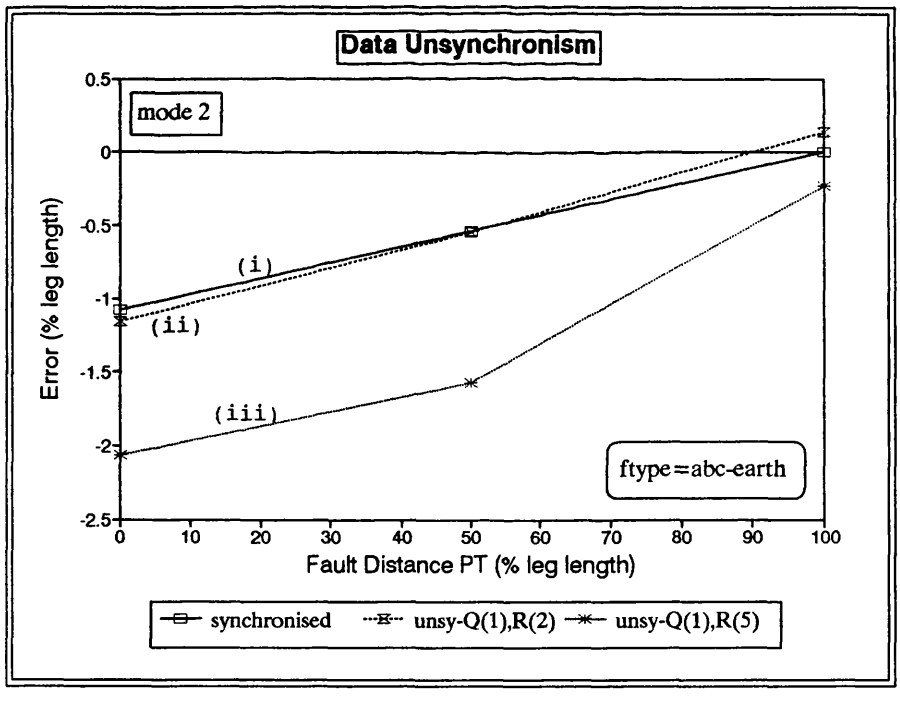

Figure 6.5 Effect of data unsynchronism on the locator's accuracy for a symmetrical system, subjected to an three phase fault.(Rf=10Ω)

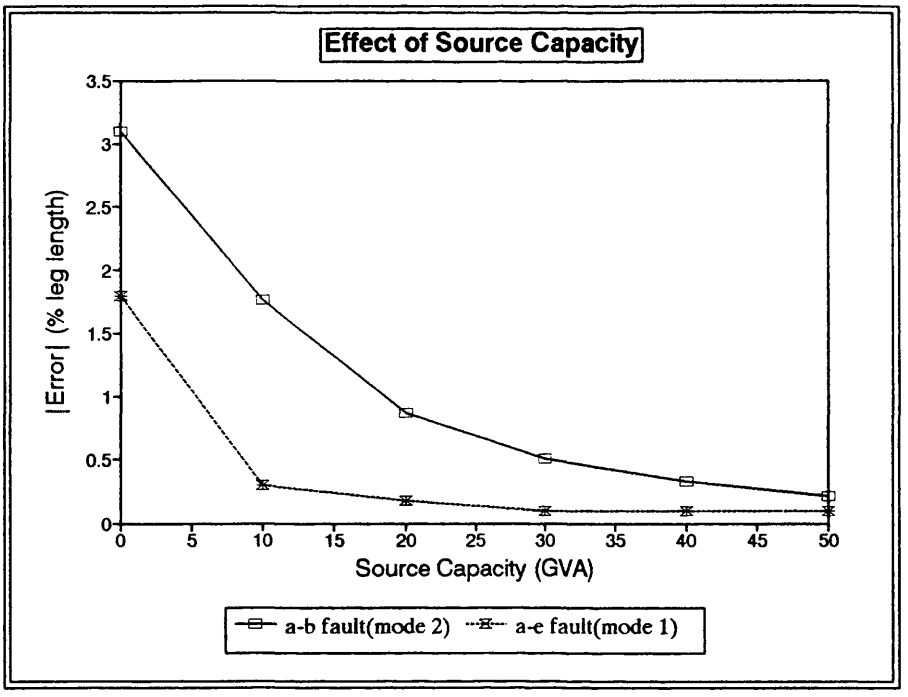

Figure 6.6 Effect of source capacity on the locator's accuracy for an a-b and a-earth fault.(Rf=10 Ω)

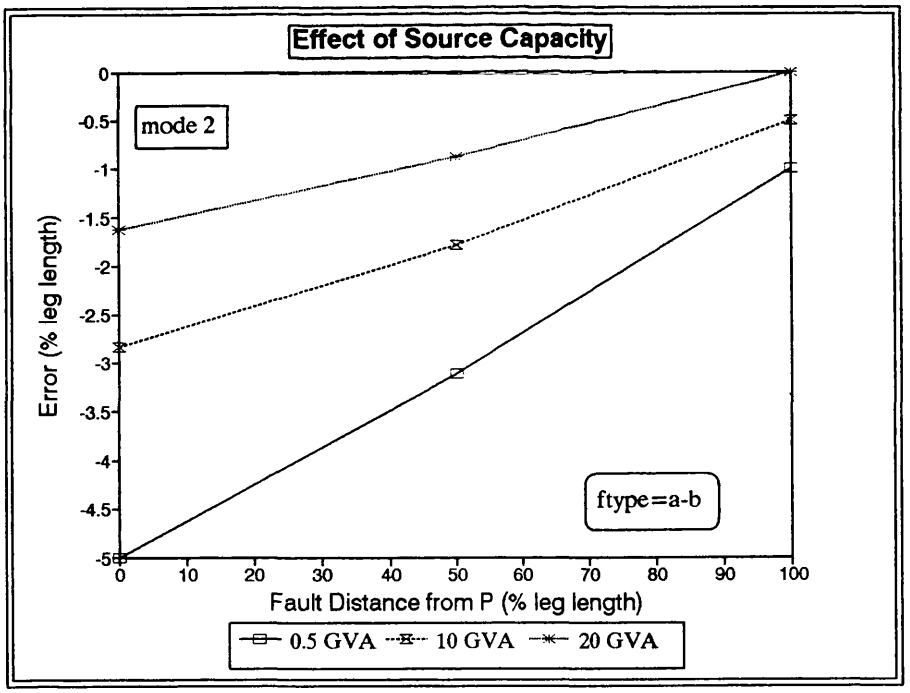

Figure 6.7 Effect of source capacity on the locator's accuracy for a symmetrical system, subjected to an a-b-earth fault.(Rf=0Ω)

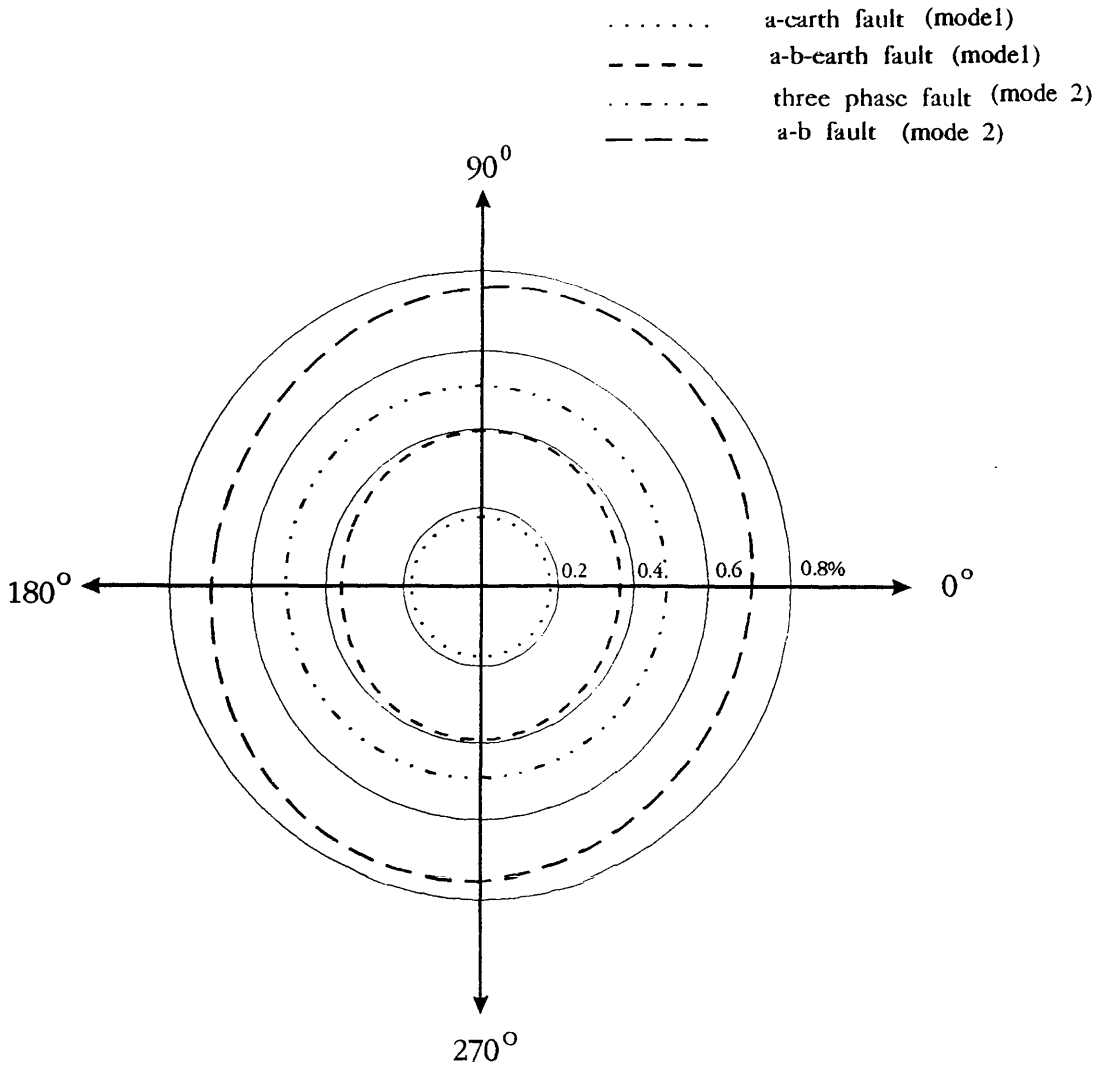

Figure 6.8 Effect of fault inception angle on measurement accuracy, for the symmetrical system, subjected to different types of fault.(Rf = 10 Ω)

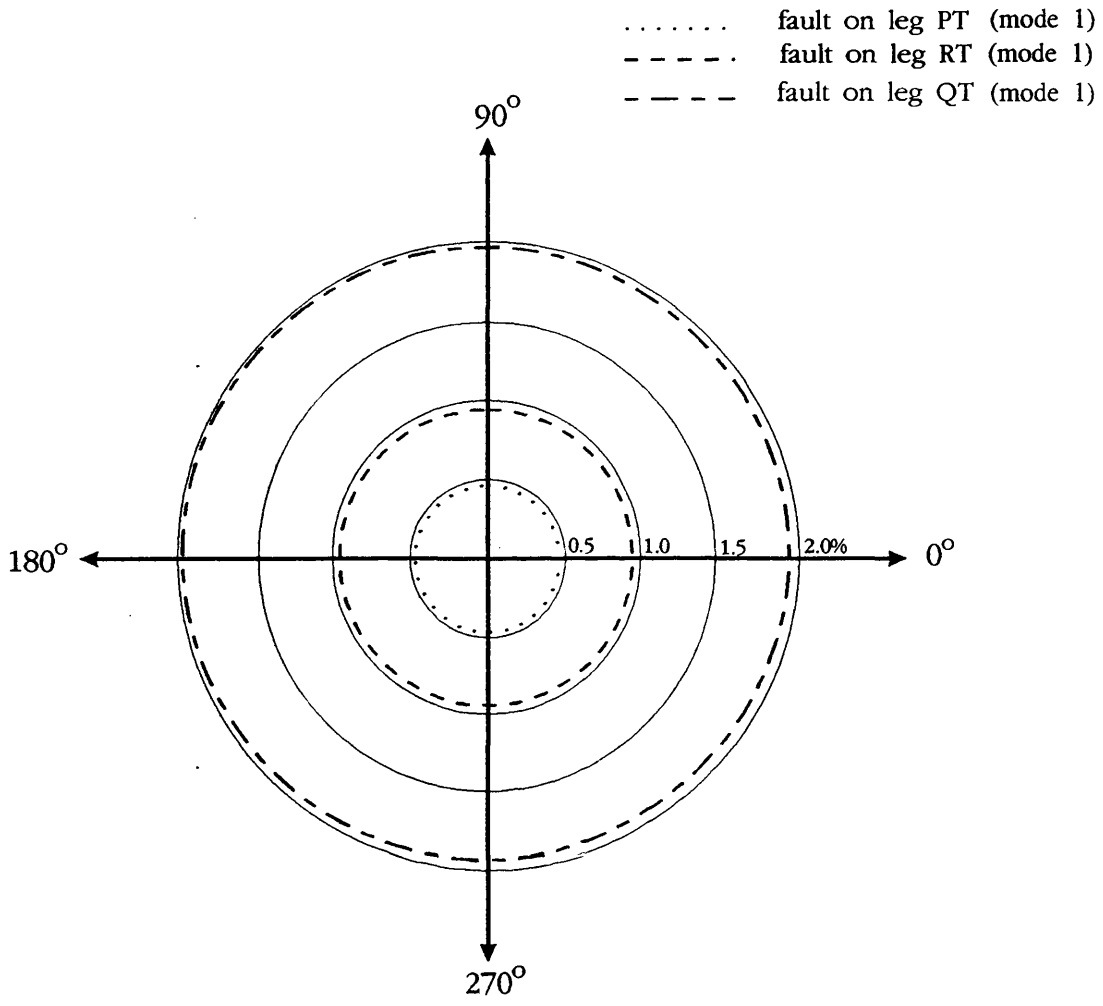

Figure 6.9 Effect of fault inception angle on measurement accuracy for the unsymmetrical system. (Rf = 60 Ω)

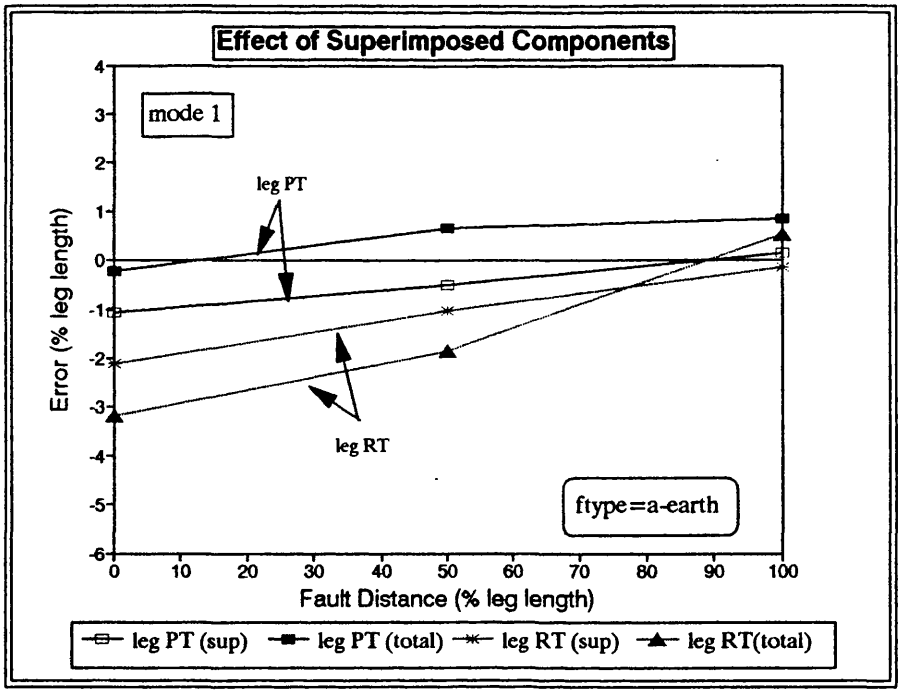

Figure 6.10 Effect of using total and superimposed components on the locator's accuracy, for an unsymmetrical system. (legs PT and RT)

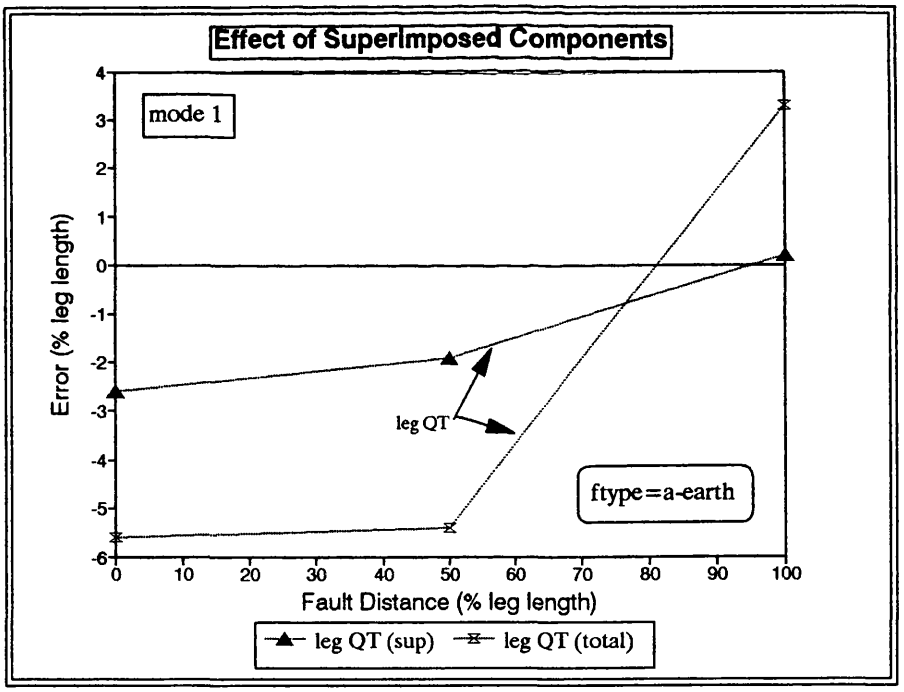

Figure 6.11 Effect of using total and superimposed components on the locator's accuracy for an unsymmetrical system. (leg QT)

actual dist. from P (Km)	Rf (Ω)	a-earth fault (mode 1)		a-b-earth fault (mode 1)	
		Distance Estimation		Distance Estimation	
		dist(Km)	Error(%)	dist(Km)	Error(%)
50	0	49.48	-0.52	49.33	-0.67
50	20	49.52	-0.48	49.00	-1.00
50	40	49.52	-0.48	49.03	-0.97
50	60	49.52	-0.48	49.06	-0.94
50	80	49.52	-0.48	49.07	-0.93
50	100	49.52	-0.48	49.08	-0.92
50	200	49.59	-0.41	49.10	-0.90
50	300	49.41	-0.59	49.11	-0.89
50	400	49.17	-0.83	49.12	-0.88

Table 6.1 Effect of fault resistance on the fault locator's accuracy, for the nonsymmetrical system, subjected to an a-earth and a-b-earth fault.

actual dist. from P (Km)	Rf (Ω)	Distance Estimation three phase-earth fault (mode 2)	
		dist(Km)	Error(%)
100	0	100.57	0.57
100	20	100.25	0.25
100	40	100.25	0.25
100	60	100.26	0.26
100	80	100.28	0.28
100	100	100.23	0.23
100	200	100.30	0.30
100	300	100.30	0.30
100	400	100.15	0.15

Table 6.2 Effect of fault resistance on the fault locator's accuracy, for the nonsymmetrical system, subjected to a three phase-earth fault.

actual dist. from P(Km)	fault type	Rf (Ω)	mode	First Cycle		Second Cycle	
				Distance Estimation		Distance Estimation	
				dist-Km	Er(%)	dist-Km	Er(%)
1	a-e	60	md 1	0.45	-0.55	0.62	-0.38
50	a-e	60	md 1	49.64	-0.36	49.82	-0.18
100	a-e	60	md 1	100.00	0.00	100.00	0.00
1	a-b-e	10	md 1	0.48	-0.52	0.35	-0.65
25	a-b-e	10	md 1	24.63	-0.37	24.45	-0.55
50	a-b-e	10	md 1	49.79	-0.21	49.61	-0.39
75	a-b-e	10	md 1	74.87	-0.13	74.81	-0.19
100	a-b-e	10	md 1	100.00	0.00	100.00	0.00
1	a-b-c-e	10	md 2	1.08	0.08	-0.08	-1.08
50	a-b-c-e	10	md 2	50.09	0.09	49.47	-0.53
100	a-b-c-e	10	md 2	100.00	0.00	100.00	0.00
1	a-b	10	md 2	-0.43	-1.43	-0.50	-1.50
50	a-b	10	md 2	49.03	-0.97	49.22	-0.78
100	a-b	10	md 2	100.00	0.00	100.00	0.00

Table 6.3 Effect of fault cycle on fault locator's accuracy.

actual dist. from P(Km)	fault type	Rf (Ω)	samp rate (kHz)	Distance Estimation (mode 1)	
				dist-Km	Er(%)
1	a-e	60	4	-0.06	-1.06
50	a-e	60	4	49.49	-0.51
100	a-e	60	4	100.15	0.15
1	a-e	60	2	-0.06	-1.06
50	a-e	60	2	49.48	-0.52
100	a-e	60	2	100.17	-0.17
1	a-e	60	1	-0.02	-1.02
50	a-e	60	1	49.49	-0.51
100	a-e	60	1	100.16	0.16

Table 6.4 Effect of sample rate on the fault locator's accuracy, for the unsymmetrical system, subjected to an a-earth fault at different positions of leg PT.

actual dist from P(Km)	fault type	Rf (Ω)	mode	samp rate (kHz)	Distance Estimation	
					dist-Km	Er(%)
100	a-b	60	md 2	4	100.28	0.28
100	a-b-e	60	md 1	4	100.25	0.25
100	a-b-c	60	md 2	4	100.49	0.49
100	a-b	60	md 2	2	100.29	0.29
100	a-b-e	60	md 1	2	100.26	0.26
100	a-b-c	60	md 2	2	100.49	0.49
100	a-b	60	md 2	1	100.32	0.32
100	a-b-e	60	md 1	1	100.28	0.28
100	a-b-c	60	md 2	1	100.48	0.48

Table 6.5 Effect of sample rate on the fault locator's accuracy, for the unsymmetrical system, subjected to different types of fault at T-point.

Distance Estimation (Km)			
	mode 1	**mode 2**	**mode 3**
Near end P	-1077	-1257	1442
Near end Q	-1008	-1132	1250
Near end R	-1192	-1380	1380

Table 6.6 Performance for an a-earth external fault.

actual dist. from P (Km)	Rf (Ω)	[Z] Error (%)		Distance Estimation (mode 1)	
		mag	arg	dist-Km	Er(%)
1	10	0	0	0.91	-0.09
50	10	0	0	49.97	-0.03
100	10	0	0	100.00	0.00
1	10	+5	0	1.11	0.11
50	10	+5	0	50.05	0.05
100	10	+5	0	100.00	0.00
1	10	-5	0	0.68	-0.32
50	10	-5	0	49.85	-0.15
100	10	-5	0	100.00	0.00
1	10	0	+5	0.90	-0.10
50	10	0	+5	49.95	-0.05
100	10	0	+5	100.00	0.00
1	10	0	-5	0.94	-0.06
50	10	0	-5	49.97	-0.03
100	10	0	-5	100.00	0.00
1	10	5	+5	1.10	0.10
50	10	5	+5	50.04	0.04
100	10	5	+5	100.00	0.00
1	10	5	-5	1.14	0.14
50	10	5	-5	50.06	0.06
100	10	5	-5	100.00	0.00

Table 6.7 Effect of the line impedance matrix errors on the locator's accuracy, for a transposed symmetrical configuration, subjected to an a-earth fault.

actual dist. from P (Km)	Rf (Ω)	[Z] Error (%)		Distance Estimation (mode 1)	
		mag	arg	dist-Km	Er(%)
1	10	0	0	0.61	-0.39
50	10	0	0	49.82	-0.18
100	10	0	0	100.00	0.00
1	10	+5	0	0.81	-0.19
50	10	+5	0	49.91	-0.09
100	10	+5	0	100.00	0.00
1	10	-5	0	0.38	-0.62
50	10	-5	0	49.71	-0.29
100	10	-5	0	100.00	0.00
1	10	0	+5	0.60	-0.40
50	10	0	+5	49.81	-0.19
100	10	0	+5	100.00	0.00
1	10	0	-5	0.64	-0.36
50	10	0	-5	49.83	-0.17
100	10	0	-5	100.00	0.00
1	10	+5	+5	0.81	-0.19
50	10	+5	+5	49.91	-0.09
100	10	+5	+5	100.00	0.00
1	10	+5	-5	0.84	-0.16
50	10	+5	-5	49.93	-0.07
100	10	+5	-5	100.00	0.00

Table 6.8 Effect of the line impedance matrix errors on the locator's accuracy, for a untransposed symmetrical configuration, subjected to an a-earth fault.

L Error (%)			1 km (mode 1)		50 km (mode 1)		T-point (mode 1)	
			Distance Estimation		Distance Estimation		Distance Estimation	
LP	LQ	LR	dist-Km	Er(%)	dist-Km	Er(%)	dist-Km	Er(%)
0	0	0	0.91	-0.09	49.97	-0.03	100.00	0.00
+5	0	0	1.08	0.08	51.68	1.68	103.33	3.33
-5	0	0	0.73	-0.27	48.22	-1.78	96.67	-3.33
0	+5	0	0.90	-0.10	49.94	-0.06	100.00	0.00
+5	+5	0	1.08	0.08	51.67	1.67	103.33	3.33
-5	+5	0	0.73	-0.27	48.21	-1.79	96.67	-3.33
0	-5	0	0.91	-0.09	49.96	-0.04	100.0	0.00
+5	-5	0	1.08	0.08	51.69	1.69	103.33	3.33
-5	-5	0	0.73	-0.27	48.23	-1.77	96.67	-3.33
0	0	+5	0.99	-0.01	50.81	0.81	101.67	1.67
+5	0	+5	1.16	0.16	52.54	2.54	105.00	5.00
-5	0	+5	0.82	-0.18	49.08	-0.92	98.33	-1.67
0	+5	+5	0.99	-0.01	50.80	0.80	101.67	1.67
+5	+5	+5	1.16	0.16	52.53	2.53	105.00	5.00
-5	+5	+5	0.82	-0.18	49.08	-0.92	98.33	-1.67
0	-5	+5	0.99	-0.01	50.82	0.82	101.67	1.67
+5	-5	+5	1.17	0.17	52.55	2.55	105.00	5.00
-5	-5	+5	0.82	-0.18	49.09	-0.91	98.33	-1.67
0	0	-5	0.82	-0.18	49.09	-0.91	98.33	-1.67
+5	0	-5	0.99	-0.01	51.08	1.08	101.67	1.67
-5	0	-5	0.65	-0.35	47.36	-2.64	95.00	-5.00
0	+5	-5	0.82	-0.18	49.08	-0.92	98.33	-1.67
+5	+5	-5	0.99	-0.01	50.81	0.81	101.67	1.67
-5	+5	-5	0.65	-0.35	47.35	-2.65	95.00	-5.00
0	-5	-5	0.82	-0.18	49.10	-0.90	98.33	-1.67
+5	-5	-5	1.00	0.00	50.83	0.83	101.67	1.67
-5	-5	-5	0.65	-0.35	47.37	-2.63	95.00	-5.00

Table 6.9 Effect of line length setting errors on the locator's accuracy, for a transposed symmetrical configuration, subjected to an a-earth fault. ($Rf = 10\Omega$)

L Error (%)			1 Km (mode 1)		50 Km (mode 1)		T-point (mode 1)	
			Distance Estimation		Distance Estimation		Distance Estimation	
LP	LQ	LR	dist-Km	Er(%)	dist-Km	Er(%)	dist-Km	Er(%)
0	0	0	-0.05	-1.05	49.52	-0.48	100.14	0.14
+5	0	0	0.64	-0.36	52.10	2.10	104.64	4.64
-5	0	0	-0.74	-1.74	46.94	-3.06	95.63	-4.37
0	+5	0	-0.05	-1.05	49.52	-0.48	100.14	0.14
+5	+5	0	0.64	-0.36	52.10	2.10	104.64	4.64
-5	+5	0	-0.74	-1.74	46.94	-3.06	95.63	-4.37
0	-5	0	-0.05	-1.05	49.52	-0.48	100.14	0.14
+5	-5	0	0.64	-0.36	52.10	2.10	104.64	4.64
-5	-5	0	-0.74	-1.74	46.94	-3.06	95.63	-4.37
0	0	+5	0.01	-0.99	49.75	-0.25	100.54	0.54
+5	0	+5	0.70	-0.30	52.33	2.33	105.5	5.05
-5	0	+5	-0.68	-1.68	47.17	-2.83	96.04	-3.96
0	+5	+5	0.01	-0.99	49.75	-0.25	100.54	0.54
+5	+5	+5	0.70	-0.30	52.33	2.33	105.05	5.05
-5	+5	+5	-0.68	-1.68	47.17	-2.83	96.04	-3.96
0	-5	+5	0.01	-0.99	49.75	-0.25	100.54	0.54
+5	-5	+5	0.70	-0.30	52.33	2.33	105.05	5.05
-5	-5	+5	-0.68	-1.68	47.17	-2.83	96.04	-3.96
0	0	-5	-0.11	-1.11	49.29	-0.71	99.73	-0.27
+5	0	-5	0.58	-0.42	51.87	1.87	104.24	4.24
-5	0	-5	-0.80	-1.80	46.71	-3.29	95.23	-4.77
0	+5	-5	-0.11	-1.11	49.29	-0.71	99.73	-0.27
+5	+5	-5	0.58	-0.42	51.87	1.87	104.24	4.24
-5	+5	-5	-0.80	-1.80	46.71	-3.29	95.23	-4.77
0	-5	-5	-0.11	-1.11	49.29	-0.71	99.73	-0.27
+5	-5	-5	0.58	-0.42	51.87	1.87	104.24	4.24
-5	-5	-5	-0.80	-1.80	46.71	-3.29	95.23	-4.77

Table 6.10 Effect of line length setting errors on the locator's accuracy, for a untransposed unsymmetrical configuration, subjected to an a-earth fault.($Rf=10\Omega$)

CHAPTER 7

SUMMARY, CONCLUSIONS AND SUGGESTIONS FOR FUTURE WORK

7.1 SUMMARY OF WORK

This thesis presents an alternative approach to accurately locating faults on three-terminal lines. The technique addresses some of the common problems in fault location and can be applied in a whole variety of practically encountered systems and fault conditions, without sacrificing the high accuracy requirements.

A general literature review of fault locator techniques for transmission lines has been outlined in Chapter 2. They are initially divided into two groups : (i) techniques for two terminal lines and (ii) techniques for three-terminal lines. The first group is subdivided into algorithms which use data from one end of the system only and those that employ data from the two ends. The second group is concerned with outlining the limited number of techniques developed for fault location on three-terminal configurations, hitherto. The advantages and limitations of using each of the methods are also summarised.

The basis of the proposed fault locator has been presented in Chapter 3. The method is based on utilising voltage and current waveforms at all three ends of typical EHV teed feeders, which are then filtered using Discrete Fourier Transform (DFT) techniques, so as to produce a measure of the steady state frequency voltage and current phasors. The technique described makes use of superimposed, modal components of voltages and current phasors for the calculation of the fault distance. The basis of accurate and effective techniques for the synchronisation of data from the three ends, fault inception time identification, fault classification and identification of the faulted leg have also been presented as part of the fault location process.

A fault transient simulation package for three terminal lines, developed at University of Bath, has been utilised for testing the proposed algorithm. As has been emphasised in Chapter 4, although the fault location technique is based on Computer Aided Design (CAD) studies, however, practical considerations such as the effect of transducers, interface modules/analog filters, quantisation errors, etc on primary system fault data are also included in the simulation, so that the data processed through the algorithm is very close to that attained from actual fault recorders.

Chapter 5 shows the performance of the fault locator algorithm when applied to some typical system

configurations as encountered in practice. Some of the configurations studied are the symmetrical and nonsymmetrical tee of the type shown in Figure 5.1. The effect of feed around paths on accuracy, for both the symmetrical and nonsymmetrical systems, are also analysed. Finally, the performance for a double circuit tee is presented. Performance relating to accuracies attained at different stages of the algorithm such as synchronisation of data, DFT filtering, fault classification, faulted leg identification and fault distance calculation are then presented.

An overall performance evaluation of the fault locator algorithm under different fault conditions is presented in Chapter 6. In particular, the effect of data unsynchronism, differing source capacities, fault resistance, fault inception angle, fault cycle, sample rate and superimposed components on the accuracy attained are examined. Finally, a sensitivity analysis of the fault locator algorithm is also presented in Chapter 6.

7.2 CONCLUSIONS

The basis of an alternative approach for accurately locating faults on teed feeders has been described in this thesis. The fault locator algorithm is based on superimposed, modal signals and special filtering

techniques are developed to accurately extract the fundamental phasors from the signals. These, together with an effective data synchronising facility, fault classification and a method for an accurate identification of the faulted leg of the tee, has culminated in a fault locator design that gives a high degree of accuracy for a majority of practically encountered systems and fault conditions.

As mentioned above, the algorithm makes use of modal signals with the purpose of eliminating the mutual coupling effects inherent in a multiphase system. The transformation matrices [Q] and [S], used in the algorithm for obtaining the modal values (Section 3.2.6), are computed from the line series impedance and shunt admittance matrices ([Z], [Y]) and these are in turn computed from a knowledge of the line conductor geometry, earth plane resistivity and the conductor parameters. In this respect it should be mentioned that, for an untransposed line, these matrices have complex elements, making it difficult to evaluate the modal quantities in practice. Moreover, the matrices need to be evaluated for each line application and then set into the locator. On the other hand, for transposed lines, irrespective of the line geometry, the transformation matrices [Q] and [S] take the simplified form given in equation (3.29), having scalar quantities only. Thus, in order to considerably simplify the processing and overcome the forgoing practical problem, for the technique described herein,

perfect line transposition has been assumed when setting the parameters into the fault locator for all the cases tested. It is clearly demonstrated that the accuracy is not unduly affected by this supposition when dealing with untransposed lines for the cases studied.

Three independent mode signals are then formed as combinations of the phase quantities: an Earth mode (mode 1) and two Aerial modes (modes 2 and 3). It is clearly shown that for single circuit vertical construction lines, of the type shown in Figure 5.1(a) and (b), a higher degree of accuracy is attained when using Earth mode based signals rather than the two Aerials for faults involving earth such as single-phase earth and double-phase earth. However, for faults clear of ground or three phase faults, Aerial modes have to be used due to absence of the Earth mode for such faults. In the technique described herein, the algorithm is thus applied to all three modes and the presence of a significant level of residual current being used to identify the existence of a fault involving earth. The fault classification subroutine, incorporated into the algorithm, is utilised for the latter purpose. However, with regard to a double tee circuit with untransposed lines of the type illustrated in Figure 5.2(a), when using data only from the faulted circuit, it is found that Aerial modes (modes 2 and 3) are always more accurate than Earth mode, for all types of fault.

It has been observed that for the majority of cases studied, especially for single-circuit configurations, the maximum error is attained for faults close to the terminal ends P, Q and R for all types of fault. It is also evident from the results that the best accuracies are always found for single-phase to earth faults when compared to other types.

The algorithm has been tested for some typical vertical configurations encountered in practice, illustrated in Figure 5.1. The first one considered is the symmetrical tee with equal lengths to the T-point and equal source capacity terminations, with transposed and untransposed lines respectively. Nonsymmetrical source capacities are also considered for the same symmetrical configuration. It is found that the algorithm has the ability to retain a high degree of accuracy for the symmetrical configuration under different types of fault.

In order to demonstrate the flexibility of the proposed algorithm for a more complicated system, a nonsymmetrical vertical configuration with differing source capacities and line lengths up to the T-point, of the type shown in Figure 5.1(b), is also analysed. It is apparent from the results attained that the percentage error for the unsymmetrical system is greater than that attained for the symmetrical system considered previously, under similar faults. The results also show that, for the different types of fault analysed, the

worst performance is attained for faults on leg QT, which is substantially shorter than the other two. A limited study is also presented for the unsymmetrical system with horizontal construction lines and in this case, it is found that the degree of accuracy attained for such lines is higher than that for the vertical construction, for the same fault conditions. This is due to the greater symmetry associated with the former .

In teed circuits, it is fairly common to have tenuous feed-around-paths as illustrated in Figure 5.1(c) and (d), which can result in an over distance calculation, particularly in conventional impedance measurements techniques. However, the proposed technique interestingly gives a better performance than that attained in the absence of the out-feed, particularly for faults on the legs connected via the out-feed.

Finally, the performance of the proposed fault locator is presented for a double circuit tee of the type illustrated in Figure 5.2(a), using data from the faulted circuit only. The lines are untransposed and assumed transposed parameters are again assumed. Studies clearly show that the degree of accuracy attained for double circuit lines (using Aerial modes, as explained earlier) is generally higher than that for the single circuit lines for the same types of fault. It is also apparent that, again, like the results for the single circuit line, the shortest leg QT presents an inferior

performance when compared with the other two legs. The case of a single tee connected into a adjacent double circuit line, as shown in Figure 5.2(b), is also analysed. The algorithm copes admirably well with this configuration and for most cases the accuracies are little different from those attained for the double circuit tee.

In summary, the results clearly demonstrate that the proposed algorithm retains its high accuracy for distance estimation for a variety of configurations presented in Chapter 5, the magnitude of errors in terms of accuracy being less than about 3% for most of the fault conditions studied. High accuracy is also found for the subroutines for data synchronisation, fault inception time identification, fault classification and identification of the faulted leg.

The second part of the tests are concerned with presenting the performance evaluation of the proposed algorithm under different fault conditions. The symmetrical and unsymmetrical systems previously described, with untransposed lines, are again considered. The effect of data unsynchronism on the fault locator's accuracy in the absence of data synchronisation technique, is analysed in the first instance. The purpose of this exercise is to establish what levels of unsynchronism can be tolerated by the algorithm, without unduly affecting the accuracy. In this respect, it is

shown that, considering the symmetrical system, if there is a small mismatch in data amongst the three ends (1 sample at end Q and two samples at end R, with respect to end P), then there is a slight deterioration in accuracy attained. If, however, for some abnormal reasons, the mismatch is by a large number of samples (say 1 at end Q and 5 at end R), then there is a significant increase in error. This identifies a need for building into the algorithm a mechanism for data synchronisation, of the type developed in the thesis, before evaluating fault distances. With the latter included in the algorithm, it is illustrated that the proposed synchronisation subroutine, performs to a high degree of accuracy. The subroutine detects the mismatch of data and then shifts the appropriate number of samples of voltages and currents at each end, in order to synchronise the data and consequently maximise the accuracy attained.

Although the fault location algorithm presents an acceptable degree of accuracy independent of the source capacities, however, it has been found that there is a deterioration in the locator's performance when a particular leg of the teed circuit is connected to a weak source. This can be attributed to the accentuation of quantisation errors for such a source as well as to the increment in the level of distortion, particularly in the faulted voltage waveforms, introducing larger errors in the extracted fundamental components via the DFT technique.

It is also shown that the fault locator gives an inherently accurate evaluation of fault position that is not significantly influenced by changes in fault resistance and fault inception angle. The former is a very significant advantage over conventional techniques, particularly those based on impedance to fault measurements, which tend to produce excessive errors when dealing with resistive faults.

The DFT technique, as implemented in the proposed fault locator, ignores the first cycle of post fault data, since the transients are more prominent during this period. However, in some cases, due to extremely fast relay clearance time, it is possible that the second cycle may not be available and the algorithm thus has to rely on making use of the first cycle of post fault recorded data information. In the technique described herein, it is shown that in such cases, the global accuracies attained remain roughly the same as those attained when there is more of the fault recorded information available.

The effect of using different sample rates, other than 4 kHz, are also analysed. It is clearly shown that accuracies attained for the two lower sample rates of 2 kHz and 1 kHz respectively are little different from those attained for the higher rate of 4 kHz. This is an added advantage of the proposed algorithm since, in

certain applications, lower sampling rates are desirable e.g. for economic reasons.

As emphasised, for the technique described in this thesis, use is made of superimposed components of voltages and currents rather than total values in order to eliminate errors caused by line loading. In this respect, the results presented clearly show that, as expected, accuracies attained using superimposed components are significantly better than those attained using total components. The improved performance associated with superimposed components can be wholly attributed to the fact that the steady state power flow component responsible for the rather large errors when employing total components, is virtually non-existent in the superimposed components.

For the fault locator described, an external fault always produces an estimation which is consistently very much higher than that expected for a internal fault. This very important feature of the algorithm makes it totally immune to any maloperation for external faults.

The final phase of the tests is dedicated to a sensitivity analysis of the proposed algorithm. Although all the results presented are based on assuming perfect setting data into the algorithm, however, in practice there are always small errors in data available and these can affect the fault locator's accuracy. It is thus

important to exercise the effect on accuracy due to incorrect settings. The setting parameters considered are the line impedance matrix and the line lengths of the teed configuration. Tests are then carried out by deliberately introducing a ± 5% error into the forementioned parameters.

Setting errors are considered in the line impedance matrix [Z] only. The line admittance matrix [Y], that represents the effect of shunt capacitance, has a much smaller effect on accuracy and the setting errors associated with this parameter is therefore not considered. It is shown that, in the case of transposed and untransposed lines, the fault location algorithm maintains its high degree of accuracy subjected to setting errors in the impedance matrix. For the tests realised, a ± 5% error in the [Z] matrix resulted in a maximum of only ± 0.23% additional error in the accuracies attained. This is a very important finding, since, as mentioned before, in practice it is never ever possible to have a precise knowledge of such a parameter.

The effect of line length errors on the accuracy attained is also analysed. Line lengths up to the T-point are subjected to, again, ± 5% error and a combination of such setting errors is then fed into the algorithm. It is shown that the algorithm is significantly affected by the line length setting errors. In particular, it is shown that as the fault position moves from that close to end P

to the T-point, the measurement accuracies attained become progressively worse. For the examples shown, considering transposed and untransposed cases for the symmetrical and unsymmetrical configurations, only up to ± 0.8% error is introduced for a fault close to end P. On the other hand, error reaches a high of ± 5% for faults at the T-point.

It is found that the accuracies achieved in the synchronisation, fault classification and identification of the faulted leg techniques are maintained in the presence of the setting errors in the [Z] matrix and line lengths.

Finally, it is important to mention that the proposed algorithm does not require any source impedance setting, and therefore any inaccuracies (or changes) in source parameters are of no consequence to this technique. This is thus a very significant advantage over other techniques.

7.3 SUGGESTIONS FOR FUTURE WORK

(a) Testing the proposed algorithm with data from real systems

As emphasised in the thesis, an extensive series of tests have been realised to ascertain the accuracy of the proposed algorithm under different systems and fault conditions, using a fault transient simulation package. Many more such tests can be performed, but very likely the ones realised hitherto in this work are conclusive for this part of the research work. As a next logical step, the algorithm should be tested by input data captured from real systems. A prototype fault locator should then be implemented for such tests as a follow up.

(b) Back-up fault locator for three terminal lines using data from one end only

As emphasised earlier, the proposed algorithm makes use of information at the three ends of the system for the fault distance estimation and consequently a communication link is necessary. Communication requirements for fault locators are very modest (and non-continuous), since it operates in an off-line mode. If, for any reason, the communication of data is discontinued or the fault recorders at one or two ends fail to record data for some reason, then fault location, employing the

technique as developed in this work, can no longer be estimated. A back-up facility comprising a fault locator based on utilising information from one end of a system is thus clearly desirable and advantageous. In this respect, some of the techniques outlined in Chapter 2, particularly those relating to two-ended systems utilising information from one end only, could be researched into in order to extend the principles to three ended systems. The latter additional facility could then be relatively easily implemented as part of the same equipment as the main fault locator.

REFERENCES

1. Saha, M.M. and Erikson, L., "Microcomputer-Based Accurate Fault Locator with Remote-End Infeed Compensation", IEE Conference Publication n° 249, April, 1985, pp 193-198.

2. IEEE Study Committee Report, "Protection Aspects of Multi-Terminal Lines", IEEE report n° 79, TH0056-2-PWR, 1979.

3. Sant, M.T. and Paithankar, Y.G., "On Line Digital Fault Locator For Overhead Transmission Lines", Proc.IEE, 126, n° 11, November 1979, pp 1181-1185.

4. Takagi, T., Yamakoshi, Y., Yamaura, M., Kondow, R. and Matsushima, T., "Development of a New Type Fault Locator Using the One-Terminal Voltage and Current Data", IEEE Trans., PAS-101, n° 8, August 1982, pp 2892-2898.

5. Muraoka, M.,Mitani, I.and Inagaki,J., "Microprocessor Based Fault Locator", Toshiba Review, n° 148, Summer 1984, pp 11-14.

6. Schweitzer, O., "Evaluation and Development of Transmission Line Fault Locating Techniques Which Use Sinusoidal Steady-State Information", Ninth Annual

Western Protective Relay Conference, 1982, Spokane, Washington, USA.

7. Takagi, T. et. al., "A New Algorithm of an Accurate Fault Location for EHV/UHV Transmission Lines: Part I - Fourier Transformation Method", IEEE Trans. on Power Apparatus and Systems, PAS-100, n° 3, March 1981, pp 1316-1323.

8. Takagi, T. et. al., "A New Algorithm of an Accurate Fault Location for EHV/UHV Transmission Lines: Part II - Laplace Transform Method", IEEE Trans. on Power Apparatus and Systems, PAS-101, n° 3, March 1982, pp 564-573.

9. Wiszniewski, A., "Accurate Fault Impedance Locating Algorithm", Proc. IEE, 130, Part C, 6, 1983, pp 311-314.

10. Erikson, L., Saha, M.M., Rockefeller, G.D., "An Accurate Fault Locator with Compensation for Apparent Reactance in the Fault Resistance Resulting form Remote-End Infeed", IEEE Trans., PAS-104, n° 2, February 1985, pp 424-436.

11. Cook, V., "Fundamental Aspects of Fault Location Algorithms Used in Distance Protection", Proc. IEE, 133, Part C, n° 6, September 1986, pp 359-368.

12. Richards, G.G. and Tan, O.T.," An Accurate Fault Location Estimator for Transmission Lines", IEEE Trans., PAS-101, n° 4, April 1982, pp 945-950.

13. Morrison, L.F. and Yang, Q., "Fault Location on High Voltage Transmission Lines Using Solid State Disturbance Recorders", IEEE/CSEE Joint Conference on High Voltage Transmission Systems in China, October 1987, pp 154-160.

14. Christoupoulous, C. and Wright, A., "The Possibility of Locating Power Systems Faults from the Travelling Waves Set Up by Them on Transmission Lines", Seventeenth Universities Power Engineering Conference, April 1982, Manchester, England.

15. Schweitzer, E.O. and Jachinowski, J.K., "A Prototype Microprocessor-Based System for Transmission Line Protection and Monitoring", Eight Annual Western Protective Relay Conference, 1981, Spokane, Washington, USA.

16. Jeayasurya, B. and Rahman, M.A., "Accurate Fault Location of Transmission Lines Using Microprocessors", IEE Fourth International Conference, 1989.

17. Johns, A.T. and Jamali, S., "New Accurate Transmission Line Fault Location Equipment", IEE Fourth International Conference, 1989.

18. Sachdev, M.S. and Agarwall, R., "Accurate Fault-Location Estimates from Digital Impedance Relay Measurements", IEE Conf. Publ. 249, 1985, pp 180-184.

19. Ibe, A.O. and Cory, B.J.," A Travelling Wave-Based Fault Locator for Two- and Three-Terminal Networks", IEEE Trans. on Power Systems, PWRD-1, n° 2, April 1986, pp 283-288.

20. Girgis, A.A., Hart, D.G. and Peterson, W.L., "A New Fault Location Technique for Two- and Three-Terminal Lines", IEEE/PES 1991 Winter Meeting, New York, USA.

21. Johns, A.T. and Jamali, S., "Accurate Fault Location Technique for Power Transmission Lines", Proc. IEE, Vol 137, Pt C, n° 6, September 1990, pp 395-402.

22. Bornard, R.,Tesseron, J.M.,Bastide, J.C. and Nourris, M., " Field Experience of Digital Fault Recorders and Distance Relay in EHV Substations", IEEE Trans. on Power Apparatus and Systems, Vol. PAS-103, n° 1, January 1984.

23. Girgis, A.A., "Application of Kalman Filtering in Computer Relaying of Power Systems", Ph.D. Thesis, Iowa State University, U.S.A., 1981.

24. Wedephol, L.M., "Application of Matrix Methods to the Solution of Travelling-Wave Phenomena in Poly-Phase Systems", Proc. IEE, 1963, 110, (12), pp 2200-2212.

25. Johns,A.T., Aggarwal,R.K., "Digital Simulation of Faulted EHV Transmission Lines with Particular Reference to Very High Speed Protection", Proc. IEE, Vol.23, n° 4, April 1976, pp 353-359.

26. "The MIDAR Touch"- Instrumentation and Control-April 1989.

27. Aggarwal, R.K., Husseini, A.H. and Redfern, M.A., "Design and Testing of a New Microprocessor-Based Current Differential Relay for EHV Teed Feeders", IEEE Trans. on PWRD ,Vol. 6, n° 3, July 1991.

APPENDIX A

TRANSPOSED AND UNTRANSPOSED LINE EIGENVALUES AND EIGENVECTORS

A.1 THE LINE EIGENVALUES AND EIGENVECTORS

The line eigenvalues and eigenvector matrix are computed from the line series impedance and shunt admittance matrices ([Z], [Y]) and these are in turn computed from a knowledge of the line conductor geometry, earth plane resistivity and the conductor parameters. From a knowledge of the line propagation constants (which are the square roots of eigenvalues) and eigenvector matrix, the line modal surge impedance are then evaluated. Propagation constants and modal surge impedances are the basic parameters set into the locator.

Although a simple eigenvector matrix with real elements can be defined for all transposed lines irrespective to their configurations, for untransposed lines, the matrix needs to be evaluated for each line application and set into the locator. Furthermore, while voltage and current eigenvector matrices are different for untransposed lines, they are identical for transposed lines.

In general, the eigenvector matrix and its inverse for an untransposed line have complex elements so that in

practice it is difficult to evaluate modal quantities from a complex combination of phasor values.

A.2 METHOD FOR EVALUATING EIGENVALUES AND EIGENVECTORS

With reference to equations (3.28) in Chapter 3, the transmission line equations for the natural modes are:

$$\frac{\partial^2 V_m}{\partial x^2} = [Q]^{-1}[Z][Y][Q]V_m = [\Gamma^2]\ V_m \qquad (A.1)$$

$$\frac{\partial^2 I_m}{\partial x^2} = [S]^{-1}[Y][Z][S]I_m = [\Gamma'^2]\ I_m \qquad (A.2)$$

Considering the voltage case, and defining $[P]=[Z][Y]$, then $[P]=[Q][\Gamma^2][Q]^{-1}$ or $[P][Q]=[Q][\Gamma^2]$, so that the k_{th} eigenvalue Γ^2_k of $[Z][Y]$ is given by:

$$[P][Q_k] = [Q_k]\Gamma^2_k$$

or (A.3)

$$([P] - \Gamma^2_k[U])[Q_k] = 0$$

Where:

[U] = Unit matrix

$[\Gamma^2]$ = Diagonal matrix of Γ^2

$[Q_k]$ = Column matrix (k_{th} column of [Q])

The trivial solution $Q_k=0$ applies unless the determinant of the coefficient is zero, i.e. unless:

$$det([P] - \Gamma^2_k[U]) = 0 \quad \text{for } k=1,2,\ldots,n \qquad (A.4)$$

This leads to n equations with n roots Γ^2_1, Γ^2_2, ..., Γ^2_n which are the eigenvalues of [P]. The elements of the [Q] matrix are then determined by returning to equation (A.3).

The root squaring method of finding eigenvalues and eigenvectors has been found particularly useful in processing the [Z][Y] matrix. It must be pointed out, however, that in the case of near equal roots direct application of the method can lead to an excessive number of squaring in order to separate them out and so reach convergence. Methods are available for improving the rate of convergence [24].

The foregoing method cannot be used to evaluate eigenvalues and eigenvectors when the line is perfectly transposed as the matrix product of [Z][Y] gives two equal eigenvalues and the routine does not converge. Instead a matrix of eigenvectors can be defined for transposed lines as shown in equation (A.5).

$$[Q] = \begin{bmatrix} 1 & 1 & 1 \\ 1 & 1 & -2 \\ 1 & -1 & 1 \end{bmatrix} \quad , \quad [Q]^{-1} = 1/6 \begin{bmatrix} 2 & 2 & 2 \\ 3 & 0 & -3 \\ 1 & -2 & 1 \end{bmatrix} \qquad (A.5)$$

As mentioned before, for a transposed line, the current eigenvector matrix [S] is exactly the same as for the voltage eigenvector, i.e. [S] = [Q].

The eigenvector matrix and its inverse given in equation (A.5) has the advantage of having real elements only and it is more suitable for the purpose of the work presented in this thesis. Also, for this special case, the modal propagation constants (which are the square root of the eigenvalues) and the surge impedances simply become functions of the positive, negative and zero sequence parameters of the line and take the simplified form as given in equation (A.6). The general form of the [Z] and [Y] matrices is shown in equation (A.7) and the

assumed self and mutual parameters (Z_s, Z_m, Y_s, Y_m) as defined in equation (A.6) are given in equation (A.8).

$$\Gamma_1 = [(Z_s+2Z_m)(Y_s-2Y_m)]^{1/2} = (Z_0Y_0)^{1/2}$$

$$\Gamma_2 = \Gamma_3 = [(Z_s-Z_m)(Y_s+Y_m)]^{1/2} = (Z_1Y_1)^{1/2} \qquad \text{(A.6)}$$

$$Z_{01} = (Z_0/Y_0)^{1/2}, \quad Z_{02} = Z_{03} = (Z_1/Y_1)^{1/2}$$

$$[Z] = \begin{bmatrix} Z_{aa} & Z_{ab} & Z_{ac} \\ Z_{ba} & Z_{bb} & Z_{bc} \\ Z_{ca} & Z_{cb} & Z_{cc} \end{bmatrix} \qquad [Y] = \begin{bmatrix} Y_{aa} & -Y_{ab} & -Y_{ac} \\ -Y_{ba} & Y_{bb} & -Y_{bc} \\ -Y_{ca} & -Y_{cb} & Y_{cc} \end{bmatrix} \qquad \text{(A.7)}$$

$$Z_s = (Z_{aa}+Z_{bb}+Z_{cc})/3 \quad , \quad Y_s = (Y_{aa}+Y_{bb}+Y_{cc})/3 \qquad \text{(A.8)}$$

$$Z_m = (Z_{ab}+Z_{ac}+Z_{bc})/3 \quad , \quad Y_m = (Y_{ab}+Y_{ac}+Y_{bc})/3$$

APPENDIX B

DIGITAL SIMULATION OF THE FAULT TRANSIENT PHENOMENA ON THREE-TERMINAL EHV TRANSMISSION LINE

B.1 FUNDAMENTAL RELATIONSHIPS

Any multiconductor transmission line section is defined by its series impedance matrix per unit length [Z] and corresponding shunt admittance [Y]. Each element of [Z] varies with frequency and is determined by the conductor types, their physical geometry and the nature of the earth plane [25].

The theory of natural modes developed by Wedephol [24] enables a solution to the system voltage steady-state equations given by equation (B.1) to be transformed into a series of independent differential equations of the form of equation (B.2).

$$\frac{\partial^2 V}{\partial x^2} = [Z][Y]V \qquad \text{(B.1)}$$

$$V = exp(-\psi x).V_i + exp(\psi x).V_r \qquad \text{(B.2)}$$

where $\psi = Q.\Gamma.Q^{-1}$, Q= voltage eigenvector matrix, Γ = propagation constant matrix.

Matrix function theory permits easy evaluation of the hyperbolic functions, the polyphase surge impedance and admittance necessary for a solution of the problem. For example, the polyphase surge admittance matrix is given by:

$$Y_o = (Q.\Gamma^{-1}.Q^{-1}.Z)^{-1} \qquad (B.3)$$

B.1.1 Transmission Line Transfer-Matrix Function

A faulted transmission line system essentially consists of a network of cascaded sections. Two-port transfer matrices are particularly useful in the solution of such a problem. For example, with reference to Figure B.1, the transfer matrix representing a line section, say up to the fault point, is given by equation (B.4).

$$\begin{bmatrix} I_s \\ I_f \end{bmatrix} = \begin{bmatrix} Y_{11} & Y_{12} \\ Y_{21} & Y_{22} \end{bmatrix} . \begin{bmatrix} V_s \\ V_f \end{bmatrix} \qquad (B.4)$$

where $Y_{11} = Y_o coth(\psi x)$, $Y_{12} = -Y_o cosech(\psi x)$

B.1.2 Source-side network matrix

The source network considered here at each terminating busbar is a general source model comprising of some local generation and a number of infeeding parallel lines, each with its own generation, all the generations being based upon arbitrarily defined short circuit levels. This is shown in Figure B.2.

It is relatively easy to define an equivalent source admittance matrix [YS] at each terminating busbar and this is then used in combination with the corresponding transmission line admittance matrices of equations (B.4) to form the full fault transient model.

B.1.3 Frequency-Transform Technique

The transient phenomenon associated with any disturbance, such as a fault, represents a wide frequency variation and is therefore necessary to be able to evaluate the transient response over the whole frequency spectrum. The inverse Fourier transform given in equation (B.5) forms the basis of the method by which the frequency spectrum is used to determine the corresponding time variation of any voltage or current of interest.

$$f(t) = (1/2\pi) \int_{-\infty}^{+\infty} f(\omega) . exp(j\omega t) d\omega \qquad (B.5)$$

In these studies, a modified half-range form of the basic Fourier integral (equation (B.6)), as has been successfully employed for plain feeder applications [25], is used.

$$f(t) = \text{Real}\left\{exp[(\omega t)/\pi] \int_0^{\Omega} \delta f(\omega - \psi\alpha)\ exp(j\omega t)\ d\omega\right\} \quad (B.6)$$

where $\delta = \dfrac{\sin(\pi\omega/\Omega)}{(\pi\omega/\Omega)}$, α = frequency shift constant.

B.2 SINGLE CIRCUIT TEED FEEDER FORMULATION

A general teed feeder as shown in Figure B.3 represents the system devised to investigate the fault transient phenomena on three-terminal EHV transmission lines.

The behaviour of a teed feeder system under faulted conditions is as dependent upon the configuration of the surrounding system as upon the individual line lengths of the feeder up to the tee point. In this respect, of particular importance is the presence of feed-around paths between any two ends of the teed feeder. The system shown in Figure B.3 can be configured so as to have one, two or three feed-around paths of arbitrary lengths. The

source networks are completely general as discussed previously. The simulation includes the facility to fault the teed feeder on any leg or on a feed-around path.

To provide these facilities, the system is represented by the 5-node model of Figure B.4. A general relationship for the system with a fault point between P and T, for example, can be defined as:

$$\begin{bmatrix} I_f \\ I_p \\ I_q \\ I_r \\ I_t \end{bmatrix} = \begin{bmatrix} Y_{11} & Y_{12} & Y_{13} & Y_{14} & Y_{15} \\ Y_{21} & Y_{22} & Y_{23} & Y_{24} & Y_{25} \\ Y_{31} & Y_{32} & Y_{33} & Y_{34} & Y_{35} \\ Y_{41} & Y_{42} & Y_{43} & Y_{44} & Y_{45} \\ Y_{51} & Y_{52} & Y_{53} & Y_{54} & Y_{55} \end{bmatrix} \begin{bmatrix} V_f \\ V_p \\ V_q \\ V_r \\ V_t \end{bmatrix} \qquad \text{(B.7)}$$

The elements of the admittance matrix in equation (B.7) are defined as:

Y_{11} = yfp11 + yft11, Y_{12} = yfp12, Y_{13} = 0, Y_{14} = yft12, Y_{15} = yft12

Y_{21} = yfp12, Y_{22} = yps + ypq11 + yfp11 + ypr11, Y_{23} = ypq12, Y_{24} = ypr12, Y_{25} = 0,

Y_{31} = 0, Y_{32} = ypq12 Y_{33} = yqs + ypq11 + yqt11 + yqr11, Y_{34} = yqr12, Y_{35} = yqt12,

Y_{41} = 0, Y_{42} = ypr12, Y_{43} = yrq12, Y_{44} = yrs + yrt11 + yrq11 + ypr11, Y_{45} = ytr12,

Y_{52} = 0, Y_{53} = yqt12, Y_{54} = yrt12, Y_{55} = yqt11 + yft11 + yrt11

It should be noted that each element in equation (B.7) represents a 3 x 3 sub-matrix for a three-phase system.

B.2.1 Pre-fault Calculation

The current constraint applied to the general relation is $I_f = I_t = 0$, where the voltages V_p, V_q and V_r are defined by a consideration of the system load condition. Thus:

$$\begin{bmatrix} I_p \\ I_q \\ I_r \end{bmatrix} = \begin{bmatrix} Z_{22} & Z_{23} & Z_{24} \\ Z_{32} & Z_{33} & Z_{34} \\ Z_{42} & Z_{43} & Z_{44} \end{bmatrix} \begin{bmatrix} Vp \\ Vq \\ Vr \end{bmatrix} \qquad \text{(B.8)}$$

The elements of the impedance matrix in equation (B.8) are attained by inverting the admittance matrix [Y] in equation (B.7). I_p, I_q and I_r are then used to define V_f form the inversion of equation (B.7). The defined node voltages, combined with the two port admittance relations are then used to define all the pre-fault currents of interest.

B.2.2 Fault Transient Component Calculation

For this calculation, equation (B.7) is constrained so that $I_p=I_q=I_r=0$ and the system can then be reduced to a fault point relation as given by:

$$\begin{bmatrix} V_f \\ V_p \\ V_q \\ V_r \\ V_t \end{bmatrix} = \begin{bmatrix} Z_{11} & Z_{12} & Z_{13} & Z_{14} & Z_{15} \\ Z_{21} & Z_{22} & Z_{23} & Z_{24} & Z_{25} \\ Z_{31} & Z_{32} & Z_{33} & Z_{34} & Z_{35} \\ Z_{41} & Z_{42} & Z_{43} & Z_{44} & Z_{45} \\ Z_{51} & Z_{52} & Z_{53} & Z_{54} & Z_{55} \end{bmatrix} \begin{bmatrix} I_f \\ 0 \\ 0 \\ 0 \\ 0 \end{bmatrix} \qquad \text{(B.9)}$$

where $[Z] = [Y]^{-1}$.

For a three phase system, this gives:

$$\begin{bmatrix} V_{fa} \\ V_{fb} \\ V_{fc} \end{bmatrix} = [Z] \begin{bmatrix} I_{fa} \\ I_{fb} \\ I_{fc} \end{bmatrix} = \begin{bmatrix} Z_{11} & Z_{12} & Z_{13} \\ Z_{21} & Z_{22} & Z_{23} \\ Z_{31} & Z_{32} & Z_{33} \end{bmatrix} \cdot \begin{bmatrix} I_{fa} \\ I_{fb} \\ I_{fc} \end{bmatrix} \qquad \text{(B.10)}$$

Now considering a single-phase-earth fault involving the a phase, the two healthy phase fault path currents I_{fb} and I_{fc} are zero. V_{fa} is the known quantity and is the transform of a suddenly applied sinusoidal voltage of the form $-V_{fsa}\sin(\omega_o t + \beta)$. h(t) i.e. is simply equal and

opposite to the pre-fault voltage at the fault point as determined in section B.2.1. Thus:

$$I_{fa} = V_{fa}/Z_{11} \qquad (B.11)$$

The current I_{fa} substituted in equation (B.9) then defines the system transient voltages for the fault condition. It should be noted that although not shown here, the modelling of a double circuit teed feeder is simply an extension of the single circuit analysis.

B.2.3 Fault Resistance Arrangements

For each type of fault, an example of fault resistance arrangement used by the line simulation program is shown in Figure B.5. Throughout the simulation studies in the thesis, these arrangements are used, but different phase(s) may be involved.

B.3 TYPICAL FAULT STUDIES

The results presented here typify the fault transients waveforms attained by faulting some typical 400 kV teed feeder applications as shown in Figure B.6.

The commonly made assumption of constant line parameters results in waveforms which contain

considerably more distortion than is the case in practice. Furthermore, the travelling-wave components exist for much longer period after fault inception than might otherwise be predicted. Both these latter points are evident from Figure B.7, which is for an a-earth fault at the T-point on circuit shown in Figure B.6(a). It can be clearly seen that the assumption of constant 50 Hz line parameters leads to the faulty-phase waveforms, in particular the voltage, being relatively very distorted.

The source parameters, particularly their capacities, significantly affect the fault transient waveforms. Figure B.8 shows the waveforms, again for an a-earth fault at the T-point, in which the end P capacity has been reduced to 5 GVA. Comparing Figures B.7(c-d) and B.8, it can be seen that in the case of the former (larger source of 20 GVA) the voltage transients are less significant than when the end P source capacity is small for the latter case. This is so because in the former case the source voltage is much stiffer than the latter. Similar effects are observed in the sound-phase voltages.

Faults not involving earth give rise to waveforms which are generally very noisy. Figure B.9 shows the waveforms observed for a b-c-phase fault and by comparing these for an a-earth fault for similar source conditions shown in Figures B.7(c-d), it is clear that the

travelling waves persist for considerably longer in the former case.

For certain internal fault conditions, a feed-around path can cause non-unit type line protection relays to see a fault as if it were external to the tee. The feed-around problem is most severe in system configurations of the type shown in Figure B.6(b), where the T-point is close to one end (in this case close to end Q). The primary-system current waveforms shown in Figure B.10(a-b) clearly shows that for a fault close to end P, there is a reversal in the polarities of the phase currents at end R only when there is a feed-around path present in the system (Figure B.1). This is due to a strong current being fed to end R via the feed-around path. The voltages polarities, on the other hand, remain unchanged in both the cases.

In double-circuit teed applications, there is a possibility of line instability on the healthy circuit when a fault occurs on an adjacent circuit. This is particularly so for certain types of earth faults which can produce a strong mutual coupling effect between the faulted and healthy circuits. The waveforms shown in Figure B.11, which are for a b-c earth fault on one circuit of the system shown in Figure B.5(c), typify the problems that can be caused by the mutual coupling effect.

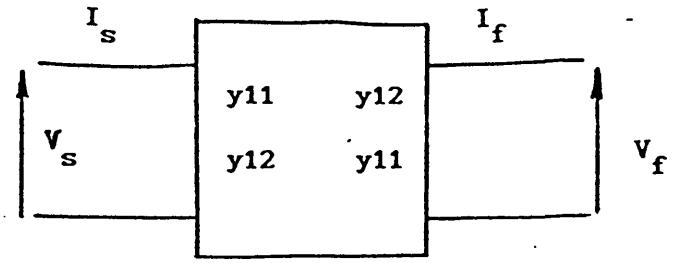

Figure B.1 Two-port transfer matrix of the line.

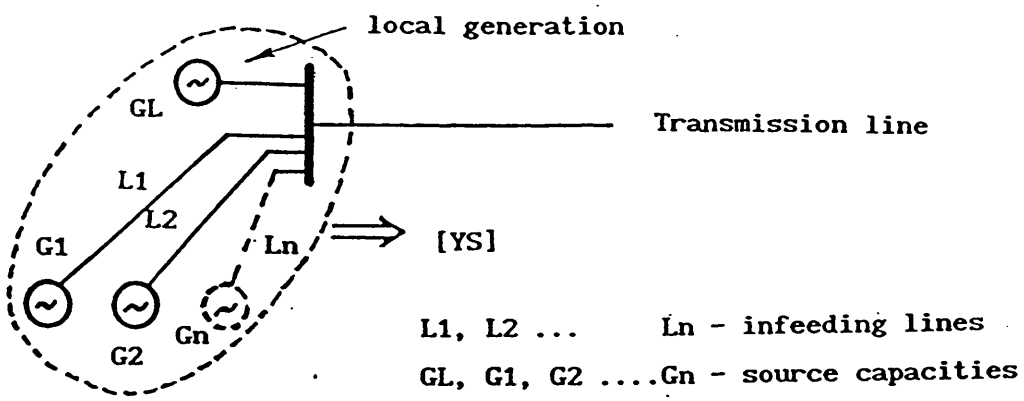

Figure B.2 General source network.

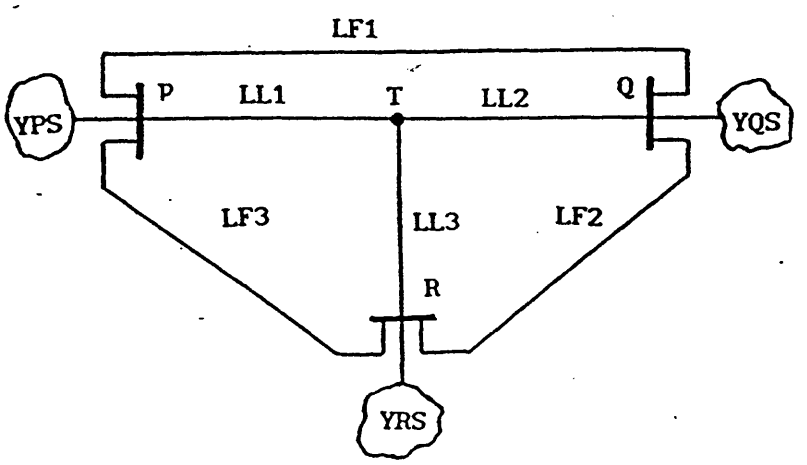

LF1, LF2, LF3 - lengths of feed-around paths

LL1, LL2, LL3 - transmission line lengths up to the tee-point

YSP, YSQ, YSR - equivalent source admittance matrices at the terminating busbars

Figure B.3 Single circuit tee system.

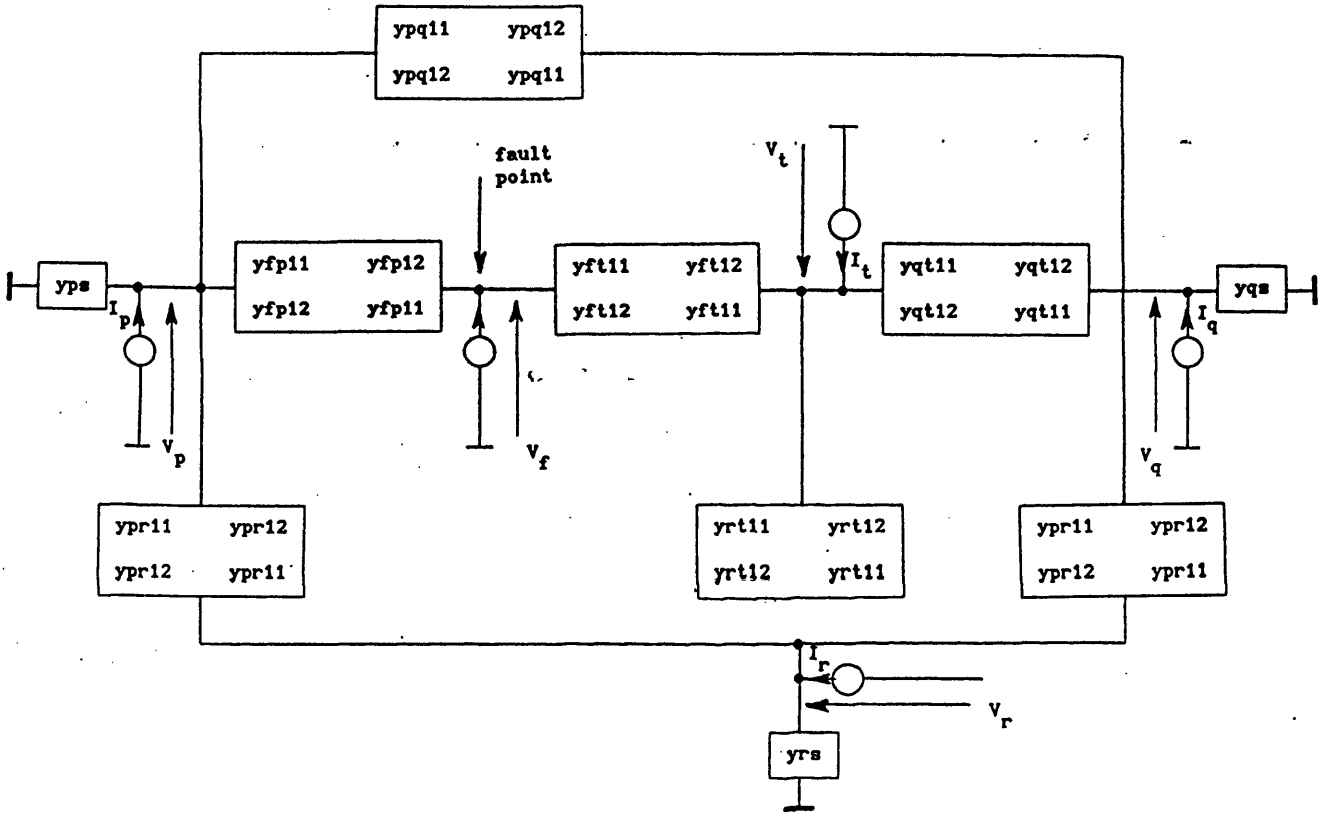

Figure B.4 Admittance format for the single-circuit tee.

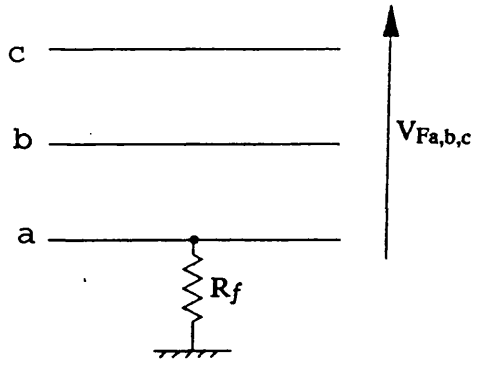

(a) a-earth fault

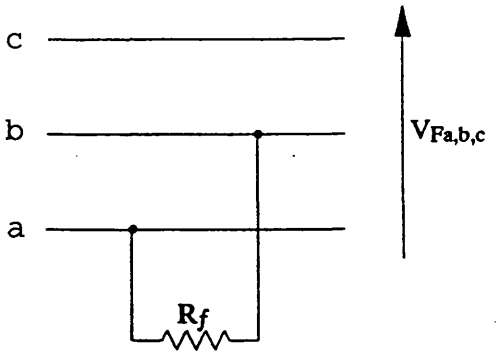

(b) a-b fault

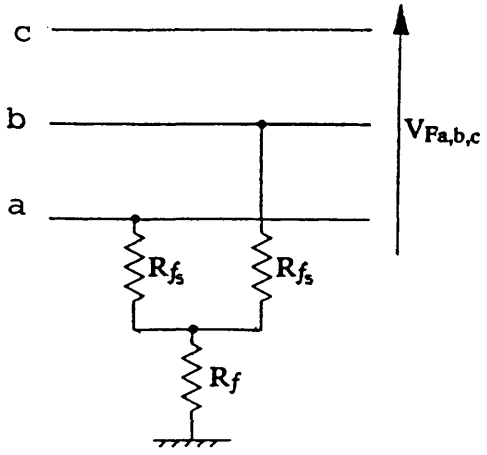

(c) a-b-earth fault

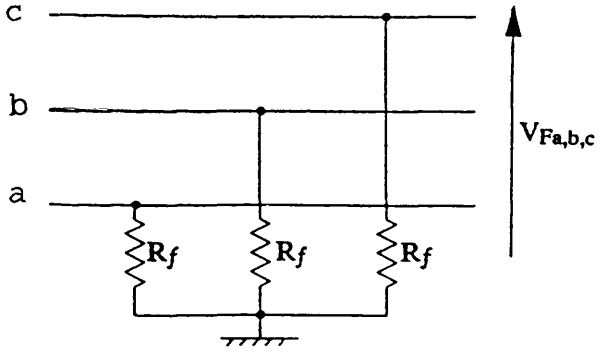

(d) three phase fault

Figure B.5 Fault resistance arrangements

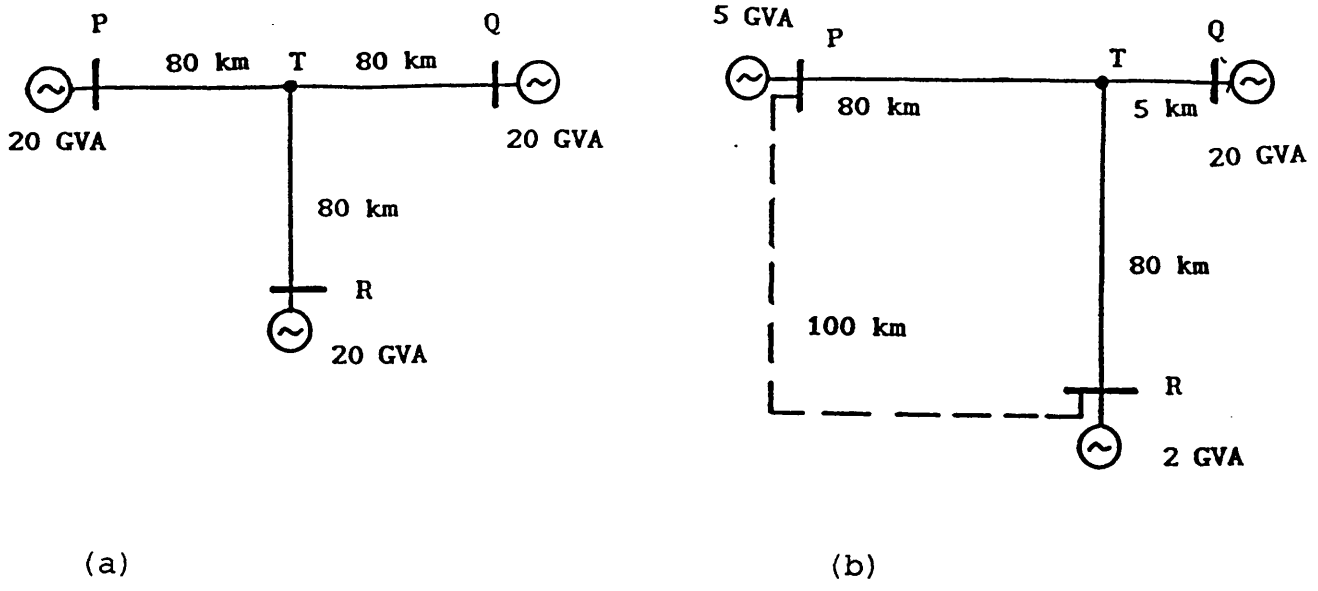

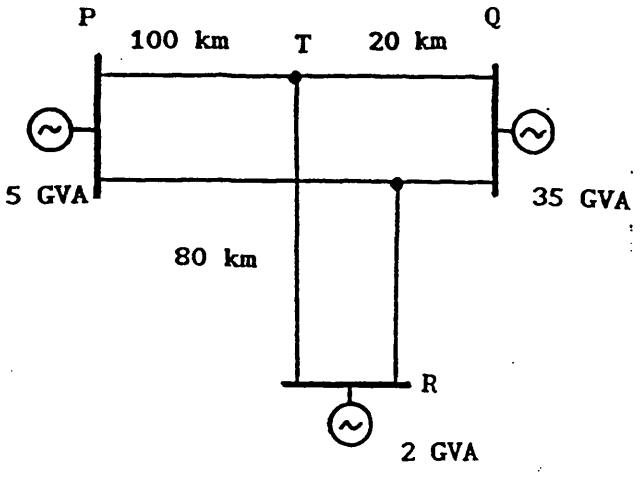

Figure B.6 System configurations studied.

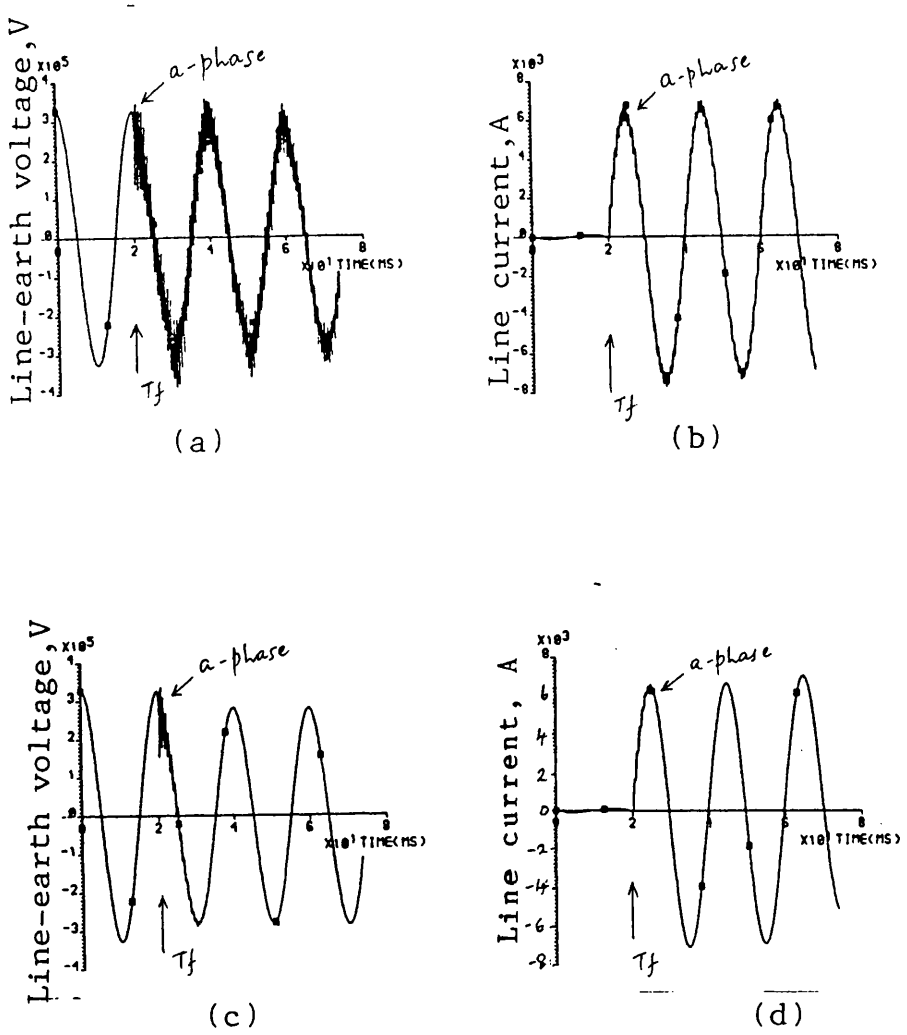

a-earth fault at $V_{a90°}$ at T-point; waveforms observed at end P;
Tf= fault inception time

(a) & (b) const. 50 Hz parameters

(c)&(d) frequency variance of parameters

Figure B.7 Effect of parameter variance on faulty-phase transient waveforms.

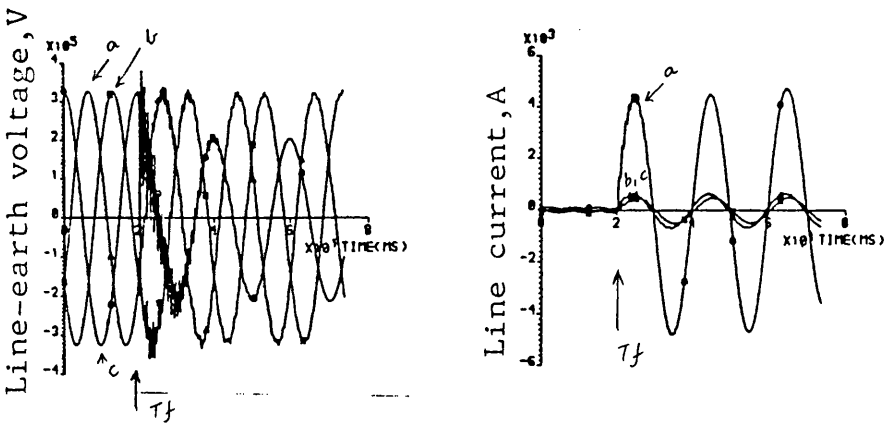

a-earth fault at $V_{a90°}$ at T-point; waveforms observed at end P
Tf= fault inception time

source capacity at end P = 5 GVA

Figure B.8 Effect of source capacity on waveforms.

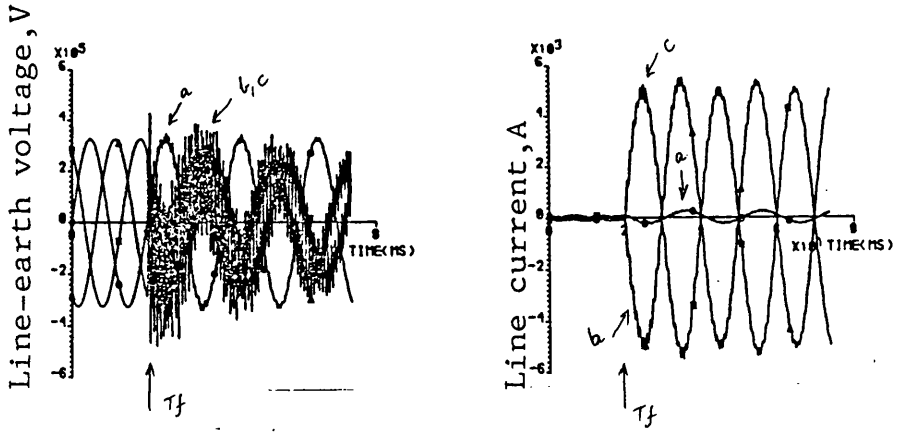

b-c phase fault at $V_{bc90°}$ at T-point; waveforms observed at end P
Tf=fault inception time

Figure B.9 Waveforms for a phase fault.

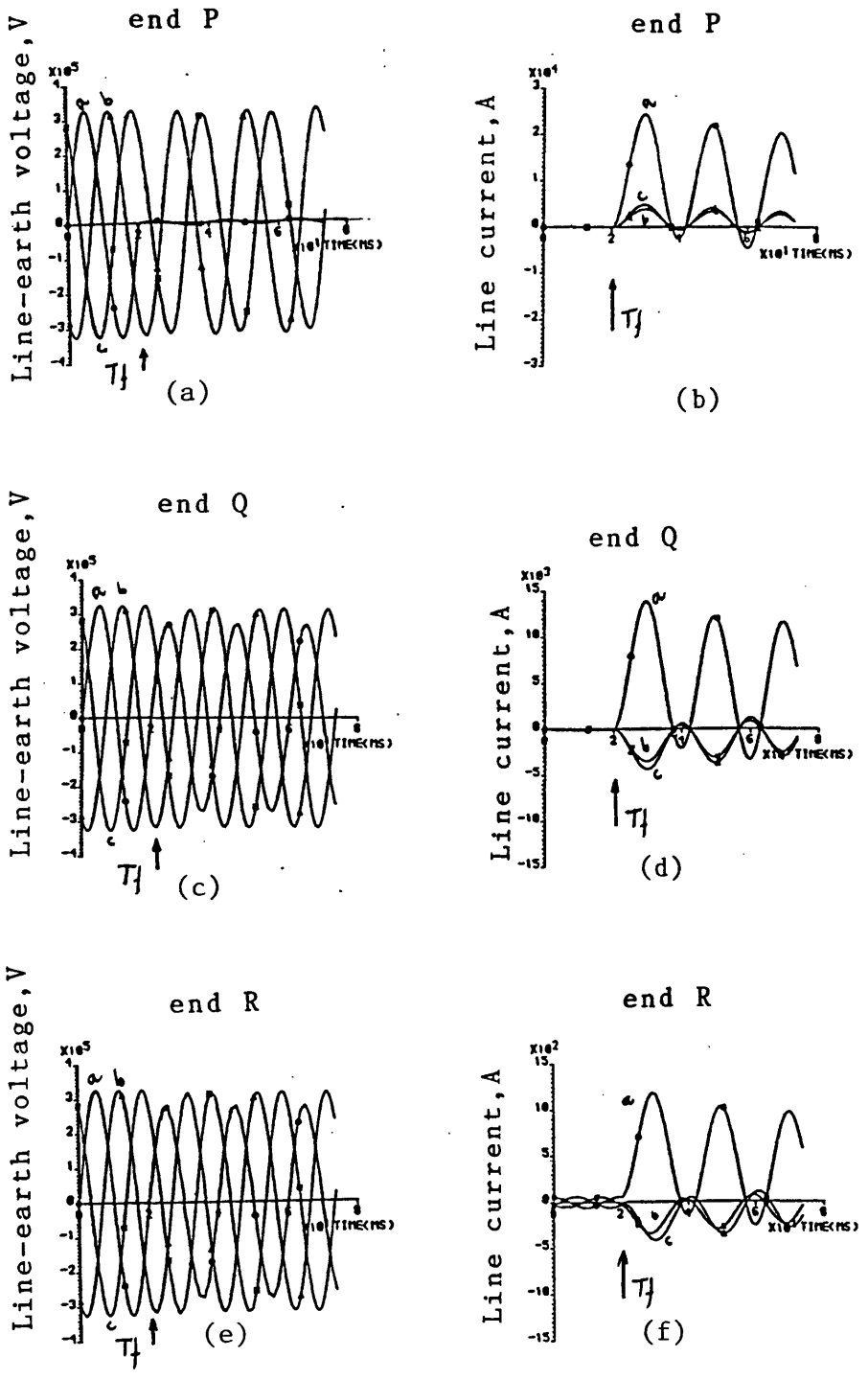

fault at 1 Km from end P, at $V_{a0°}$
Tf=fault inception time

(a) to (f) no feed-around path

Figure B.10(a) Effect of feed-around path on busbar waveforms.

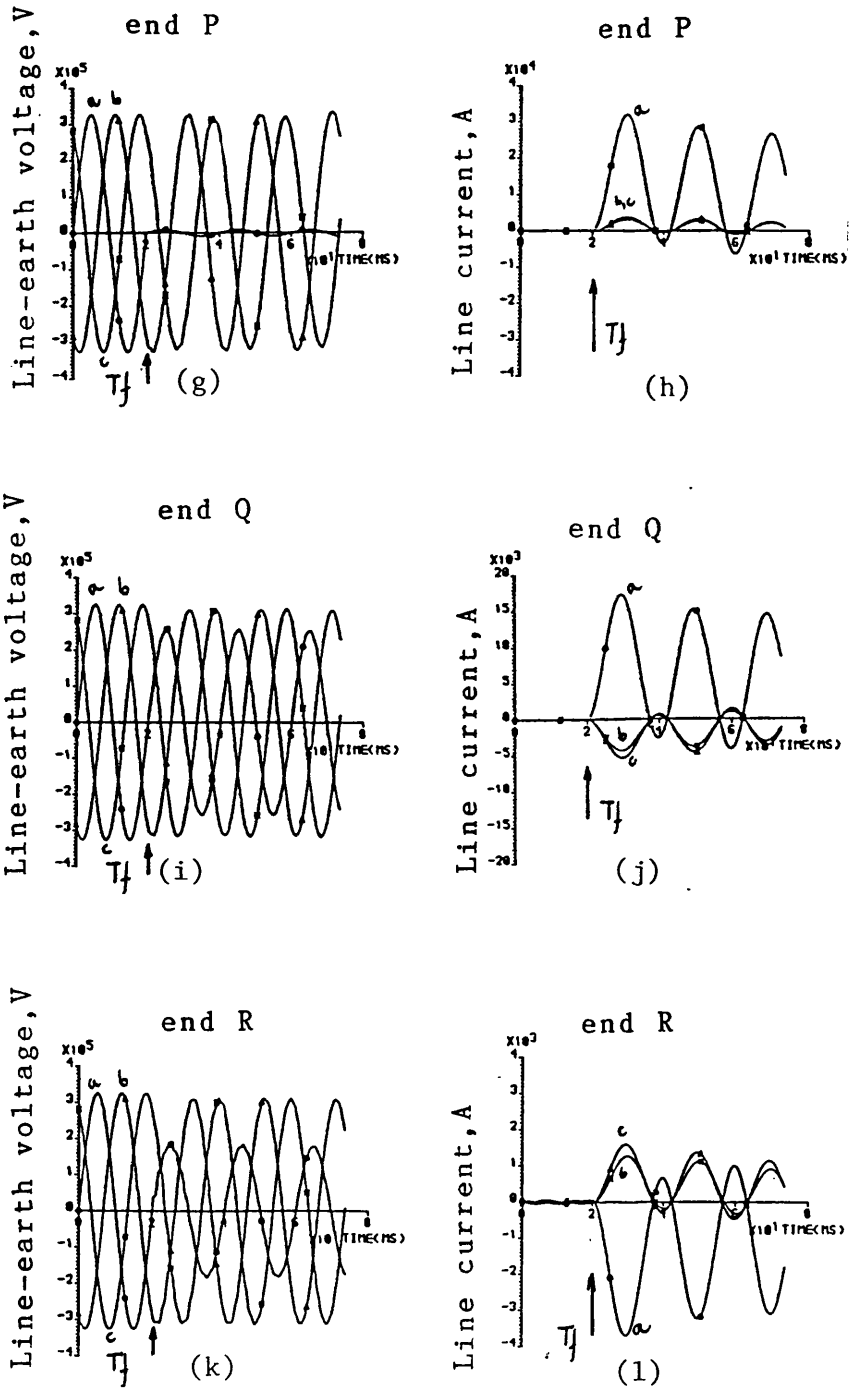

fault at 1 Km from end P, at $V_{a0°}$
Tf=fault inception time

(g) to (l) with feed-around path

Figure B.10(b) Effect of feed-around path on busbar waveforms.

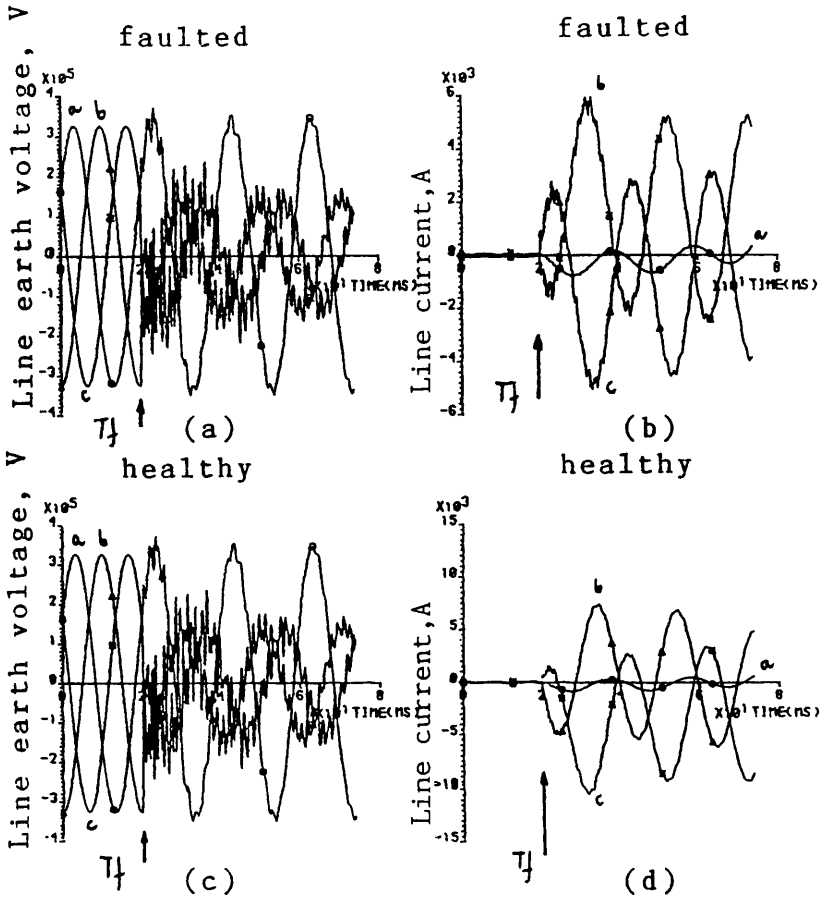

fault at 60 Km from end P, waveforms observed at end R
Tf=fault inception time

b-c-earth fault at $V_{b90°}$

Figure B.11 Waveforms for a double circuit fault.

PUBLISHED WORK

The following papers are based on the work described in this thesis:

1. Coury,D.V. and Aggarwal,R.K. ,"A New Algorithm for Fault Classification and Fault Location on Three-Terminal Lines", 26th Universities Power Engineering Conference at Brighton Polytechnic, UK, September, 1991.

2. Aggarwal,R.K., Coury,D.V., Johns,A.T. and Kalam,A., "A Practical Approach to Accurate Fault Location On Extra High Voltage Teed Feeders", to be presented at IEEE Power Engineering Society Meeting, Seattle, USA, July, 1992.

Paper 1

A NEW ALGORITHM FOR FAULT CLASSIFICATION AND FAULT LOCATION ON THREE-TERMINAL LINES

D.V. Coury and R.K. Aggarwal

University of Bath, U.K.

INTRODUCTION

Protection relays are designed to detect faults reliably, selectively and in the shortest possible time and it is not their function to pinpoint the exact location of the fault. A fault locator, on the other hand, is designed for pinpointing accurately the transmission line faults, both transient and permanent. In the case of the former, detection of weak spots in the system results in the prevention of future problems or faults and in the case of the latter, faster repair and restoration of the system is facilitated. Like fault detection, the development of accurate fault locators for 3-terminal lines, however, has posed difficult problems. This is particularly so when using conventional impedance to fault measuring techniques [1].

This paper outlines the basis of a new approach to accurately locating faults on 3-terminal lines. The method is based on utilising voltage and current waveforms recorded at the three ends of a circuit. The signals for estimation of fault location are based on modal components rather than phase values as the former approach eliminates the effect on accuracy by the source impedances, the latter being a common cause of error with a majority of other fault location techniques developed. The method also includes a technique for precisely synchronising the data from the three ends, an accurate identification of the faulted branch and also means developed to classify the type of fault, and it is shown that these criteria are essential for achieving a high degree of accuracy.

Finally, the fault location technique is evaluated using results from a typical 400 kV 3-terminal line configuration.

FAULT LOCATION TECHNIQUE

Fig 1 shows a block diagram of the different stages involved in the fault-locating technique. The starting point is the voltage and current waveforms recorded during a fault and includes a number of cycles of pre-fault data. Fig 2 typifies the data as attained from an accurate model of the system. The sampling frequency used throughout is 4kHz.

Synchronisation of Data From The Three Ends

As a first step, it is very important to be able to synchronise the data from the three ends i.e. have a common reference point. Failing to ensure the latter could result in large unacceptable errors in the accuracy.

The technique employed here hinges upon evaluating the voltage at the Tee point, from a knowledge of the pre-fault power frequency voltage and current phasors at the three ends using Fourier Transform techniques. With reference to the single-line diagram shown in Fig 3a, the voltage relationships are given succinctly as:

$$V_{PT} = \text{Cosh}(\gamma L_P)V_P - Z_o \,\text{Sinh}(\gamma L_P)I_P \qquad (1)$$

$$V_{QT} = \text{Cosh}(\gamma L_Q)V_Q - Z_o \,\text{Sinh}(\gamma L_Q)I_Q \qquad (2)$$

$$V_{RT} = \text{Cosh}(\gamma L_R)V_R - Z_o \,\text{Sinh}(\gamma L_R)I_R \qquad (3)$$

where γ = polyphase line propagation constant.
Z_o = polyphase line surge impedance.

It is apparent that if the data is synchronised then taking, say end P as reference, $V_{PT} = V_{QT} = V_{RT}$. If, however, there is unsynchronism at any of the two ends Q or R, then although the magnitudes of the voltage phasors attained via equs 1-3 would still be the same, the phase angles would nevertheless be different. It is then a relatively simple matter to shift an appropriate number of samples of voltages and currents for the unsynchronised end(s) data until such time as synchronism is achieved.

Filtering Process

In order to attain a high degree of accuracy in the location of a fault, it is important to be able to accurately extract the power frequency voltage and current phasors from the post-fault waveforms which in practice can have significant transients ranging from high frequencies down to DC levels (Fig 2 is a typical example). Since these transients are quite severely attenuated after about a cycle after the occurrence of a fault, an extensive series of studies have shown that the application of filtering techniques based on Fourier Transform methods [2] produces very accurate voltage and current fundamental phasors, provided that the first cycle of post-fault data is ignored.

Since the technique described herein is based on the superimposed components, the latter are attained by simply subtracting the pre-fault phasors from the post-fault phasors. It should be mentioned that the employment of superimposed components rather than total values gives added accuracy by virtue of the fact that any errors due to line loading are eliminated.

Fault Classification

As discussed later, the technique is based on modal values of voltages and currents rather than phase values. Of the three modes (one Earth and two Aerial) choice of the appropriate mode, in terms of accuracy, very much depends upon the type of fault. It is thus important to be able to classify the fault type before determining the fault location.

The method developed here is based on a comparison between the superimposed and zero-sequence fundamental phasors of currents I'_a, I'_b, I'_c, I'_o at an end and is summarised in Table 1.

(Criterion): If	(Fault type): Then
$\lvert I'_b\rvert$ and $\lvert I'_c\rvert < K\lvert I'_a\rvert$	a - earth
$\lvert I'_c\rvert < K\lvert I'_a\rvert$ and $\lvert I'_b\rvert \simeq \lvert I'_a\rvert$ and $\lvert I'_o\rvert > I'_{min}$	a - b - earth
$\lvert I'_c\rvert < K\lvert I'_a\rvert$ and $\lvert I'_b\rvert \simeq \lvert I'_a\rvert$ and $\lvert I'_o\rvert < I'_{min}$	a - b
Likewise for faults involving other phase(s):	
$\lvert I'_a\rvert \simeq \lvert I'_b\rvert \simeq \lvert I'_c\rvert$ and $\lvert I'_a\rvert > I'_{min}$	3-phase-earth

Table 1

K is the ratio of unfaulted to faulted phase current and depends upon the system configuration. A series of results have shown that for the system studied here, K = 0.4 gives correct fault classification for all fault types. In practice it is also necessary to apply a small threshold I_{min} to the measurements owing to transducer, filtering errors etc.

Modal transformation

As mentioned before, the fault location algorithm developed here is based on modal components of currents rather than phase values as the former allows the three-phase system to be treated like three single circuits independent of each other, thus simplifying the calculations very considerably. Without going into the details, the phase values are transformed into three modes: an Earth mode and two Aerial modes using the theory of natural modes [3] and are given as:

$$\begin{bmatrix} I_a \\ I_b \\ I_c \end{bmatrix} = [Q] \begin{bmatrix} I_1 \\ I_2 \\ I_3 \end{bmatrix} \quad . \quad \begin{bmatrix} V_a \\ V_b \\ V_c \end{bmatrix} = [S] \begin{bmatrix} V_1 \\ V_2 \\ V_3 \end{bmatrix} \qquad (4)$$

Although for an unbalanced system, the transformation matrices [Q] and [S] are different, however, if perfect line transposition is assumed, then they become identical and are given by:

$$[Q] = [S] = \begin{bmatrix} 1 & 1 & 1 \\ 1 & 0 & -2 \\ 1 & -1 & 1 \end{bmatrix} \qquad (5)$$

Results have shown that this assumption of perfect line transposition does not add significantly to the inaccuracy and the error is well within the acceptable limits for most applications. The big advantage of the aforementioned assumption is that the need to calculate the transformation matrices is obviated. Furthermore, the modal propagation constants and the surge impedances simply become functions of the sequence values of series line impedance (Z_o, Z_1, Z_2) and the shunt admittances (Y_o, Y_1, Y_2).

Identification of the faulted branch

Since the fault location algorithm described herein is based on designating the line end closest to the fault as reference, it is thus important to be able to correctly identify the faulted branch before determining the distance to fault.

The technique is based on evaluating the voltages at the Tee point from a knowledge of the post-fault voltage and current phasors at the three ends. With reference to fig 3b, if for example the fault is nearest to end P, then the voltage attained at the T-point using phasors at ends Q and R would be identical whereas that attained from end P would be quite different, indicating that the faulted branch is PT. The other faulted branches can be similarly identified. If, however, there is no discernable difference in the voltages attained with data from all the three ends, then it can be assumed that the fault is at the T-point.

Fault distance calculation

The final step in the fault location technique is the to ascertain accurately the actual distance of the fault from the nearest end. With reference to fig 3b, if for example the fault is on branch PT, then using two-part matrix relationship, both the fault point and the T-point phasors as functions of the phasors at the three ends are given as:

$$V_{Fk} = \text{Cosh}(\gamma_k \chi) V_{Pk} - Z_{0k} \text{Sinh}(\gamma_k \chi) I_{Pk} \qquad (6)$$

$$V_{Fk} = \text{Cosh}(\gamma_k L_P - \gamma_k \chi) V_{Tk} + Z_{0k} \text{Sinh}(\gamma_k L_P - \gamma_k \chi) I_{PTk} \qquad (7)$$

$$V_{Tk} = \text{Cosh}(\gamma_k L_Q) V_{Qk} - Z_{0k} \text{Sinh}(\gamma_k L_Q) I_{Qk} \qquad (8)$$

$$I_{PTk} = Y_{0k} \text{Sinh}(\gamma_k L_Q) V_{Qk} - \text{Cosh}(\gamma_k L_Q) I_{Qk} + Y_{0k} \text{Sinh}(\gamma_k L_R) V_{Rk} - \text{Cosh}(\gamma_k L_R) I_{Rk} \qquad (9)$$

Where k = 1: Earth mode, k = 2,3: Aerial modes, γ_k = modal propagation constant, $Z_{0k} = 1/Y_{0k}$ = modal surge impedance, χ = fault distance.

A simple manipulation of equs 6 - 9 yields:

$$\chi = \text{Arctanh}\,(X_{Bk}/X_{Ak})/\gamma_k \qquad (10)$$

where

$$X_{Ak} = -Z_{0k} I_{Pk} + V_{Tk} \text{Sinh}(\gamma_k L_p) - Z_{0k} I_{PTk} \text{Cosh}(\gamma_k L_p)$$

$$X_{Bk} = -V_{Pk} + V_{Tk} \text{Cosh}(\gamma_k L_P) - Z_{0k} I_{PTk} \text{Sinh}(\gamma_k L_P)$$

PERFORMANCE EVALUATION

The modelling techniques used for obtaining the instantaneous values of the voltages and currents at each end of the Tee circuit are an extension of those used for plain feeders [4]. The results presented in this paper relate to the 400 kV Teed feeder applications as shown in fig 4. It is assumed that there is zero line loading.

An extensive series of studies have revealed that the parts of the algorithm relating to data synchronisation, fault classification and faulted branch identification perform to an extremely high degree of accuracy.

Effect of fault type

Figs 5a and 5b shows a comparison of the accuracies attained in fault location when employing mode 1 (Earth) and mode 2 (Aerial) for an 'a' earth fault on the unsymmetrical Tee Configuration shown in Fig 4a. It is apparent that for this type of fault, the Earth mode gives a significantly better accuracy than the Aerial mode. In this respect, results have clearly shown that for all faults involving earth, fault distance calculations should be based on the Earth mode components. In the case of a phase-phase fault, the Earth mode component is virtually nonexistent and the calculations have thus to be based on one of the two Aerial modes, fig 6 being an example of the precision attained for such a fault. The aforementioned thus illustrates the importance of incorporating a fault classifier into the technique.

It should be appreciated that the degree of accuracy attained very much depends upon the type of configuration. Fig 7 clearly shows that for faults on a symmetrical Tee of the type shown in Fig 4b, the fault locator developed gives an extremely accurate evaluation of fault position that is largely independent of the actual fault position.

Effect of unsynchronised data

In practice it is rarely ever possible to have digital data recorded at the three ends to be absolutely synchronised. Depending upon the degree of unsynchronism, this can often lead to unacceptably large errors. Curve d in Fig 6 shows the increase in error for faults on limb PT when the data at ends Q and R are unsynchronised by two and four samples respectively. This clearly identifies a need for building into the algorithm, a mechanism for data synchronisation before evaluating fault position.

CONCLUSIONS

An algorithm for accurately locating faults on 3-terminal lines is presented. A need for data synchronisation, fault classification and faulted branch identification is clearly identified as failure to include anyone of them could result in large errors. The limited study presented shows a high degree of accuracy attained for an unsymmetrical Tee and the locator becomes extremely accurate when the Tee is symmetrical, particularly when the source capacities at the three ends are identical.

REFERENCES

1) Cook, V.: Fundamental aspects of fault location algorithms used in distance protection', Proc IEE, Vol 133, Pt C, No. 6, September 1986.

2) Burrus, C.S., Parks, T.W.: 'DFT/FFT and Convolution algorithms', text book published by John Wiley and Sons, 1985.

3) Wedephol, L.M.: 'Application of matrix methods to the solution of travelling-wave phenomena in polyphase systems', Proc IEE, Vol. 110, No. 12, 1963.

4) Johns, A.T., Aggarwal, R.K.: 'Digital Simulation of faulted ehv transmission lines with particular reference to very-high-speed protection, Proc IEE, Vol 123, No. 4, 1976.

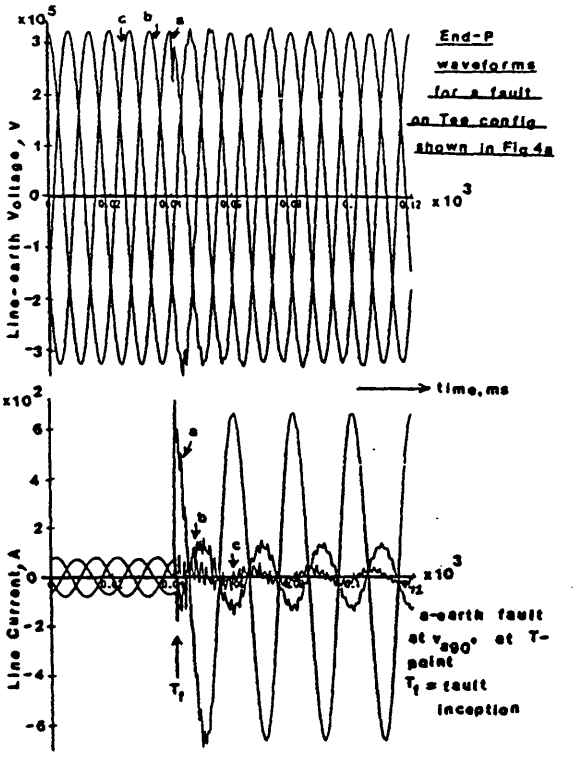

Fig 2 Typical primary system waveforms

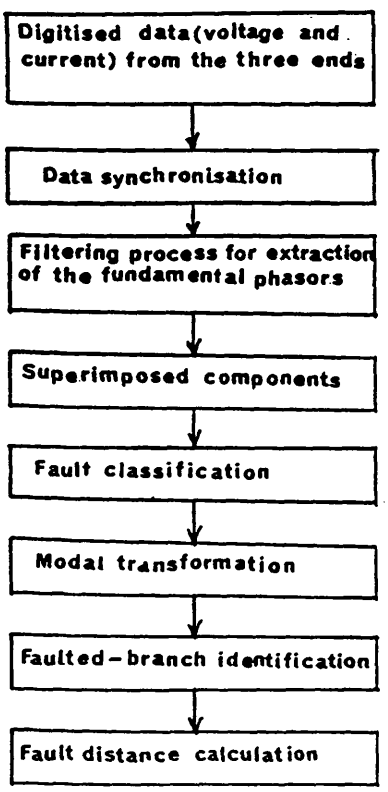

Fig 1 A block schematic of the complete process

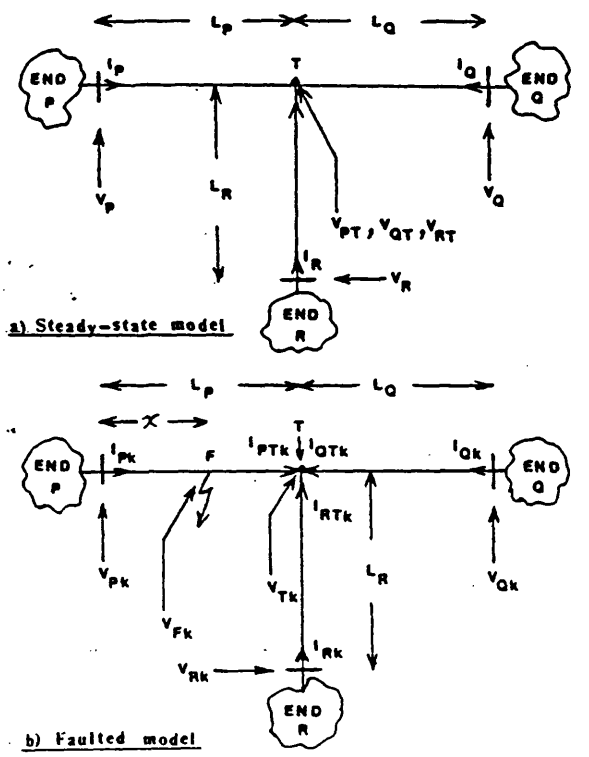

Fig 3 Basic teed-feeder model

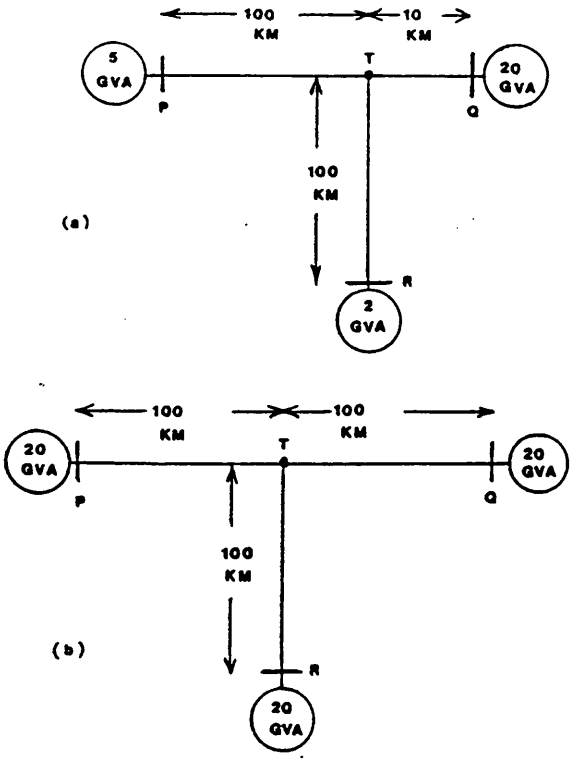

Fig 4 Typical tee configurations studied

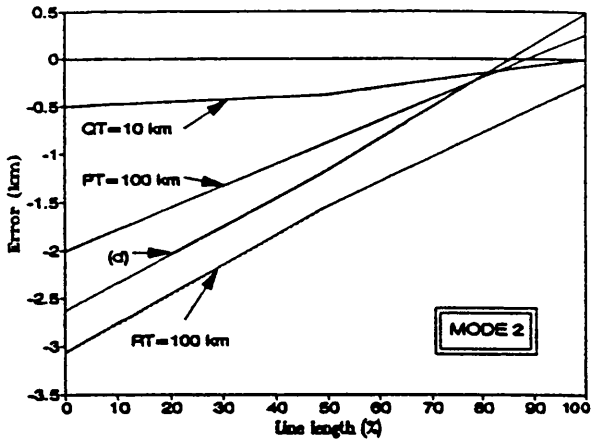

a–b phase fault at $v_{ab120°}$ on tee config shown in fig 4a; curve (d) for faults on PT but with unsynchronised data

Fig 6 Measuring accuracy for a phase-phase fault

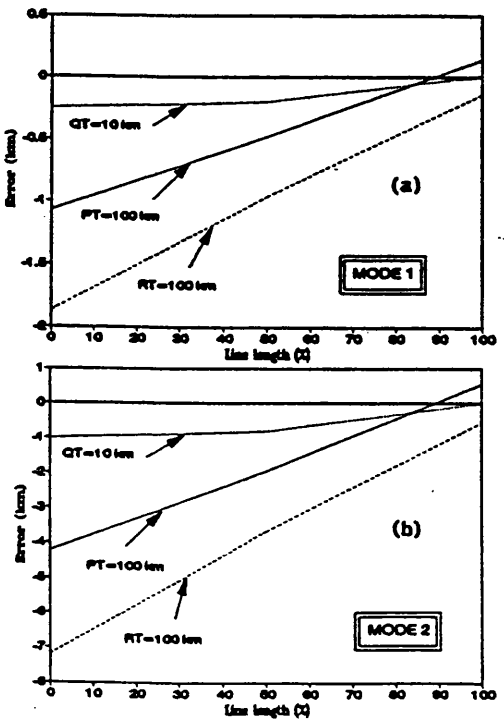

a–earth fault at $v_{a90°}$ on tee config shown in fig 4a

Fig 5 Measuring accuracy for a phase-earth fault

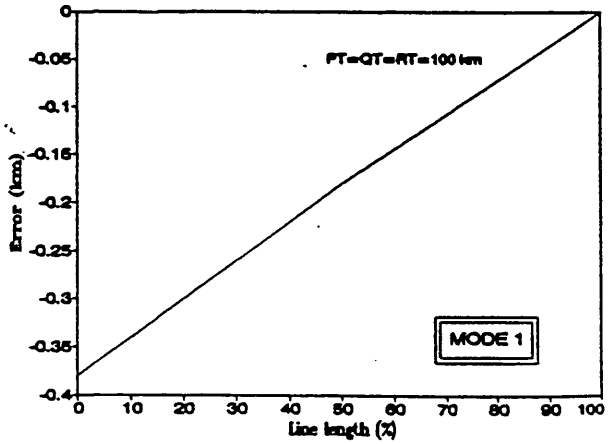

a–earth fault at $v_{a90°}$ on tee config shown in fig 4b

Fig 7 Measuring accuracy for faults on a symmetrical tee

Paper 2

A PRACTICAL APPROACH TO ACCURATE FAULT LOCATION ON EXTRA HIGH VOLTAGE TEED FEEDERS

R K Aggarwal, Senior Member, IEEE
D V Coury, Member, IEEE
A T Johns, Senior Member, IEEE
A Kalam, Non-member

School of Electronic and Electrical Engineering,
University of Bath,
Claverton Down,
BATH, Avon, BA2 7AY, U.K.

Victoria University of Technology,
Ballarat Road,
Footscray,
Victoria, Australis 3011

ABSTRACT - This paper describes the basis of an ative approach for accurately locating faults on teed rs and the technique developed utilises fault voltages currents at all three ends. The method is virtually endent of fault resistance and largely insensitive to ions in source impedance, teed and line configurations, ding line untransposition. The paper presents the basic y of the technique which is then extensively tested using ated primary system voltage and current waveforms in turn include the transducer/hardware errors ntered in practice. The performance clearly shows a degree of accuracy attained.

WORDS: fault location, teed feeders, three-terminal lines.

INTRODUCTION

ction relays are designed to detect faults reliably, tively and in the shortest possible time and it is not their ion to pinpoint the exact location of the fault. A fault r on the other hand, is designed specifically for inting the exact location of faults, both transient and anent, with a concomitant requirement to achieve a very degree of accuracy. In the case of transient faults, tion of weak spots in the system would result in the ntion of future problems or faults and in the case of anent faults, faster repair and restoration of the system d be facilitated.

rate fault location on transmission systems using ntional techniques such as impedance to fault surements, represents a problem [1], primarily due to the te-end infeeds and fault resistance. In this respect, teed rs (or three-terminal lines), although attractive both from nvironmental and economical points of view, however, additional problems and therefore require special tion. The main difficulties are caused by the intermediate d from the third terminal. A high under-distance lation thus occurs normally but occasionally, when there outfeeds present, an over-distance calculation is also ble. The inaccuracies in distance calculations are ounded by different line lengths to the tee point and rent source impedances behind the terminals [2].

The majority of work reported hitherto is concerned with developing techniques for fault location on two terminal lines [3,4,5,6]. However, the methods presented give results which are very much dependent on different system and fault conditions due to one or more assumptions such as line transposition, negligible line shunt capacitance, etc, being made. Furthermore, some of the practical limitations, for example, due to the limited bandwidth of the CVT's, which can severely affect the high frequency transients in voltage waveforms recorded by fault recorders, are not considered. A direct consequence of this is that very often, the results presented show either large unacceptable errors or extremely high accuracies, both of which do not reflect the true practical situation. With regard to teed feeders, Girgis et al [7] have recently presented a technique for locating faults on such lines and the method is based on utilising information from all three ends. Although this technique adequately deals with some of the forementioned problems relating to teed feeders, however, the limited study presented is based on neglecting the line shunt capacitance, which would imply that the high accuracy attained can only be sustained on relatively short line lengths. Moreover, practical considerations such as transducer and hardware errors are not considered.

This paper describes the basis of an alternative approach to accurately locating faults on teed feeders which has been recently developed specifically for two-terminal lines [8]. In particular, the technique developed addresses the forgoing problems and takes into account the practical limitations in the design, thus extending the range of applicability of the new scheme for a whole variety of practically encountered system and fault conditions, without sacrificing the high accuracy requirements. The method is based on utilising voltage and current waveforms at all three ends of typical EHV teed feeders, which are then filtered using Discrete Fourier (DFT) techniques so as to produce a measure of the steady-state power frequency voltage and current phasor. The latter are obtained as data described by means of fault processing applied to data captured during the fault clearance process. The technique described makes use of superimposed, modal components of voltages and currents rather than total, phase values. The former approach has the advantage that any errors arising in accuracy due to line loading or source impedances are very significantly reduced. Means is also developed for effectively synchronising the data from the three ends and an accurate identification of the faulted leg, both essential requisites for achieving high degrees of accuracy. Finally, the fault location technique is evaluated using simulated results from practical 400kV and 500kV teed-feeder configurations, including those that pose some of the most difficult problems.

FAULT LOCATION TECHNIQUE

Fig 1 shows a block diagram of the different stages involved in the fault locating technique. The starting point is the

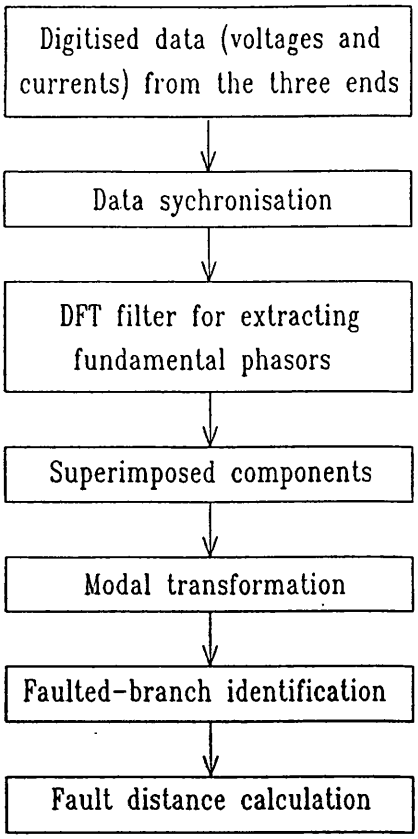

Fig.1 A block schematic of the fault locator algorithm

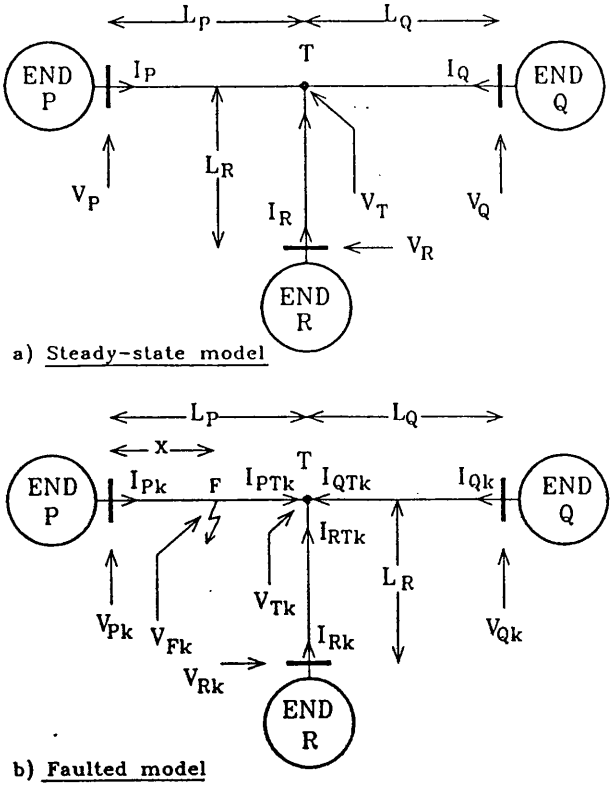

Fig.2 Basic teed-feeder model

digitised voltages and currents at all three ends during a fault and include a number of cycles of pre-fault data. It should be mentioned here that although the technique described herein is based on Computer Aided Design (CAD) studies, however, practical considerations (as described later in more detail), such as the effect of transducers, interface modules/analogue filters, quantisation, etc, on primary system fault data are also included in the simulation so that the data processed through the algorithm is very close to that attained from actual fault recorders.

Synchronisation of data from three ends

As a first step, the data from the three ends is synchronised ie, it has a common reference point. In this respect, it should be mentioned that in practice, if one end is designated as reference, then the mismatch in recorded data at any of the other two ends rarely ever exceeds two samples when compared to the reference-end data [9] and the technique is designed to tolerate these levels with little effect on accuracy. It is nonetheless important to incorporate a means for synchronising data within the algorithm to maintain the high degree of accuracy, particularly in abnormal situations where there is an exceptionally large mismatch in data due, for example, to non-simultaneous triggering of fault recorders at the three ends, on fault inception.

The technique employed here hinges upon evaluating the voltage at the tee point from a knowledge of the pre-fault power frequency voltage and current phasors which are obtained using the DFT technique (this is described in detail in the next section). With reference to the single-line diagram shown in Fig 2a, the voltage relationships attained at the T point as functions of the voltages and currents at the three ends are given succinctly as:

$$V_{PT} = \cosh(\gamma L_P)\, V_P - Z_O \sinh(\gamma L_P)\, I_P \quad (1)$$

$$V_{QT} = \cosh(\gamma L_Q)\, V_Q - Z_O \sinh(\gamma L_Q)\, I_Q \quad (2)$$

$$V_{RT} = \cosh(\gamma L_R)\, V_R - Z_O \sinh(\gamma L_R)\, I_R \quad (3)$$

where γ = polyphase line propagation constant

Z_O = polyphase line surge impedance

It is apparent that if the data is synchronised then taking, say end P as reference, $V_{PT} = V_{QT} = V_{RT} = V_T$. If, however, there is a mismatch at any of the two ends Q and/or R, then although the magnitudes of voltage phasors attained via eqns 1-3 would be identical, the phase angles would nonetheless be different. It is then a matter of shifting the data at the unsynchronised end(s) by an appropriate number of samples of voltages and currents until such time as errors due to non-synchronous sampling at the three ends are minimised. This approach has the added advantage in that, the need for data synchronisation via communication links is obviated.

Extraction of fundamental phasors

In order to attain a high degree of accuracy in the location of a fault, it is vitally important to be able to accurately extract the power frequency voltage and current phasors from the post-fault waveforms which can have significant transients ranging from high frequencies down to DC level. In this respect, although in practice, the transients in primary systems

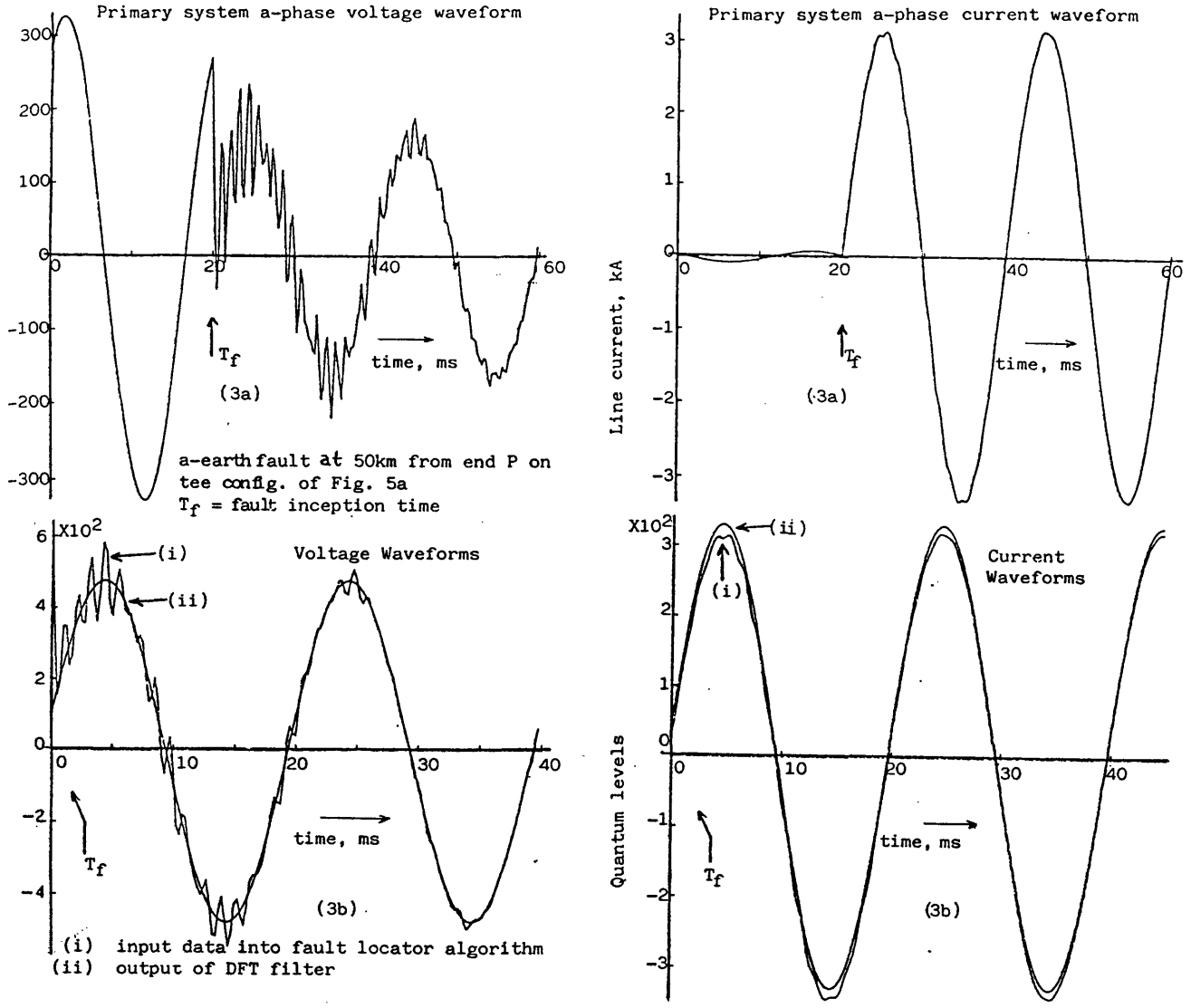

Fig 3 Effect of transducer/digital filtering on Primary System waveforms

Waveforms are attenuated by the transducers, low-pass filters, etc, the waveforms as recorded by fault recorders can still contain quite significant transient components before they are processed through the fault locator algorithm, as shown by comparing Figs 3a and 3b (graph (i)); hence the necessity to employ special digital filtering techniques to reject them.

The method used here is based on one cycle of information and the general DFT equation which gives both magnitude and phase of the fundamental phasor $X(\omega)$ is given as:

$$X(\omega) = 2/N \sum_{n=0}^{n=N-1} \left[x(n)\left\{\text{Cos}(\omega n\Delta T) - j\,\text{Sin}(\omega n\Delta T)\right\}\right] \quad (4)$$

where N= number of samples in a cycle
ΔT= time step length
ω = frequency of the phasor to be extracted
x(n) =sampled voltage or current waveforms

An extensive series of studies have shown that the aforementioned DFT technique is very effective in rejecting the transient components (Fig 3b graph (ii) is a typical example) and the resultant fundamental phasors attained give a high accuracy in fault location in a majority of practically encountered faults.

Superimposed component extraction

As mentioned earlier, since the technique described herein is based on superimposed components, which are effectively the information available on a de-energised system, the latter are attained by simply taking the difference between fault and pre-fault fundamental phasors. Again as mentioned before, the employment of superimposed components rather than total values gives added accuracy by virtue of the fact that any errors due to line loading are very substantially reduced.

Modal transformation

The fault location algorithm developed here is based on modal components of voltages and currents rather than phase values as the former allows the three phase system to be treated like three single circuits independent of each other, thus simplifying the calculations very considerably. Basically, the phase values are transformed into three modes: an Earth mode and two Aerial modes, using the theory of natural modes [10] and are given as:

$$\begin{bmatrix} I_a \\ I_b \\ I_c \end{bmatrix} = [Q] \begin{bmatrix} I_1 \\ I_2 \\ I_3 \end{bmatrix} \cdot \begin{bmatrix} V_a \\ V_b \\ V_c \end{bmatrix} = [S] \begin{bmatrix} V_1 \\ V_2 \\ V_3 \end{bmatrix} \quad (5)$$

Although for an unbalanced system, the transformation matrices [Q] and [S] are different, however, if perfect transposition is assumed, then they become identical and are given by:

$$[Q] = [S] = \begin{bmatrix} 1 & 1 & 1 \\ 1 & 0 & -2 \\ 1 & -1 & 1 \end{bmatrix} \quad (6)$$

Results have shown that this assumption of perfect line transposition does not add significantly to the inaccuracy and the error is well within the acceptable limits for most practical applications. The big advantage of the aforementioned assumption is that the need to calculate the transformation matrices is obviated. Furthermore, the modal propagation constants and the surge impedances simply become functions of the sequence values of series line impedance (Z_0, Z_1, Z_2) and the shunt admittances (Y_0, Y_1, Y_2).

Identification of the faulted leg

Since the fault location algorithm described here is based on designating the line end closest to the fault as reference, it is thus important to be able to correctly identify the faulted leg of the tee before determining the distance to fault.

The technique is based on evaluating the voltages at the tee point from a knowledge of the fault current and voltage phasors at the three ends. With reference to Fig 2b, if for example the fault is nearest to end P, then the voltage attained at the tee point using phasors at ends Q and R would be identical whereas that attained from end P would be very different, indicating that the faulted leg is PT. The other faulted legs can be similarly identified. If, however, there is no discernable difference in the voltages attained with data from all three ends, then it can be safely assumed that the fault is at the tee point itself.

Fault distance calculation

The final step in the fault calculation technique is to ascertain accurately the actual distance of the fault from the nearest end. With reference to Fig 2b, if for example the fault is on leg PT, then using two-port matrix relationship, both the fault point and the tee point phasors as functions of the phasors at the three ends are given as:

$$V_{Fk} = \text{Cosh}(\gamma_k x)\, V_{Pk} - Z_{Ok}\, \text{Sinh}(\gamma_k x)\, I_{Pk} \quad (7)$$

Also:

$$V_{Fk} = \text{Cosh}(\gamma_k L_{Pk} - \gamma_k x) V_{Tk} + \quad (8)$$

$$Z_{Ok}\, \text{Sinh}(\gamma_k L_{Pk} - \gamma_k x)\, I_{PTk}$$

And:

$$V_{Tk} = \text{Cosh}(\gamma_k L_{Rk}) V_{Rk} - Z_{Ok}\, \text{Sinh}(\gamma_k L_{Rk}) I_{Rk} \quad (9)$$

$$I_{PTk} = Y_{Ok}\, \text{Sinh}(\gamma_k L_{Qk})\, V_{Qk} - \text{Cosh}(\gamma_k L_{Qk}) I_{Qk} + \quad (10)$$

$$Y_{Ok}\, \text{Sinh}(\gamma_k L_{Rk})\, V_{Rk} - \text{Cosh}(\gamma_k L_{Rk})\, I_{Rk}$$

where k=1 for Earth mode, 2 and 3 for Aerial modes; γ=modal propagation constant; $Z_{Ok} = 1/Y_{Ok}$ = modal surge impedance; x=fault distance.

A simple manipulation of eqns 7-10 yields:

$$x = \text{Arctanh}\,(D_k/C_k)\,/\gamma_k \quad (11)$$

where

$$D_k = - V_{Pk} + A_k\, \text{Cosh}(\gamma_k L_{Pk}) + Z_{Ok}\, B_k\, \text{Sinh}(\gamma_k L_{Pk})$$

$$C_k = - Z_{Ok}\, I_{Pk} + A_k\, \text{Sinh}(\gamma_k L_{Pk}) - Z_{Ok}\, B_k\, \text{Cosh}(\gamma_k L_{Pk})$$

$$B_k = - \text{Cosh}(\gamma_k L_{Qk})\, I_{Qk} + Y_{Ok}\, \text{Sinh}(\gamma_k L_{Rk})\, V_{Rk} -$$

$$\text{Cosh}(\gamma_k L_{Rk})\, I_{Rk} + Y_{Ok}\, \text{Sihn}(\gamma_k L_{Qk})\, V_{Qk}$$

$$A_k = \text{Cosh}(\gamma_k L_{Qk})\, V_{Qk} - Z_{Ok}\, \text{Sinh}(\gamma_k L_{Qk})\, I_{Qk}$$

PRACTICAL CONSIDERATIONS IN CAD DESIGN

Fault recorder

The complete fault locator scheme is as shown in Fig 4. In practice, on fault inception, the fault recorders at all three ends are triggered simultaneously and the captured data provides a number of cycles of both pre-fault and fault data [9]. The data from the remote ends is then transferred to the local end where the processing is done in order to deduce the distance to fault. Here it is worth mentioning that unlike the communication requirements for protection schemes, those required for fault locators of the type described here, are very modest. Very often manual medium such as disks or relatively simple and cheap automatic means such as a telephone line, suffice.

Transducer/hardware errors

In the simulation described here, the primary system fault information is derived using the Frequency Domain technique as described in reference [11]. The digital simulation is run at 4 kHz. Conventional CVT's have a very low cut-off frequency typically of 600 Hz whereas the CT's have a much wider bandwidth of typically 10 kHz. Within the fault recorders are interface modules comprising input transformers and low-pass filters. The current interface module (CIM) is employed to give a proportional voltage over a specified frequency range which is much less than 10 kHz; typically the bandwidth of receptability of a CIM extends from about 2.5 Hz to 1 kHz [12]. The low-pass filter (in this case a second order Butterworth with a cut-off frequency of 1.5 kHz) has to be employed to avoid aliasing. The digitisation of the analogue information is achieved via a 12-bit A/D converter before the data is finally stored in the recorder. Inevitably, the latter process introduces further errors due to quantisation.

As mentioned before, in any fault locator design based on CAD techniques, it is extremely important to take into account the effect on primary system waveforms of forementioned equipments as they can have a significant bearing on the accuracies attained and therefore on any inferences drawn concerning a particular fault locator technique. In the fault locator described herein, these effects are incorporated into the simulation via the impulse responses of both the primary system transducers and the interface modules, which in turn have been generated from frequency tests carried out on practical models of the equipments. Furthermore, the data is

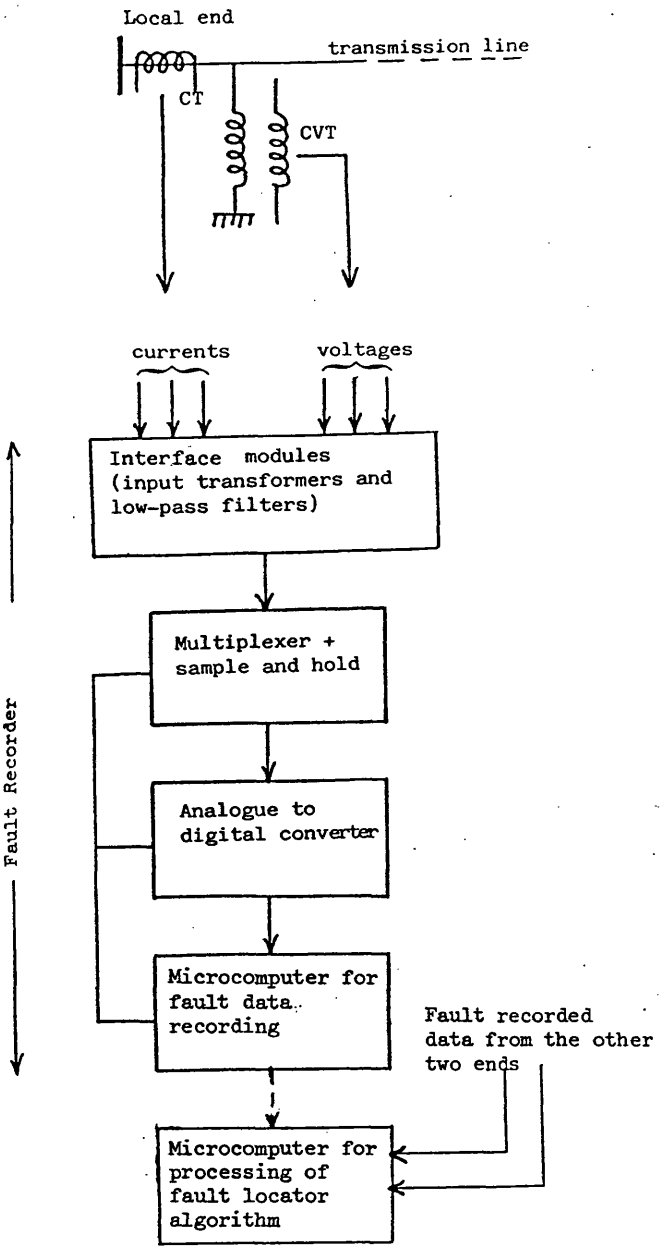

Fig 4 A block schematic of the complete fault locator scheme.

quantised to a 12-bit resolution before it is processed through the algorithm. A comparison between Figs 3a and 3b (graph (i)) typifies the differences in simulated fault transient data before and after the forementioned transducer/hardware effects have been taken into account in the CAD design. An extensive series of studies have shown that the foregoing approach is justified and accurately emulates both transducer and hardware errors.

PERFORMANCE EVALUATION

The modelling technique used for attaining the primary system fault transient waveforms at each end of the teed circuit is essentially an extension of that used for plain feeders [11]. The latter is a well tried and tested technique which has been validated using fault data from field trials. It includes both the distributive nature of the line and its frequency dependence parameters and gives very realistically, the instantaneous values of voltages and currents at the terminating busbars for any type of fault and source condition.

The results presented in this paper relate to single and double circuit teed configurations as shown in Fig 5, which comprise typical 400 kV vertical construction lines of the type commonly encountered in the UK. A limited study is also presented for a typical single circuit 500 kV horizontal line commonly used in the USA. Details of line construction are given in reference [8] and the relevant parameters used are:

(i) earth resistivity (assumed homogeneous) =100Ω m
(ii) source X/R ratio =30, Z_{S0}/Z_{S1} =0.5

The error is expressed as a percentage of the length of a particular leg of the tee and is given as:

$$\% \text{ error} = \frac{(\text{estimated location} - \text{actual location}) \times 100}{\text{length of the leg of tee}}$$

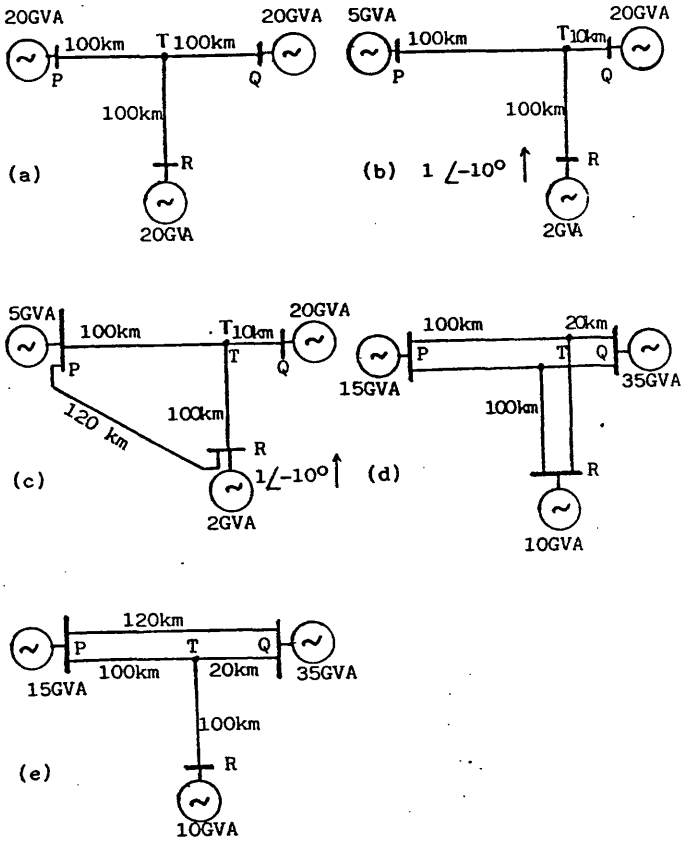

Fig 5 Teed configurations studied

Faults on a symmetrical tee

Fig 6 typifies the results attained for different types of fault on the symmetrical tee configuration shown in Fig 5a, based on a 400kV vertical construction single-circuit line of the type described in reference [8].

Type of mode selection: First of all considering faults involving earth, it is apparent from Figs 6a and 6b that a higher degree of accuracy is attained when using Earth-mode (mode 1) based signals rather than the two Aerial modes (modes 2 and 3). A series of studies have shown that this is

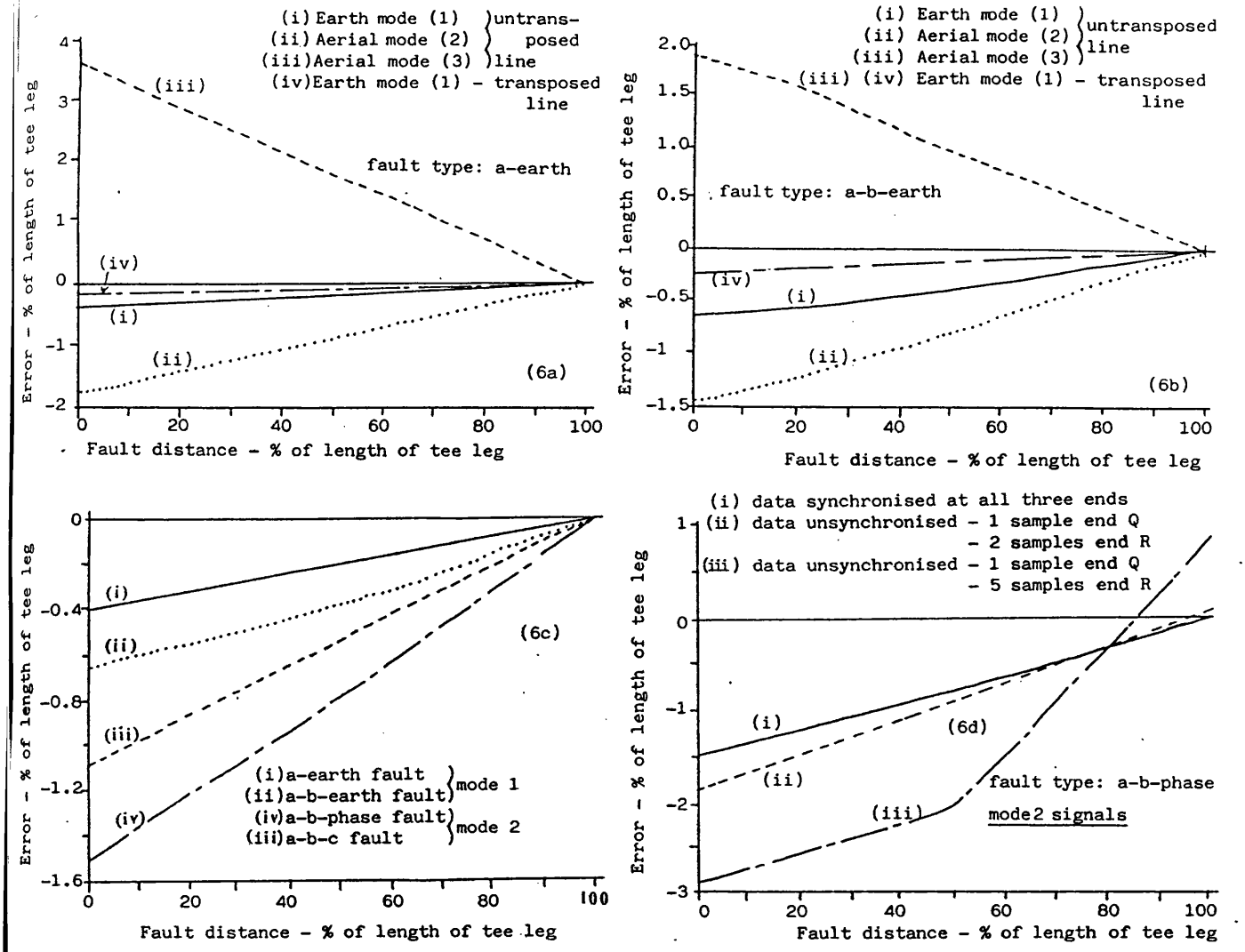

Fig 6 Measurement accuracy for faults on symmetrical tee

always the case for single-circuit vertical construction lines and is primarily due to the relatively high degree of asymmetry associated with them. It is generally found that the asymmetry associated with such lines manifests itself into causing larger errors when utilising Aerial-mode rather than Earth-mode based signals.

It should be mentioned that for faults clear of ground or three phase faults, fault location has to be based on Aerial modes due to the absence of the Earth mode for such faults. This effectively means that in the forementioned applications the fault locating algorithm would be applied to all three modes, the presence of a significant level of residual current being used to identify the existence of a fault involving earth.

Effect of line transposition: The results presented in this paper are for untransposed lines which, in practice constitute a vast majority of transmission systems. However, as mentioned before, in order to considerably simplify the processing, perfect line transposition has been assumed when setting the parameters into the fault locator described herein. Untransposed lines have parameters which differ (albeit slightly) as between phases i.e. such lines are, to a small degree, unbalanced. In teed circuits, the degree of unbalance very much depends on the level of unsymmetry i.e. on line lengths relative to each other, and its effect on accuracy of measurement is therefore carefully considered in the following sections.

Comparing curves 1 and 4 in Figs 6a and 6b which are for an a-earth and a-b-earth faults respectively and based on Earth mode, it is apparent that there is a small improvement in the measurement accuracy attained for the transposed case. This would be expected for reasons stated above, but the important point to note is that the accuracy is not unduly affected by untransposition and the percentage error is always less than about 0.6 as compared to about 0.25 for the transposed line, for all fault positions on the symmetrical tee considered.

Effect of fault type: Fig 6c shows a comparison of the accuracies attained for different types of fault. First of all when comparing faults involving earth, it is apparent that the error for multi-phase earth faults is greater than for the corresponding single-phase-earth faults. The error tends to be accentuated for three phase and pure phase-phase faults, the maximum error attained for the latter being approximately 1.5% for a close-up fault. This can be attributed to the fact that for the two latter types of fault, the estimation of fault location has to be based on Aerial modes rather than the Earth mode.

Effect of data unsynchronism: As mentioned previously, although in practice, it is relatively uncommon for mismatch in recorded data to exceed two samples between data at the reference end and the two other ends, however, it is important

o establish what levels of unsynchronism can be tolerated by he algorithm without unduly affecting the accuracy. it is vident from Fig 6d that taking end P as reference, if there is mismatch in data at ends Q and R of 1 and 2 samples espectively, then as expected, there is a slight deterioration in ccuracy attained, but it is still well within the acceptable imits. However, if for some abnormal reasons, the data at nd R is in unsynchronism by a large number of samples, say , then there is a significant increase in error, again as shown y the figure. This clearly identifies a need for building into he algorithm a mechanism for data synchronisation before valuating fault distances.

Effect of source capacity: In conventional fault location techniques, particulary those based on impedance to fault measurements, a major source of error in accuracy is the dependence of the algorithm on source capacity and therefore source impedance. In practice, this is undesirable since capacities constantly change according to changing load conditions. The algorithm described herein, however, does not require any source impedance setting (this is apparent from eqn 11). Fig 7 illustrates the measurement accuracies attained when the source capacity at end P is varied from a large value to a small one. It can be clearly seen that for the faults considered (a-earth and a-b-phase faults at 50 km from end P), the algorithm gives an accurate evaluation of fault position. The small variations in accuracy particularly at very low capacities, are a direct consequence of the associated reduction in current signal levels under such source conditions. It is once again evident from the figure that this has a more detrimental effect for pure phase faults based on Aerial modes rather than earth faults based on the Earth mode.

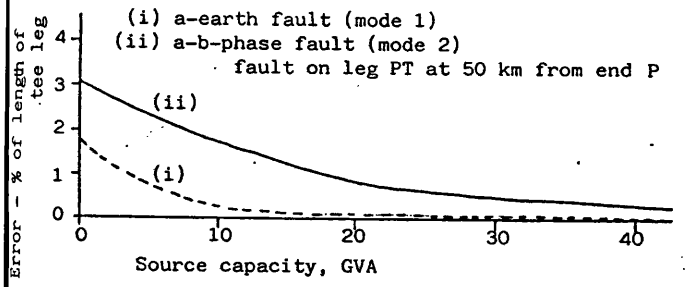

Fig 7 Effect of source capacity on measurement accuracy

Faults on an unsymmetrical tee

The performance of the fault locator discussed so far in this paper has been in relation to a symmetrical tee, ie equal line lengths up to the tee point. Although this type of system is one amongst a large number of different tee configurations encountered in practice, it nevertheless very usefully illustrates some of the salient features of the locator, particularly in its ability to retain a high degree of accuracy under a number of different practical situations. However, it is also vitally important to examine the performance for an unsymmetrical tee since very often a major cause of error is due to the unequal lengths of a teed feeder. Fig 8 typifies the performance of the locator for faults on a teed configuration of the type shown in Fig 5b. First of all considering faults on different legs of the tee, it can be clearly seen from Fig 8a that the degrees of accuracy attained are different for the three legs and this is in marked contrast to the symmetrical tee case in which absolutely identical performances are obtained for faults on all three legs. Furthermore, the percentage error for the former is greater than that for the

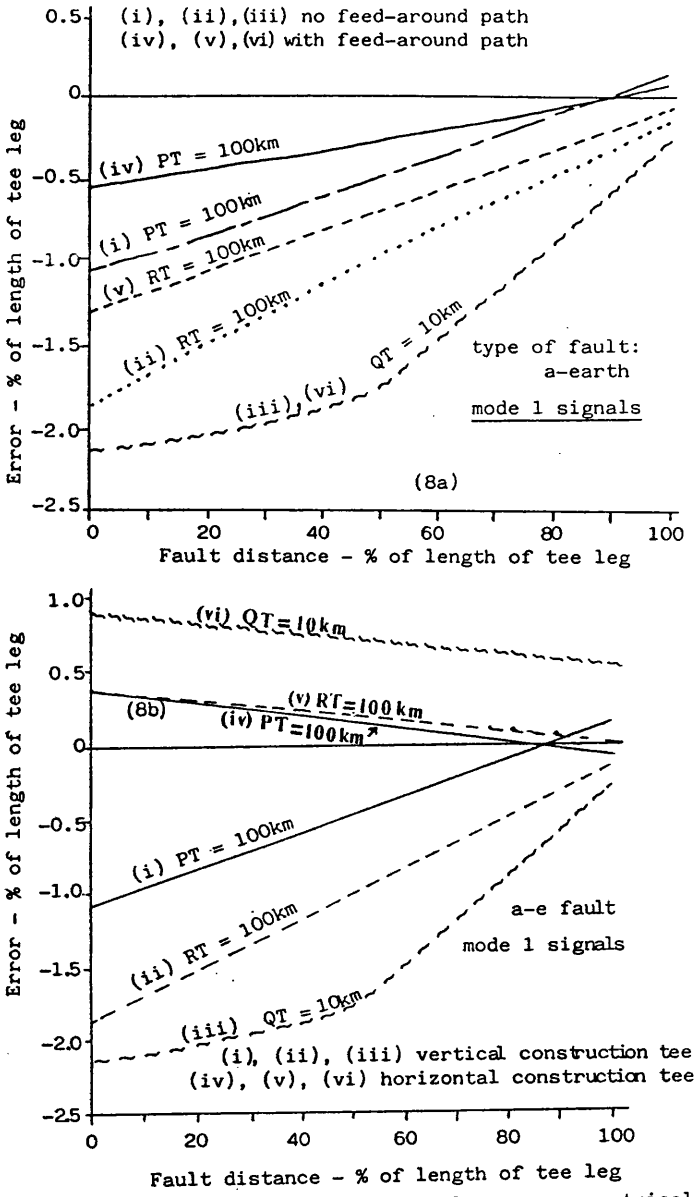

Fig 8 Measurement accuracy for faults on unsymmetrical tee

latter. As mentioned before, the unsymmetrical tee performance can be attributed to an increase in line unbalance (due to line untransposition) caused by the unequal lengths of the tee. The figure also shows that the worst performance is attained for faults on leg QT which is substantially shorter than the other two, but the magnitude of the error is still always less than about 2% for all fault positons. This compares to an overall accuracy of about 0.4% for the symmetrical tee for an idential a-e fault, as shown in Fig 6c.

It should be mentioned that although the teed circuit has some line loading, however, this is of little consequence as far as the measurement accuracy is concerned, since the employment of superimposed rather than total components of modal signals, virtually eliminates any errors caused by line loading.

Effect of an out-feed: In teed circuits, it is fairly common to have tenuous feed-around paths (Fig 5c is an example) which can result in an over-distance calculation, particularly in conventional impedance measurement techniques. The latter occurs due to a current out-feed at end R, which for certain fault positions, can cause the current at R to undergo a

transition from one direction of current flow to another. However, the fault locator algorithm described here interestingly gives a performance, as shown by Fig 8a, that is better than that attained in the absence of an outfeed, particularly for faults on legs PT and RT which are the two legs connected via the outfeed.

Effect of line configuration: Although 400kV vertical construction lines are commonly encountered in the U.K. 500 kV horizontal construction lines of the type described in Reference [8] are also quite common in other parts of the world. It is thus important to examine the performance of the algorithm for faults on such configurations. It is evident from Fig 8b that the degree of accuracy attained for such lines is both consistently and significantly higher than that for the vertical construction line. An extensive series of studies have shown that this is always the case for all types of fault and is essentially due to the greater symmetry associated with the former.

Effect of fault resistance: It is clearly evident from Fig 9 that the fault locator gives an inherently accurate evaluation of fault position that is largely independent of the fault resistance, this being so for both single-phase-earth and double-phase-earth faults. This is a very significant advantage over conventional techniques, particularly those based on impedance to fault measurements, which tend to produce excessive errors when dealing with resistive faults [1].

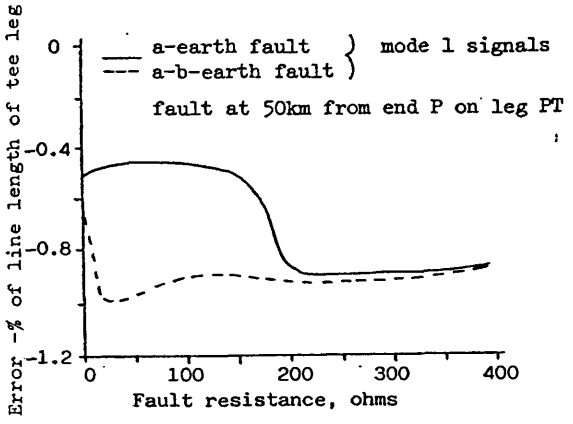

Fig 9 Effect of fault resistance on measurement accuracy

Effect of fault inception angle: Fig 10 shows the degree of accuracy attained with point-on-wave of fault, for mid-point a-earth faults on legs PT, QT and RT respectively of the tee configuration shown in Fig 5b. In common with the previous study, the results clearly show that the algorithm maintains a high degree of accuracy which is almost independent of the fault inception angle. This feature is important since in practice, faults can occur at any point on wave i.e. the fault inception angle cannot be predefined in advance. This study clearly demonstrates that the fault location algorithm is virtually immune to any errors caused by either the higher frequency transients, which are associated with faults near voltage maximum or DC offsets caused by faults near voltage zero. This feature can be primarily attributed to the effectiveness of the DFT filter in rejecting such transients.

Performance under external faults: In a fault locator, although a high accuracy for internal faults is the primary concern, nonetheless, it should also be stable under external faults. For the fault locator described herein, an external fault produces

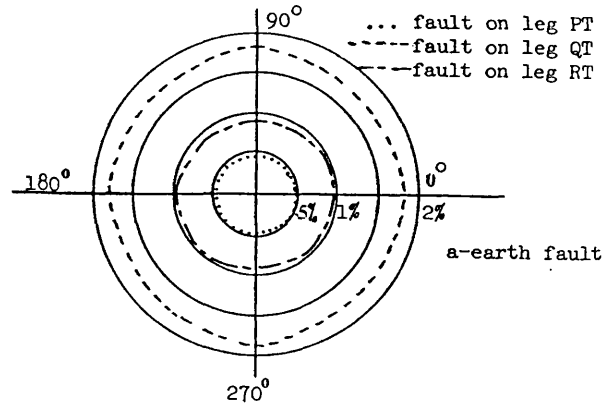

Fig 10 Effect of fault inception angle on measurement accuracy

an estimation which is consistently very much higher than that expected for an internal fault, Table 1 being a typical example. Judging from the results, it is evident that when the algorithm indicates such abnormally high values, then it can be safely assumed that the fault is external. Studies have shown that the forementioned is the case for all practically encountered external faults.

Table 1: Performance for an a-earth external fault

Fault location estimation, km			
Mode	Near end P	Near end Q	Near end R
1	-1077	-1008	-1192
2	-1257	-1132	-1380
3	1442	1250	1380

Double circuit line performance

Fig 11 illustrates the performance of the fault locator when applied to a 400 kV vertical construction double circuit line configuration of the type shown in Fig 5d. First of all considering the earth faults, it is apparent from Fig 11a that unlike the single circuit line, better accuracy is achieved when employing Aerial mode rather than Earth mode signals. This is an important finding since for such configurations, it eliminates any need for mode selection and Aerial mode based signals suffice. Moreover, any chance of a false indication of a fault on a healthy circuit due to mutual coupling between the faulted and healthy circuits is minimised since this coupling is primarily associated with Earth-mode signals.

A series of studies have also shown that the degree of accuracy attained for double circuit lines is generally higher than that for the single circuit lines for all types of fault. This can be attributed to the greater symmetry associated with the former.

In double circuit teed feeders, very often there is only a single circuit tee connected into an adjacent double circuit line, as shown in Fig 5e. A second tee circuit is normally added at a later stage. Because of the unsymmetry created resulting in a peculiar current distribution in the two circuits, such configurations can often pose difficult problems. It is therefore useful to examine the fault locator's performance for such type of teed configurations. Comparing the results for faults involving earth, it is evident from Fig 11b that the algorithm copes admirably well and the accuracies are little

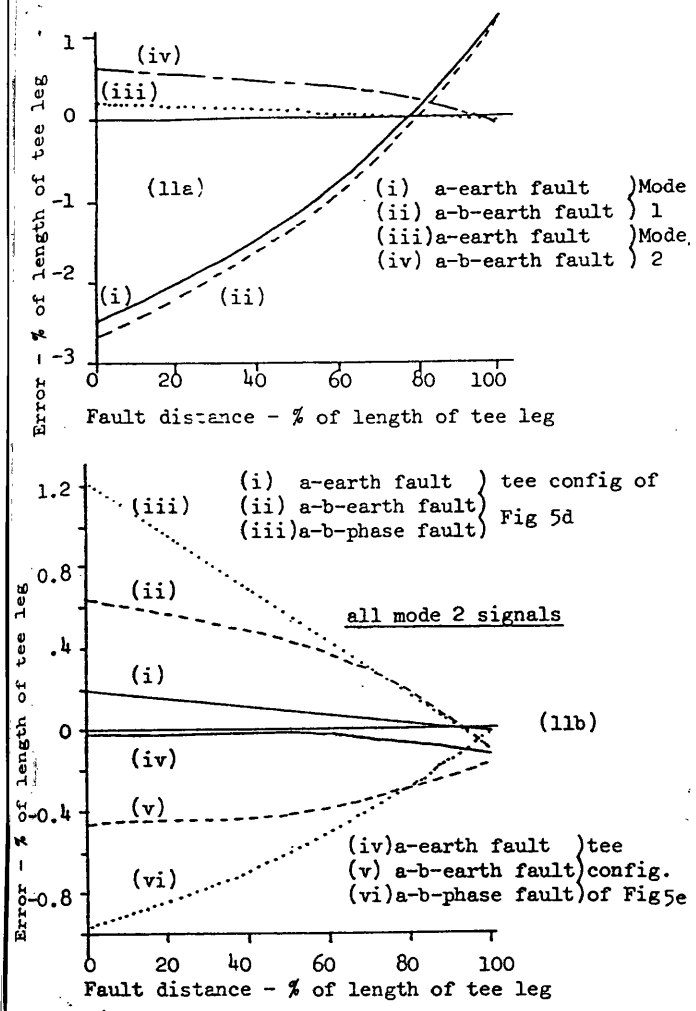

Fig 11 Measurement accuracy for double circuit tee

different from those attained for the double circuit tee.

CONCLUSIONS

The basis of an alternative approach for accurately locating faults on teed feeders is described. Although the technique utilises information from all three ends, however, there is no requirement for any continuous communication channels for data transfer.

The fault locator algorithm is based on superimposed modal signals and special filtering techniques are developed to accurately extract the fundamental phasors from the signals. These, coupled with an effective data synchronising facility and a method for an accurate identification of the faulted leg of the tee, has culminated in a fault locator design that gives high degrees of accuracy for a majority of practically encountered system and fault conditions such as different line and tee configurations, line untransposition, fault type, differing source capacities, fault resistance, etc.

Although the algorithm is based on CAD techniques, however, particular emphasis is places on examining its performance using data as though it were captured using practical fault recorders, ie, the simulated primary system voltage and current signals are subjected to the same transducer/hardware errors as those encountered in practice. It is clearly shown that the algorithm retains its high accuracy in the presence of such errors, the magnitude of errors in terms of accuracy being always less than about 2% for all practical system and fault conditions, studied. Equally importantly, with this approach, the performance attained from simulated studies more closely pertains to an actual practical situation than would otherwise be the case.

REFERENCES

1. Cook, V: "Fundamental aspects of fault location algorithm used in distance protection", Proc IEE, Vol 133, Pt C, No.6 September 1986.

2. "IEEE study committee report on protection aspects of multi-terminal lines", IEEE report No 79, TH0056-2-PWR, 1979.

3. Takagi, T., Yamakoshi, Y., Yamaura, M., Kondow,R. and Matsushima, T: "Development of a new type of fault locator using the one-terminal voltage and current data", IEEE trans, 1982, PAS-101, pp 2892-2898.

4. Sachdev, M.S. and Agarwal, R.:"A technique for estimating transmission line fault location from digital relay measurement", IEEE trans, 1988, PWRD-3, (1), pp 121-129.

5. Scheweitzer, E.O.: "Evaluation and development of transmission line fault locating techniques which use sinusoidal steady-state information". Computers and Elect Enging USA, 1983, 10, (4), pp 269-278.

6. Lawrence, D.J. and Waser, D.L.: "Transmission line fault location using digital fault recorder", IEEE trans, 1988, PWRD-3, (2), pp 496-502.

7. Girgis, A.A., Hart, D.G. and Peterson,W.L.: "A new fault location technique for two and three-terminal lines", paper no.91WM 167-7 PWRD, presented at the IEEE Winter PES meeting, New York, Feb 1991.

8. Johns, A.T. and Jamali, S.: "Accurate fault location technique for power transmission lines", Proc IEE, Vol 137, Pt C, No.6, Sept 1990, pp 395-402.

9. Bornard, P., Tesseron, J.M., Bastide, J.C. and Nourris, M.: "Field experience of digital fault recorders and distance relay in EHV substations", IEEE trans on power apparatus and systems, Vol. PAS-103, No.1, January 1984.

10. Wedephol, L.M.: "Application of matrix methods to the solution of travelling-wave phenomena in poly-phase systems", Proc. IEE, 1963, 110, (12), pp 2200-2212.

11. Johns, A.T. and Aggarwal, R.K.: "Digital simulation of faulted ehv transmission lines with particular reference to very-high-speed protection", Proc IEE, 1976, 123, (4), pp 353-359.

12. Aggarwal, R.K., Husseini, A.H. and Redfern, M.A.: "Design and testing of a new microprocessor-based current differential relay for ehv teed feeders", IEEE trans on PWRD, Vol 6, (3), July 1991.